

Topic 2: Remote sensing of sea ice

Decomposition of laser altimetry waveforms

Introduction

- At the time of writing, waveform processing methods didn't consider surface type nor its effect on the shape of the return laser pulse
- This study decomposes laser altimetry waveforms into components, the sum of which approximate the complete waveform and the location of which can be used to improve the geolocation accuracy of the lidar system
 - Decomposing waveforms provides information of the unique reflecting surfaces present within the footprint, allowing one to differentiate between surface features
 - Focusing on complex (multimodal) waveforms here, not simple (unimodal) waveforms
- They assume the return waveform is Gaussian (and each component waveform)**

Data

- LVIS – laser vegetation imaging sensor – 20m diameter footprints over Sequoia National Forest

Statement of the problem

- Levenburg-Marquardt non-linear least squares method used → minimizes the weighted sum of squares btw the observed waveform and the sum of its Gaussian decomposition
 - Need good initial guess of Gaussian parameters so LSM solution isn't a local minima
 - They do this by looking at number of inflection points of a smooth copy of the waveform and retrieving initial positions/half widths of each component
- Criteria for good fit → the stdev of the residual difference btw sum of Gaussians and observed waveform must be less than 3X the std of the background noise of observed waveform

Fitting algorithm

Identifying the number of Gaussians

- Smooth waveform to prevent high-frequency noise from giving spurious inflection points
 - Done by convolving a Gaussian of predetermined half-width w/observed waveform
 - After smoothing, the number of Gaussians is computed based on # inflection pts

Generate initial parameter estimates

- Positions, x_i , and half-widths, σ_i , of Gaussian components estimated from the positions of consecutive inflection points, l_{2i-1} and l_{2i} , on smoothed version of the observed waveform:

$$x_i = (l_{2i-1} + l_{2i}) / 2 \text{ and } \sigma_i = |(l_{2i-1} - l_{2i})| / 2 \rightarrow \text{initial amplitudes estimated w/nonnegative LSM}$$

$$(\text{intensity of pulses must be nonzero and positive})$$

Flag and rank Gaussians in terms of importance

- Flagging and ranking needed as most identified Gaussians are within background noise
- Gaussians w/half-widths \geq that of **impulse response (the laser output pulse shape)** and amplitudes 3X the stdev of mean noise level are flagged as "important"
 - Then, remaining Gaussians are ranked w/respect to their distance from the "important" one, with smaller distance giving higher ranking
 - Remaining Gaussians used if optimal fit statistic says more Gaussians needed
 - This minimizes the # of Gaussians needed for waveform decomposition

Perform parameter optimization

- This is done via non-linear LSM method Levenburg-Marquardt and mathematically looks like this:

$$\chi^2 = \sum \left[\frac{y_i - f(x_i)}{\omega_i} \right]^2$$
 where ω_i is 1 sigma uncertainties the observations, y .
- If stdev of fit is less than 3X the stdev of the background noise of observed waveform, the fit is considered reasonable

Demonstration of algorithm on observed laser altimetry data

- Decomposing the waveform, instead of focusing solely on waveform centroid/peak amplitude, is that multiple ranging points provide information on vertical diversity of surface structure within the laser footprint → in their case, they find 4 different layers within the canopy using LVIS
 - They were able to ID the ground over forested regions, whereas a simple peak-amplitude processing approach would only return information of height from within the canopy
- Comparing Gaussians from footprint to footprint can help you clearly identify vertical structures in a surface → similar Gaussians across footprints can provide confidence in IDing structures

Discussion

- Return laser pulses are generally not Gaussian → algorithm could easily be modified, though
 - Decomposing signals using the sum of Gaussians will not always be appropriate

Impressions

I provided details on the algorithm here to help me understand while reading. The algorithm is actually very straightforward and intuitive. The important point is that decomposing lidar waveforms can provide valuable insights on vertical structures within a footprint that would be ignored if ranging point was determined using a waveform centroid-based approach or peak amplitude approach. It is worth thinking about how this could be done over sea ice with diffuse waveforms and whether this has been done before?

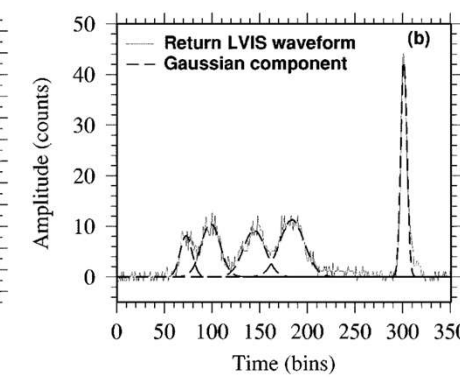
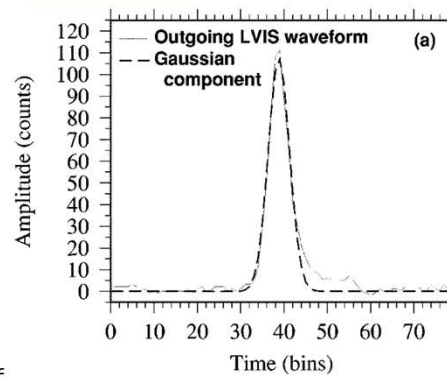


Fig. 5. Digitized LVIS laser (a) output and (b) return pulses (solid lines) and their Gaussian components (dashed lines) from the Sequoia National Forest, CA.

Satellite observations of Antarctic sea ice thickness and volume

Introduction

- This study uses laser altimetry and PMW data to provide a first estimate of basin-wide Antarctic SIT and SIV, plus the changes which occurred over 2003-2008
- Laser preferable over radar due to returns from snow surface rather than somewhere within the snowpack

Data Sets

- IS data is over all 13 campaign periods from 2003-2008 during the satellite's lifetime
 - Elliptical footprint w/mean major axis range btw 51-100m over the campaigns
 - Laser shot to shot spacing of 172m
- Areal coverage of sea ice (i.e., SIC) estimated from SSM/I using NT2
- Freeboards only used in areas w/areal coverage (SIC) was greater than 50% to reduce the impact of ocean waves which can bias retrieved freeboard

Methodology of SIT and SIV retrievals

- IS SIT observations are gridded to 25km
- Initial SSH estimate, $h_{\text{sst-est}}$, made by summing contributions of geoid, tides, and atm pressure variations at each IS measurement and subtracting sum of contributions from surface elevation estimates
 - SSH reference points taken as avg of lowest 3 values of $h_{\text{sst-est}}$ within $\pm 12.5\text{km}$ along-track distance from each measurement and $\pm 7\text{ cm}$ vertical difference of a SSH estimate (described in Markus et al. 2011)
 - $\pm 12.5\text{km}$ used to estimate length scale over which expected SSH is constant after contributions of geoid/tides/atm pressure variations are removed (also fits well w/25km gridding)

Errors in ice thickness retrieval follow Spreen et al. (2006):

$$\sigma_{hi} = \left[\left(\frac{\rho_w}{\rho_w - \rho_i} \right)^2 \sigma_{hf}^2 + \left(\frac{\rho_s - \rho_w}{\rho_w - \rho_i} \right)^2 \sigma_{hs}^2 + \left(\frac{(h_s(\rho_s - \rho_w) + h_f \rho_w)}{(\rho_w - \rho_i)^2} \right)^2 \sigma_{\rho_i}^2 + \left(\frac{h_s}{\rho_w - \rho_i} \right)^2 \sigma_{\rho_s}^2 \right]^{1/2}$$

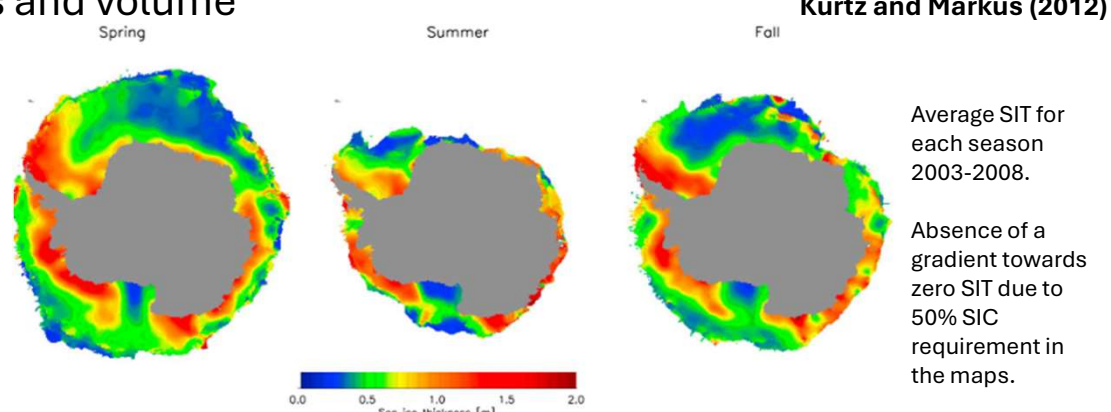
- Random error in freeboard negligible due to large number of estimates
- They assume zero ice freeboard, thus IS freeboards are equivalent to snow depth ... so no snow depth dataset is required → SIT estimates, and by extension SIV, are lower bounds
- Absolute uncertainty of 23 cm is estimated for SIT results

Comparisons With Ship-Based Observations

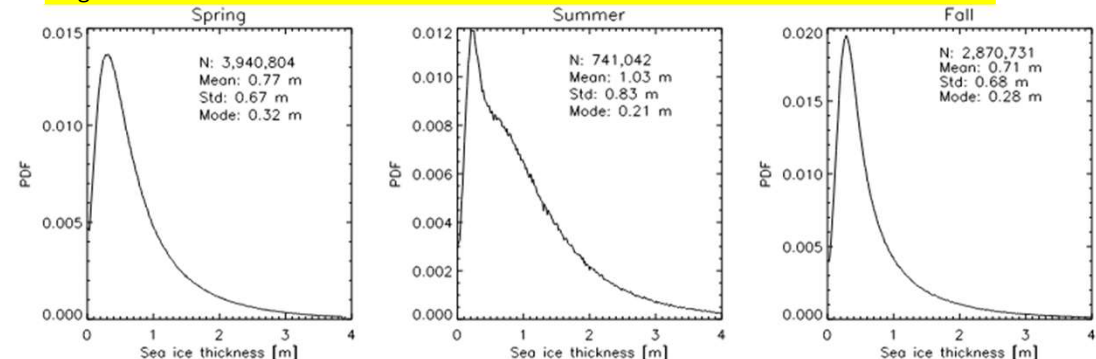
- IS results compared with estimates from ASPeCT dataset → they grid ASPeCT for comparison
- Mean SIT for ASPeCT within the $\pm 1\sigma$ uncertainty of IS estimates

Sea Ice Thickness and Volume Results

- Large annual cycle of SIV, w/mean SIV over 2003-2008 at a min of $3,357\text{ km}^3$ in summer, growing to $8,125\text{ km}^3$ in fall, and reaching a max of $11,111\text{ km}^3$ in spring
 - Amplitude of this seasonal cycle is therefore $\sim 8,000\text{ km}^3$ compared to $\sim 3400\text{ km}^3$ in the Arctic → all driven by the strong seasonal extent fluctuations



- Modal SIT $\sim 20\text{-}30\text{cm}$ for all seasons → around the max SIT that's been observed to grow thermodynamically before it's deformed → undeformed ice is most common type in Southern Ocean
- Large tails of distributions and mean SIT values $>70\text{cm}$ indicate much of SIV is deformed ice



- Very small negative SIT trends, + SIV trend in summer ($4.8\% \text{ yr}^{-1}$), - SIV trend in spring ($-2.4\% \text{ yr}^{-1}$)
- Statistical significance of SIT and SIV trends depend primarily on interannual variability of ρ_i and ρ_s
- Confidence in trends is limited; Monte Carlo simulation shows only trends in spring W Weddell and summer Indian/A-B seas are significant
 - Basin-scale estimates, along w/all others except the above, have a significant chance (>10%) of being due to interannual variability in snow/ice densities

Impressions

Uncertainty analysis is good. I didn't include random error estimate, but worth taking note of. Trend analysis is quite limited.

Antarctic | IS | ASPeCT | SIT | SIV

ICESat observations of Arctic sea ice: A first look

Introduction

- GLAS on IS had 1064nm and 532nm wavelengths, but 1064 was used for surface altimetry
- IS orbital inclination of 94°, footprint diameter of ~70m and measurements every 170m
- The first estimate of freeboards from radar altimetry came from Laxon et al. (2003)
 - I believe this study is the first to look at freeboards using lidar (not 100% sure)

Data/Methods

- IS data from March 4 - March 20
- At 1064nm, the lidar penetrates the cold/dry winter atmosphere remarkably well
- Warren et al. (1999) snow climatology → snow depth applied via sigmoidal function so it never exceeds freeboards
- Surface roughness determined as stdev over 10-km tracks (~60 samples)

Freeboard and Thickness Estimation

- Leads / flat thin ice show low reflectivity values and can be used as local SSH
 - Reflectivity not used here as determination of SSH as algorithms to correct for detector saturation/atm not finalized, but authors write that “the reflectivity would serve as an ideal indicator of thin ice or open water.”
 - Overshoots at right edge of leads due to detector saturation at transition points from ocean-ice/snow
- SIT within leads from Lebedev parameterization: $SIT = 1.33F^{0.58}$ where F is accumulated freezing days from NCEP NCAR reanalysis 2m temp → used to estimate local SSH
 - # freezing days determined as half the time separation btw RADARSAT images
 - Ice within leads estimated btw 0-25cm
- Mean SIT of 3.9m and 2.7m over two transects
- Stable and higher reflectivity over predominantly MYI regime North of Ellesmere Island, whereas E. Siberian Sea reflectivity is lower with more variability due to mixed ice types

Surface roughness

- IS allows first analysis of pan-Arctic surface roughness
- Range of roughness is from several cm to ~30cm
- Strong correspondence btw IS surface roughness and backscatter fields from QuikSCAT scatterometer which provides delineations of boundaries btw seasonal and perennial ice

Conclusions/Impressions

- The 3 lasers of IS had shorter than expected operating lifetime, meaning that continuous operation over 3-5 years was not possible → therefore, data collection periods limited to 33 days for a total of 8 periods over 3 years
- Most interesting part is how they estimated local SSH to derive freeboards due to inability to use reflectivity → consecutive RADARSAT images used w/parameterization to determine amount of time ice was forming in a lead, and this freeboard used as a reference to level the IS elevation profiles
 - “Near-coincident RADARSAT and ICESat observations allow us to identify and estimate the [SIT] of open leads for estimation of the sea level.”
 - Freeboards and SITs biased low, then, as SSH is higher than open water?... unclear methodological description though
- Not too much to take away from this paper, but interesting to see how far we've come in altimetry freeboard retrievals

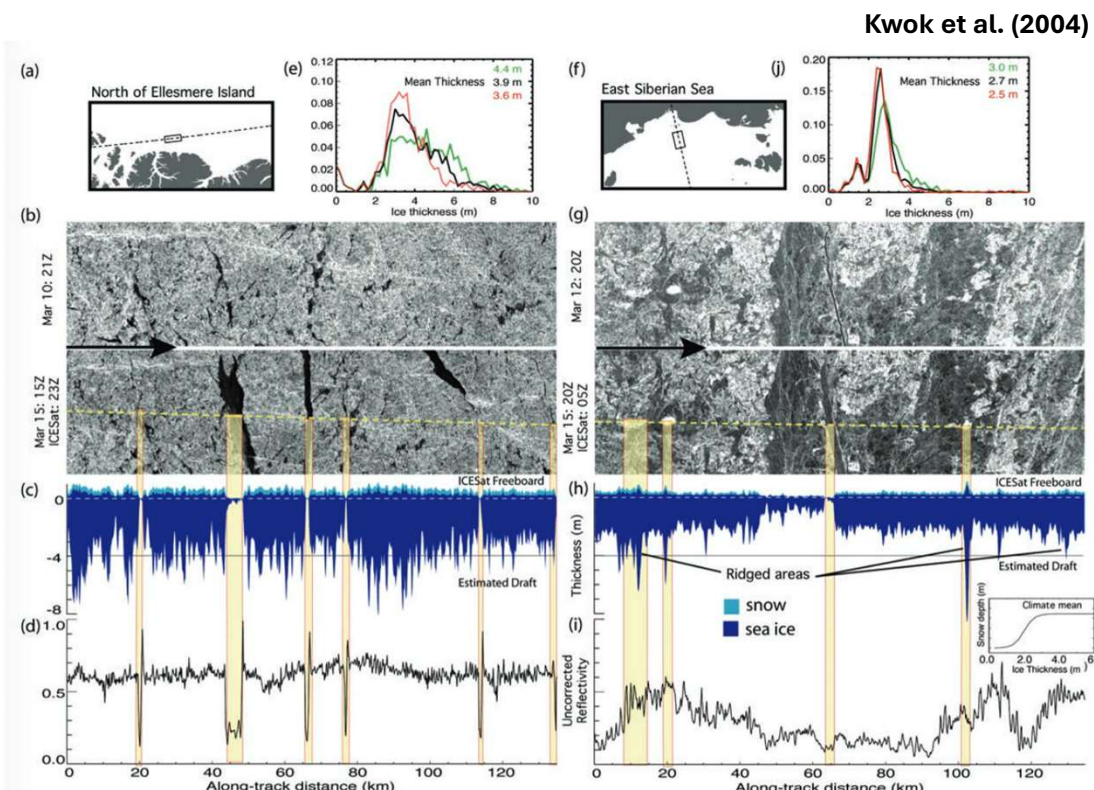


Figure 2. Two near-coincident RADARSAT and ICESat datatakes. (a, f) Geographic location of data. (b, g) ICESat track (dashed yellow line) and new leads/openings seen in time-separated RADARSAT images over the same area on the ice cover. (c, h) ICESat freeboard profile and estimated ice draft (snow: light blue; ice: dark blue). (d, i) Uncorrected reflectivity along the track. (e, j) The thickness distribution with three superimposed snow covers (red: climatological mean+10 cm; black: mean; green: mean-10 cm). (RADARSAT imagery ©CSA 2004). The inset in (i) shows the sigmoidal function for applying snow depth. The vertical scale depends on the climatological snow depth at the geographic location of interest. Yellow bands highlight features referred to in the text.

Lidar | ICESat | RADARSAT |
Freeboard | SIT | Surface roughness

ICESat over Arctic sea ice: Interpretation of altimetric and reflectivity profiles

Kwok et al. (2006)

Introduction

- This study follows Kwok et al. (2004), focusing on the geophysical signals embedded in the altimetric profiles on small and large scales

"The retrieval of freeboard and thickness estimation is not within the scope of this paper"

Data

- IS data over 3 winters, 2 falls, and 1 spring (2003-2005): FM03, ON03, FM04, MJ04, ON04, and FM05
- RADARSAT C-band SAR w/HH polarization at spatial resolution of ~150m; 3-day coverage of Arctic
- Gridded MYI fractions from QuikSCAT (ku-band scatterometer at V and H polarizations)
- NCEP NCAR reanalysis for SLP fields

ICESat Data Characteristics

- Three parameters they from ICESat they use:
 - Reflectivity (R): ratio of received energy after being scaled for range and transmitted energy
 - Time-varying Gain (G) of detector → high time-varying gain means low SNR and vice versa
 - S → the difference btw the fitted Gaussian and the received waveform
- Detailed discussion and modeling of detector saturation → they show received echo energy, E_r , can be significantly correlated with S ... this shouldn't be the case as S should be dependent on surface characteristics and not E_r → but, when saturation occurs the Gaussian fit is poor (S)

Variability of ICESat Elevations

- Retrieved surface elevation, h_{obs} , can be written as: $h_{obs}(x, t_i) = h_f(x, t_i) + h_{ssh}(x, t_i) + \varepsilon(x, t_i)$
 - h_f is total freeboard, h_{ssh} is SSH relative to reference ellipsoid, ε is instrument error (14cm)
- h_{ssh} can be expanded: $h_{ssh}(x, t_i) = h_g(x) + h_a(x, t_i) + h_T(x, t_i) + h_d(x, t_i) + O^2$
 - h_g is due to geoid undulations, h_a represents sea surface response to atm pressure loading, h_T is from tidal contributions, and h_d is the dynamic topography

Variability due to h_a (sea surface response to atm pressure loading) → causes ~70cm variation in ssh

- Regression btw elevation and ΔSLP shows that lower SLP results in higher surface elevation and vice versa → the slope is -1.12cm/hPa and $r = -0.81$
 - 1.12 cm/hPa is only slightly higher than the inverted barometer effect (IBE: the response of ssh change to changes in atmospheric pressure) of -1cm/hPa
- Applying the IBE correction results in 10-fold (2-fold) reduction in mean (variance) in elevation estimates btw two 8 day repeat cycles → so influence of h_a minimal once IBE correction is applied

Variability due to h_g (geoid undulations)

- Incorporating GRACE data into geoid models dramatically reduces residuals ... but some features in residual field remain corresponding to bathymetric relief w/high surface slopes
 - Geoid is model of global mean sea level based on Earth's gravity (no tides and currents)

Variability due to h_T (elevation changes due to ocean, load, and solid earth tides)

- At time of writing, Arctic ocean tide models quite poor
- Magnitude of ocean load tide (elastic response of Earth's crust to ocean tides, deforming the seafloor) correction typically <10cm, w/accuracy better than 1cm

- Solid Earth tide (displacement of Earth's crust due to gravitational attraction of moon/sun) varies in range ±30 cm w/uncertainty <<1cm

Variability due to h_d (dynamic topography)

- Time-varying dynamic topography → surface elevation differences due to mantle convection
- Contributions range from 2.5cm in central Arctic up to 25cm in shallow coastal regions

Large-Scale Variability → looking at differences in elevation fields

- Surface roughness highest north of Ellesmere Island/Greenland (~30cm), less so over MYI in central Arctic (~15cm) and smoothest in seasonal ice zone (<10cm)
 - Perennial ice zone distinguishable from seasonal ice zone via just surface roughness

Small-Scale Variability → using RADARSAT to verify features being detected w/IS altimetry

- Presence of snow drives up reflectivity (albedo) far more than thickening of sea ice
 - Snow on thin ice within a lead may result in reflectivity values similar to surrounding ice
 - Thus, changes in surf elevation may need to be used w/reflectivity to ID leads
 - Low reflectivity at dips in surface elevation can be used to estimate ssh
- Open-water/near-specular returns saturate detector, but postiori correction can be applied
- Stdev of elevations over flat ice is ~2cm, consistent w/the surface roughness of 1.5-2cm over this ice → indicating high precision of elevation retrievals over flat/smooth ice
- GLAS footprint not fine enough to capture individual ridges, but can get groups of them
- Radar backscatter of ridges higher bc (a) lower salinity and density, higher porosity enhance volume scattering and (b) orientation of some surf facets can reduce local incidence angles
- Waveforms of FYI and MYI look similar, unless there is large scale roughness (e.g., ridges), within a footprint as surface returns are dominated by the properties of snow cover
 - Surface relief broadens altimetric waveforms
 - New ice has similar waveform shape as FYI/MYI, just lower reflectivity (smaller)

Conclusions

- Highly reflective waveforms and near-specular returns from open-water are beyond the range of valid adjustments → which is unfortunate as these would be great local ssh estimates
- Response of sea ice cover to inverted barometer effect is near ideal and the IBEcorrection significantly decrease variance of IS fields → residuals are dominated by geoidal height
 - Effect of dynamic topography remains in question
 - Overall, though, these residuals indicate need for many local SSH references
- At the end they state that it is of immediate geophysical interest to develop a robust procedure to estimate ssh to ultimately attain freeboard estimates

Impressions

Great overview of the corrections needed to derive surface elevation and their associated uncertainties. PDFs in Figure 17 are useful to look at and Figure 3 is very interesting (looking at IBE effect). This paper emphasizes need for direct, instantaneous SSH measurements.

Lidar | IS | Reflectivity | Geophysical corrections | Detector saturation | SSH

Ice, Cloud, and land Elevation Satellite (ICESat) over Arctic sea ice: Retrieval of freeboard

Kwok et al. (2007)

Introduction

- Follow on paper from Kwok et al. (2004, 2006); objective of this paper is freeboards/tie points
- This paper puts forth three approaches for estimating local tiepoints of the sea surface

Data

- IS data from 21 Oct-24 Nov 2005 (35 days; ON05) and 22 Feb-27 Mar 2006 (34 days; FM06)
- RADARSAT; QuikSCAT data for MYI fractions; Ice motion from PMW; SLP from NCEP NCAR

ICESat Elevations, Freeboard, Sea Surface, and Tiepoints

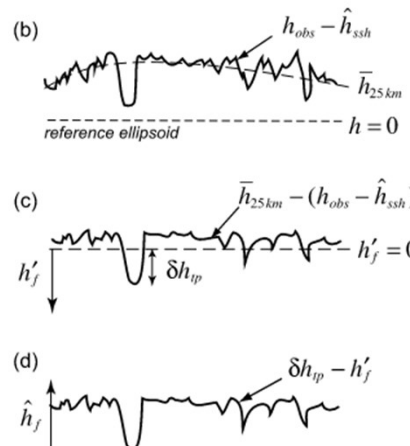
- First, $\widehat{h_{ssh}}$ estimated (modeled) w/:
$$h_{ssh}(x, t_i) = h_g(x) + h_a(x, t_i) + h_T(x, t_i) + h_d(x, t_i) + O^2$$
- Second, 25 km running mean of $h_{obs} - h_{ssh}$ (IS elevation – estimated ssh) removed
$$h'_f = \overline{h_{25km}} - (h_{obs} - \widehat{h_{ssh}})$$
 - This is written such that elevations below 25-km running mean are positive
 - Assumption is that the mean captures spatial variability of residuals in ssh, and remaining diffs are mostly due to h'_f
- Third, freeboard adjusted: $\widehat{h_f} = \delta h_{tiepoint} - h'_f$
- Lastly, tie points used to improve local ssh estimate: $h'_{ssh} = \overline{h_{25km}} - \delta h_{tiepoint}$

Data filtering

- R, G, S used to filter data: all samples with $G > 30$ (low SNR samples) removed, samples with $S > 60$ are not used (poor Gaussian fits), and $R > 1$ (saturated detector) are removed

Estimation of Local Sea Surface Height (i.e., tie points)

- For this section, $h'_f = \delta h_{tiepoint}$ and $\widehat{h_f} = 0$ → this is because estimated freeboard is detrended and the adjusted freeboard is equal to the change in tie point height
- Approach 1 (H_{op}):** same as Kwok et al. (2004, 2006) → identifying openings w/IS elevation profiles, then estimating age of openings w/RADARSAT → tie points selected from openings < 1 day old → Lebedev's parameterization tells us that the freeboard of this ice $< 2\text{cm}$ → low-reflectivity and low-elevation points selected visually, spurious jumps due to detector saturation omitted
 - They observe H_{op} and the 25-km stdev of detrended h'_f, σ_{f-25} , are linearly related, w/expected freeboard (which we said is equal to tiepoint height, $H_{op} = h'_f = \delta h_{tiepoint}$) $\sim 3X$ that of σ_{f-25} → this is used to derive Approaches 2 and 3



Approach 2 ($H_{\Delta R}$): low-reflectivity IS samples → ID ssh using low-reflectivity values and dips in elevation profile → basin-scale reflectivity of IS data is generally around $R=0.67$ —an expression of snow cover on the ice → so they find all samples where reflectivity is at least 0.3 lower than surrounding ice cover ($\Delta R > 0.3$) → they show that samples w/ $\Delta R > 0.3$ have a linear relationship btw h'_f and σ_{f-25}

- Mean differences btw H_{op} and $H_{\Delta R}$ are $-1.6 \pm 4.8\text{cm}$ in ON05 and $-4.0 \pm 5.6\text{cm}$ in FM06
 - Mean $H_{op} > H_{\Delta R}$ → expected as $H_{\Delta R}$ samples don't always contain the thinnest ice
 - Reasonably good, but slight underestimation of sea surface tie points up to 4cm

Approach 3: relation btw sea surface level and stdev of ICESat elevations ($\delta h_{tiepoint} = H_o$) → no reflectivity requirement, just elevation → samples selected where expected freeboard h'_f is $> 3X \sigma_{f-25}$

- Mean differences btw H_{op} and H_o are $-1.3 \pm 5.6\text{cm}$ in ON05 and $-3.1 \pm 5.8\text{cm}$ in FM06
 - Again, mean $H_{op} > H_o$ → expected as H_o samples don't always contain the thinnest ice
- Approach 1 provides the highest quality estimates of ssh, with the cost of more sparse sampling

Seasonal variability in freeboard

- They combine tiepoint estimates within IS segments → gives uncertainty of 6cm or better
- Mean and stdev of gridded freeboard are $27.5 \pm 15.5\text{ cm}$, seasonal increase in freeboard is 7.5cm
 - FYI mean $\sim 14.4\text{cm}$ w/increase of 12.4cm ; MYI mean $\sim 35.1\text{cm}$ w/increase of 8.5cm
- Mean stdev $\sim 3\text{cm}$ in both fall/winter datasets, indicating consistent freeboard retrievals
- IMBs estimate snow depth and SIT, which they use to convert to freeboard w/ p_s of Warren et al. (1999) and p_i , calculated two different ways
 - Freeboards from IS and IMBs within several cm of each other → they say "the level of agreement could be entirely fortuitous" → only 5 IMB point samples
 - Implies long correlation length scales of freeboard as IMBs are point measurements
- Changes in IS freeboard over MYI give good insights into changes in snow depth

Residual Sea Surface Height

- $h_{res} = h'_{ssh} - \widehat{h_{ssh}} = \overline{h_{25km}} - \delta h_{tiepoint}$ → a crude measure of errors in estimating ssh
 - Estimated ssh – the modeled ssh gives the residual
- Means $\sim 26\text{ cm}$ w/stdev of $\sim 22\text{-}23\text{ cm}$ for fall/spring
- Residuals thought to be largely due to geoid and mean dynamic topography

Summary/conclusions

- Best quality tie points from the new openings identified using IS and RADARSAT
- Intermediate quality tie points from (approach 2) comparing reflectivity of the samples w/that of the background ice and the expected deviation of these samples from the mean surface
- Worst quality: approach 3: tie points obtained via expected deviation of samples from mean surface
- Strength of approaches 2/3 for getting tie points is much more data w/no reliance on RADARSAT
- Preferred estimate of ssh created by weighted average of approaches 2/3
- Key to this paper: just know the three basic ways tie points are estimated (starred)

ICESat over Arctic sea ice: Estimation of snow depth and ice thickness

Kwok and Cunningham (2008)

Introduction

- Follow on from Kwok et al. (2004, 2006, 2007) → finally focusing on snow depth and SIT

Data/Methods

- IS data from ON05, FM06, ON06, and MA07
- QuikSCAT, SIM and SIC from AMSR-E, meteorological data from ECMWF
- WHOI moorings from Beaufort Gyre Observing System – operational since 2003

ICESat Freeboard

- Freeboards, and by extension SIT, estimated with all 3 tiepoint approaches: H_{op} , $H_{\Delta R}$, and H_o
- Reminder, $H_{\Delta R}$, and H_o underestimate freeboard because (a) IS elevations represent mean surface within footprint, thus lowest elevation surfaces contaminated by neighboring ice cover and (b) snow on thin ice increases elevation of tie point and leads to underestimated freeboard
 - No known correction for (a), but nominal adjustment applied to tie points based on their observed reflectivity → $R_{background} - R \rightarrow$ high $R =$ minimal snow adjustment added, low R (close to value of nearby sea ice surface) = snow adjustment (up to 5cm added to tiepoint)
 - This reduces biases a lot, especially for H_o which doesn't factor R in at all

Construction of Fields of Snow Depth

- They used ECMWF snow fall estimates (in SWE) instead of W99
- Ice parcels tracked along drift trajectories and accumulation is determined based on parcel's location within reanalysis grid cells → accumulation permitted if $2m \text{ temps} < \text{freezing} \& \text{SIC} > 50\%$
- Seasonally varying snow density (used w/SWE to get snow depth) from W99, but they shift early fall portion of the curve by 1 month → merges w/original climatology in late winter
- Initial MYI snow depth/density assumed to be the same as reported in W99
- Frost/rime deposition, sublimation, and wind redistribution of snow (most important) all ignored

Estimation of SIT

- Instead of estimating sea ice freeboard as difference btw total freeboard and snow depth (they are on different scales), they adjust snow depth to account for local freeboard variability
 - Especially important when freeboard < snow depth → no negative sea ice freeboards
- Effective snow depth taken to be a fraction of the total freeboard as defined by sigmoidal curve
 - "Our choice of this function is quite arbitrary"
- Unlike the previous papers (Kwok et al. 2006, 2007) SITs are compared across different seasons using a Lagrangian tracking to ensure ice types don't get mixed
- They find that variance in SIT explained mostly (>80%) by uncertainties in total freeboard and snow depth, with ice density explaining only 3-12% of variability

Comparison with ice draft from moorings

- To compare moorings (point data) with IS, they match the spatial length of IS by including mooring observations over the time where the ice has traveled 25 km
- Overall difference is $-0.21 \pm 0.42 \text{ m}$ w/correlation of 0.65 between the two populations

Ice Volume/Thickness for Two Winters

- Mean SITs around ~2-2.5m
- To estimate volume, they need to interpolated over polar data hole → they use MYI fraction as a proxy of local avg ice thickness → they compare MYI fraction from QuikSCAT with SIT in neighborhood of the hole
- SIV estimates across the four IS campaigns range from ~10,600-14,000 km³

Impressions

Not as technical as the previous few, but a good overview of the first lidar-derived basin-scale SIT and SIV estimates. The nominal snow depth adjustment was new compared to the previous papers. The sensitivity analysis section was very interesting, and I should apply this to my own work (see Table 1). Interestingly, they state that freeboard and snow depth explain >80% of the variance in SIT... which is not what later studies have found (I think; Alexandrov et al. 2010)? The comments about making sure data are on the same length scales (moorings and IS) was important. I need to consider this in my own work.

5.4. Sensitivity Analysis

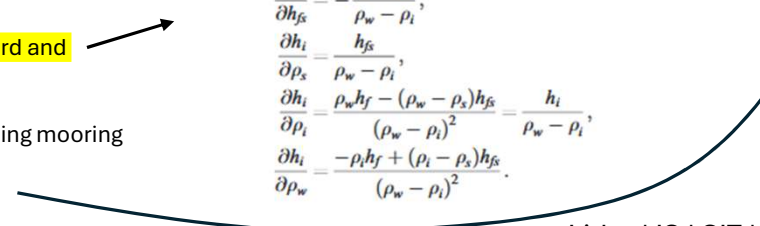
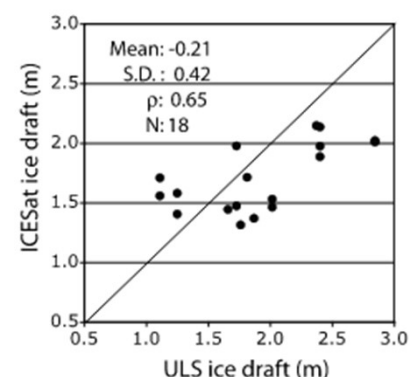
[42] At this point, it is useful to examine the uncertainty in the thickness estimates, h_i , associated with uncertainties in the five variables (h_f , h_{fs} , ρ_w , ρ_i , ρ_s) in equation (4). Assuming that the variables are uncorrelated, the sensitivity of the thickness estimates can be evaluated according to the following expression:

$$\sigma_{h_i}^2 = \sigma_{h_f}^2 \left(\frac{\partial h_i}{\partial h_f} \right)^2 + \sigma_{h_{fs}}^2 \left(\frac{\partial h_i}{\partial h_{fs}} \right)^2 + \sigma_{\rho_w}^2 \left(\frac{\partial h_i}{\partial \rho_w} \right)^2 + \sigma_{\rho_i}^2 \left(\frac{\partial h_i}{\partial \rho_i} \right)^2 + \sigma_{\rho_s}^2 \left(\frac{\partial h_i}{\partial \rho_s} \right)^2, \quad (6)$$

where

$$\begin{aligned} \frac{\partial h_i}{\partial h_f} &= \frac{\rho_w}{\rho_w - \rho_i}, \\ \frac{\partial h_i}{\partial h_{fs}} &= -\frac{\rho_w - \rho_s}{\rho_w - \rho_i}, \\ \frac{\partial h_i}{\partial \rho_s} &= \frac{h_{fs}}{\rho_w - \rho_i}, \\ \frac{\partial h_i}{\partial \rho_i} &= \frac{\rho_w h_f - (\rho_w - \rho_s) h_{fs}}{(\rho_w - \rho_i)^2} = \frac{h_i}{\rho_w - \rho_i}, \\ \frac{\partial h_i}{\partial \rho_w} &= -\frac{\rho_i h_f + (\rho_i - \rho_s) h_{fs}}{(\rho_w - \rho_i)^2}. \end{aligned}$$

c) Overall Differences



Lidar | IS | SIT | SIV | ECMWF | Tie points | SSH

Five years of Arctic sea ice freeboard measurements from the Ice, Cloud and land Elevation Satellite

Farrell et al. (2009)

Introduction

- IS coverage $\sim 86^\circ\text{N}$; before IS, radar altimetry from ERS-1 and ERS-2 satellites were limited to $\sim 81.5^\circ\text{N}$ which means that IS gets 15% more coverage over sea ice during winter max
- First study to look at freeboards over full 5 years of the IS mission
- This study also presents new method of ssh retrieval distinct from Kwok et al. (2007)

Data

- IS data from 11 campaigns spanning Feb-Mar (one is Mar-Apr) and Oct-Nov from 2008 to 2008
- GLA06 Global Elevation Data Product for elevation, reflectivity, and saturation range correction
- GLA01 Global Altimetry Data Product for waveforms (T_x and R_x)/detector gain/received energy
- MODIS visible imagery w/resolution of 250m and imagery every $\sim 1\text{-}2$ days
- SSM/I SIC used for sea ice mask to get IS data over sea-ice covered regions of Arctic

Data Filtering

- Only consider regions w/SIC $\geq 35\%$ \rightarrow removes MIZ data, accounts for less than 5% total data
- Elevations deviating from geoid by more than 5m omitted
- Discard terms w/reflectivity > 1 (these waveforms likely due to detector saturation)
- Discard terms w/detector gain > 30 counts

Detecting Sea Surface Elevations and Measuring Freeboard

- Surface elevation anomalies, h_a , calculated: $h_a = h_{alt} + \Delta h_{IBC} + \Delta h_{sat} - h_g$ \rightarrow where h_{alt} is the altimetry elevation measurement, Δh_{IBC} is the IBE correction, Δh_{sat} is saturation range correction and h_g is the geoid (which is subtracted off)
- Lead detection algorithm here differs from Kwok et al. (2007) as it uses a combination of 6 IS parameters to ID leads, whereas Kwok uses ~ 1 in each of his 3 approaches
 - This study uses elevation, reflectivity, gain, and properties of the waveform
- Waveform properties computed: peak power and FWHM of T_x and R_x
 - Parameter 1: $\Delta\text{fwhm} = R_x\text{ fwhm} - T_x\text{ fwhm}$
 - Parameter 2 (skewness of waveforms): $\Delta\text{skew} = R_x\text{ skew} - T_x\text{ skew}$
 - Parameter 3: cross correlation of R_x and T_x $\rightarrow 1$ indicates perfect Gaussian for both
- Breakdown of what the six parameters tell us: (1) reflectivity is low (high) for leads (sea ice/snow), (2) cross correlation indicates reflection from smooth/rough topography, (3) gain indicates cloud-free returns, and (3-6) $\Delta\text{fwhm}/\Delta\text{skew}/R_x\text{ fwhm}$ indicate presence or lack of waveform broadening due to surface topography or atm forward scattering
 - Leads have low reflectivity, high cross correlation, low gain, and similar waveform parameters for R_x and T_x
- MODIS used to ID leads and then IS parameter ranges selected based on these data
- SSH calculated by averaging elevations associated w/leads over 35-km along-track search range
- Freeboard estimated: $h_f = h_a - h_{ssh}$
- Reflectivity alone is not a great estimator of local sea surface height

Arctic Freeboard

- Mean freeboard grew by 4.2cm, 10.2cm, 9.9cm, 9.1cm, 6.7cm over the 5 winter seasons

- Bimodal SIT distributions for the early fall campaigns, clearly showing FYI vs MYI, but this is not as apparent in the later fall campaigns (indicating thinning) or in winter
- Autumn (winter) mean freeboard trend is -1.8cm/yr (-1.6 cm/yr) with $R^2 = 0.86$ ($R^2 = 0.59$)

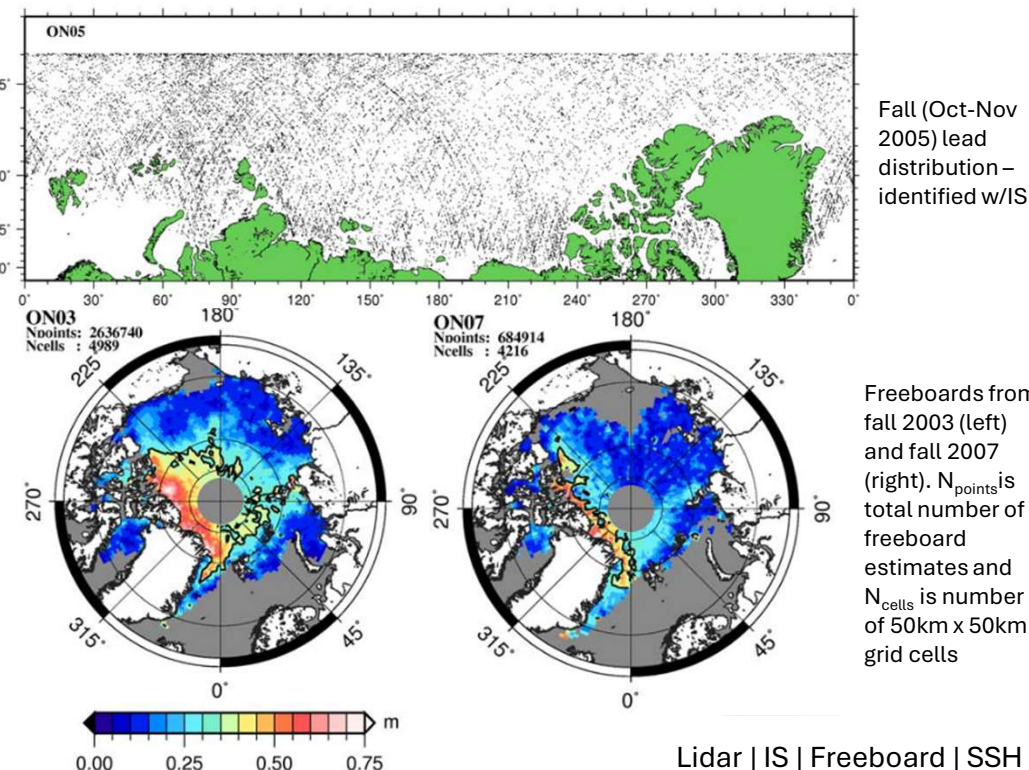
- Seasonal mean freeboards: fall = 26 cm and winter = 35cm

Conclusions

- Average $\sim 8\text{cm}$ increase in freeboard from autumn-winter
- Fall 2007/winter 2008 mean freeboards below seasonal avg by -4.5cm and -6.8cm , respectively
- 5-year period too short to determine whether freeboard changes are due to internal variability or anthropogenically forced change

Impressions

SSH estimation makes a lot of sense and seems robust compared to earlier studies (e.g., Kwok et al. 2007). Good overview of how freeboard is calculated.



Arctic sea ice freeboard from IceBridge acquisitions in 2009: Estimates and comparisons with ICESat

Kwok et al. (2012)

Introduction

- Giles et al. (2007) provided first analysis of coincident lidar and radar over sea ice, showing that they could be combined to estimate snow depth
- The first study demonstrating large-scale operational use of OIB ATM

Data

- ATM is conical-scanning lidar at 532nm and off-nadir incidence angle of 15°
 - Across-track scan swath of 250m, near center of swath the footprints are ~1m and spaced ~3-4m in the along and across track directions
- ATM campaigns flown 31 March, 2 April, 5 April, and 21 April 2009
- CAMBOT aerial photos along ATM swaths used to help w/lead ID
- IS data from 9 March through 11 April → freeboard derived using Kwok et al. (2007) and Kwok and Cunningham (2008) procedures
- QuikSCAT for MYI area/regions

Data Analysis

- Elevation estimated based on location of leading edge at 75% of waveform peak (i.e., a TFMRA)
 - Due to this, the estimated range is surface reflectivity or signal strength dependent
 - Weaker signal, retracking displaced more towards peak → increased range to sea surface → leads to overestimated freeboard
 - Polynomial fit to data and used to correct signal-dependent biases
- Leads determined with apparent reflectivity, R, only → validated w/CAMBOT imagery

Steps to ID sea surface reference samples

- Remove cloud-contaminated samples
- To select samples suitable for use as sea surface segments, elevation distributions of consecutive 250m ATM segments are compared to elevation distribution of local 30km segment
 - 30km segments used as measures of elevation for larger ice-only surface
 - Multiple modes are ID'd in the 250m distribution, then the mode w/lowest elevation that is at least 1 RMS standard deviation below 30km segment mode is selected
- Select candidate elevation samples in neighborhood of designated mode that was selected^
- Filter out candidate elevation samples with $R \geq 0.25$

Estimation of sea surface height profile

- $\tilde{h}_{ssh}(x) = h_{ATM}^{50km}(x) - \bar{h}_f(x)$ → they assume h_{ATM}^{50km} is a close replica of the residual sea surface and thus a good estimate of the local sea surface profile because most of the small-scale variability due to ridges/leads has been averaged out and the remaining variations are due to slowly varying changes in mean freeboard and residuals in sea surface
 - Then, by subtracting off the mean freeboard, you can get a good estimate of the local ssh
- Mean freeboard, \bar{h}_f , is estimated as weighted mean of diff btw 50km running mean of ATM profile and mean height of tie points along 200km segment → \bar{h}_f is updated every 250m

Results

- Overall difference btw ATM and IS freeboards are $0.7 \pm 8.5\text{cm}$ with an $R = 0.78$
- Mean variability of tie points is ~8cm
- ATM freeboard estimates over regions of high MYI are larger as the observations can capture more of the deformational features rather than IS which gets a broader average over the region
- Short-scale variations in ssh driven by residual undulations in the geoid

Impressions

Main takeaway is the close agreement between IS and OIB ATM. Description of ssh retrieval procedure is quite technical. Fair amount of discussion about corrections applied to ATM data.

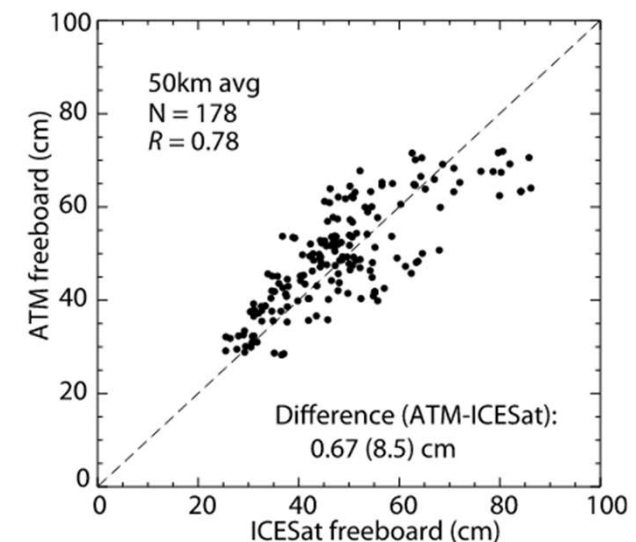


Figure 10. Comparison of ATM and ICESat derived freeboards from the four transects (50 km averages).

Interesting approach;
makes sense

The ICESat-2 Laser Altimetry Mission

Abdalati et al. (2010)

Background

- IS: ~65m footprint diameter, footprints every ~172m, elevation prevision and accuracy of ~2cm and ~14cm per shot, respectively.
 - GLAS had three 1064nm lasers, and a frequency doubler in the beam path that converted portion of main 1064nm beam to 532nm to get better atm measurements
 - 3rd laser was the only one that really survived

ICESat-2 Mission Objectives

Ice Sheets

- Science Definition Team determined that IS2 must be capable of resolution of winter/summer elevation change to 2.5cm at subdrainage basin scales ($25 \times 25 \text{ km}^2$), annually resolved changes of 25 cm/yr on outlet glaciers (100km^2) areas, and annually resolved elevation changes of 25 cm/yr at outlet glacier margins (along linear distances of 1km)

Sea Ice

- The primary measurement driver for sea ice is precision (i.e., consistency of retrievals btw adjacent pulses) rather than accuracy → because estimating SIT requires scaling of freeboard by ~10X, small errors in precision can translate to large errors in SIT
- 3cm precision in freeboard is the minimum required capability, corresponding to ~0.3m in SIT and an overall uncertainty of better than 25% of the current annual SIV production in the Arctic
 - Allows for determination of spatial ranges in SIT in Arctic (2-4m) and Antarctic (2-3m) as well as resolving seasonal cycles of growth melt (amplitude of ~1m)

Vegetation

- Goal is to get vegetation height surface within 3m accuracy at 1-km spatial scale

ICESat-2 Mission Considerations

- Goal is to match IS w/91-day repeat orbit with a 94° inclination at 600km altitude
- IS2 will point to RGTs to within 30m (1σ) to minimize separation btw observations along each repeat pass
- Reducing FOV can reduce forward scattering biases since more of the scattered photons are outside the smaller FOVs
- 5-year minimum mission duration

- 50 Hz PRF and 50mJ of laser energy thought to be sufficient to reduce stress on lasers

Mission Status

- At time of writing, mission is in Phase A which is preliminary design and project planning
- Initial launch planned for 2015

Mission Configuration Options

- Both IS and IS2 are not sun-synchronous, thus they complete a series of 90° yaw maneuvers twice a year to maintain sufficient surface illumination of the solar panels
- With one beam, you can't determine the surface slope w/o multiple passes (~around 5), which motivated the science team to explore the (a) multibeam option and (b) the micropulse option

- The multibeam approach (which they eventually went for) is limited by the amount of laser energy available
- The micropulse approach was to use one beam with its output split into many beams
- Traditional analog pulse laser has more history, micropulse is a more novel approach

Conclusions/Impressions

- Since the time of the paper acceptance, the science team opted to use the micropulse lidar with no analog central beam as the implementation approach for IS2

This was a first look at IS2 and what it could be in the early stages of its development.

Science Goals	Science Requirements	Measurement Requirements	Instrument Functional Requirements	Mission Functional Requirements
Ice Sheets Quantify polar ice sheet mass balance to determine contributions to current and recent sea level change and impacts on ocean circulation	Annual elevation change of 0.2 cm/yr over entire ice sheet Surface elevation change of 25 cm/yr annually in 100 km^2 areas and along linear distances of 1 km	Ability to penetrate optically thin clouds Precise repeatability of ground tracks	4.5 m pointing knowledge 5 years continuous operation with 7-year goal	Orbit parameters comparable to those of ICESat (600 km altitude; 94 deg. incl., 91-day repeat). 10 arcsec (30-m) pointing control
Determine seasonal cycle of ice sheet changes	Resolve winter and summer ice sheet elevation change to 2.5 cm over $25 \times 25 \text{ km}^2$ areas	Repeat sampling 4x per year, uniformly spaced in time	Measurement capability in the cross-track direction within the vicinity of the primary beam	1.5 arcsec (4.5-m) pointing knowledge
Determine topographic character of ice sheet changes to assess mechanisms driving that change and constrain ice sheet models	Continuous observations through for at least 5 years Direct comparability to ICESat-1 measurements for 15-year dh/dt	Continuous measurements for no less than 5 years	Surface reflectivity capability of 5% to enable characterization of snow conditions for gain and range corrections	2 cm radial orbit accuracy requirement 5 year continuous operation with 7-year goal
Sea Ice Estimate sea ice thickness to examine ice/ocean/atmosph ere exchanges of energy, mass and moisture	Discriminate freeboard from surrounding ocean level to within 3 cm Capture seasonal evolution of sea ice cover on $25 \times 25 \text{ km}$ scales	Vertical precision of <2 cm between leads and sea ice freeboard height Monthly near-repeat coverage of Arctic and Southern Oceans at $25 \times 25 \text{ km}$ scales Coverage up to at least 86 deg. latitude	Telescope FOV of 100 m (160 µrad) or better to minimize atmospheric forward-scattering effects Atmospheric vertical resolution of 75 km to enable atmospheric corrections plus studies of clouds	91 day repeat orbit to capture seasonal effects and maximize comparability to ICESat for trend detection

Lidar | IS2 | Science requirements | Mission overview

Spacing between ascending and descending grounds tracks in ICESat's 91-day, 94° inclination, 600km altitude orbit. You get closer RGTs near the poles with higher orbital inclination.

Geodetic Latitude (deg)	Track Spacing (km)
0	29.60
5	29.48
10	29.14
15	28.58
20	27.80
25	26.81
30	25.61
35	24.22
40	22.64
45	20.89
50	18.99
55	16.94
60	14.76
65	12.47
70	10.09
75	7.64
80	5.12
85	2.57

Refining the sea surface identification approach for determining freeboards in the ICESat-2 sea ice products

Kwok et al.(2021)

Introduction

- Classification algorithm for discriminating surface type of a height segment in IS2 data utilizes photon rate (r_{surf}), width of photon distribution (w_s), and background rate (r_{bkg})
 - Photon rate (photons/shot) is the average # of detected surface photons divided by the # of laser shots required to construct a 150-photon aggregate → proxy for reflectivity
 - Gaussian width (w_s) of height distribution provides a measure of surface roughness
 - Background rate (r_{bkg}) → the solar background count rate (B_s) is the solar zenith radiance due to solar energy scattered by the surface/atm and this provides a useful reflectance measure for surface identification → usefulness varies seasonally w/sun angle
- Specular and smooth dark leads used as candidate height samples to estimate sea surface reference heights → this was the approach in R001 and R002 of the data
- Beam 3 is weaker than Beam 1 and 5 (yes, the strong beam) → this was intentional/expected

Data

- IS2 ATL07 and ATL10 products → strong beams only
 - In ATL07/10 leads identified within 10km along-track sections for each beam
 - ATL10 freeboards provided where SIC > 50% and samples are at least 25 km from coast
- CAMBOT imagery from spring 2019 OIB campaign

Ice-water discrimination

- In R001 and R002, each height segment is assigned a surface type: specular, dark lead (smooth), dark lead (rough), gray ice, snow-covered ice, rough, and shadow → primary purpose of these classifications is to ID usable sea surface height samples
- Post-classification (using r_{surf} , w_s , and r_{bkg}), upper and lower bounds of heights provided for smooth surfaces ($w_s < 0.13\text{m}$) and data is further filtered
- For each lead, ssh is calculated as weighted (w/distance) sum of selected height samples
 - Estimates from individual leads combined to obtain sea level reference on 10km track
- Fixed # of photons use in surface finding, thus photon rates are determined by the number of shots (or along-track distance) needed to construct 150-photon aggregates
 - Height segments longer when returns are lower (e.g., dark leads, mode ~60m) and shorter when returns are higher (smooth, specular/quasi-specular leads, mode ~27m)

Effect of clouds on leads with low surface reflectance

- Clouds reduce photon rates bc energy is scattered away from lidar → leads to misclassifications
- Areas like refrozen leads may have low surface reflectance, exacerbated by cloud cover, so this surface may be classified as a dark lead due to a dip in photon rates
 - This is then averaged with other leads and inflates the avg reference sea surface because this “dark lead” is really refrozen ice → this leads to net decrease in total freeboard
- Why are cloud flags not used? IS2 cloud flags are sampled every 400m and not compatible with the size of the leads used here (~27-80m)
 - Cloud flags are also conservative, so a large number of leads would be removed if the clouds flags were used to filter returns

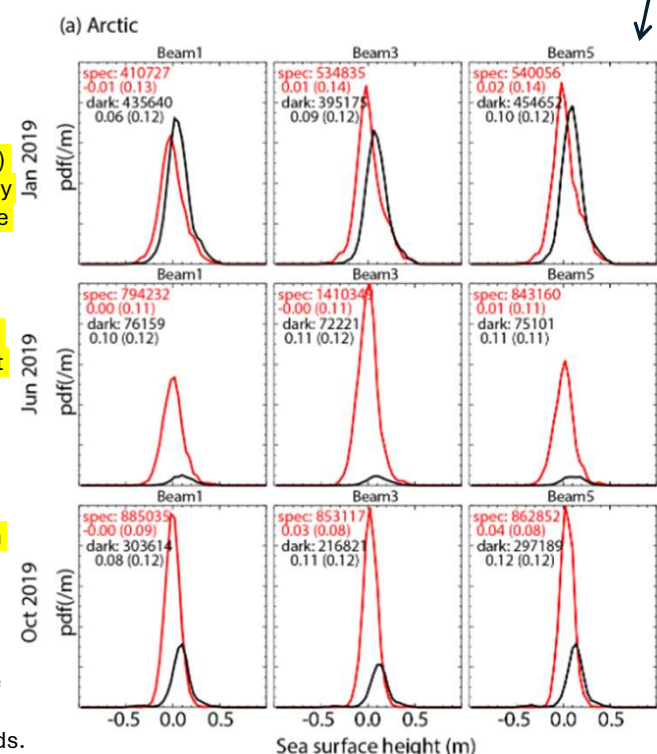
Sea surface height distribution of specular and/or dark leads

- Sea surface distributions derived using specular and dark leads overlap, although the mean of the dark leads is higher by up to 10cm and the modes are skewed relative to each other
 - Differences in the tails of distributions quite distinct
 - This provides (indirect) evidence that the height distribution of dark leads is contaminated by incorrect classification of the surface
- The population of sea surface height segments classified as specular leads >> dark leads, except for Jan 2019 in Arctic, meaning the impact of dark leads is not as significant

They proposed using a contrast ratio $R = \frac{PR_{max}}{PR_{dark\ lead}}$ between the photon rate of dark leads and the height segment w/highest photon rate → could help address cloud misclassification issue

An algorithm revision: R001 and R002 to R003

- In R003, only specular surface returns are used to derive reference sea surface
- The impact of this change is: (a) area coverage has decreased by ~10-20% due to fewer reference ssh estimates, (b) means have increased by 0-4cm



Conclusion/Impressions

- Photon rates attenuated due to clouds which leads to incorrect classification of dark leads
- Sea surface heights over dark leads biased high, causing freeboards to be biased low
- Cloud flags are of insufficient resolution to be used in the sea ice data products
- R003 no longer includes dark leads – only specular leads for reference sea surface height

Important to understand the issue with dark leads and how misclassification biases freeboards. Good background on surface type classification in this paper.

Lidar | IS2 | SSH | Dark leads | Clouds

Mapping Sea Ice Surface Topography in High Fidelity with ICESat-2

Farrell et al. (2020)

Introduction

- Goal of paper is to demonstrate that IS2 can resolve fine-scale sea ice properties

Data

- IS2 ATLAS Release 003 Level 2 ATL03 product –geolocated photons w/accuracy of 0.05m in vertical direction and precision better than 0.13m
 - They also use Release 002 Level 3 ATL07 sea ice heights
- IS2 estimates validated w/OIB ATM under flights in April 2019 and Sentinel-2 visible imagery
- IS2 footprints are ~12m every ~0.7m along-track vs. ~50m footprint and ~172m spacing between shots w/IS

Surface roughness and pressure ridges

- For all fine-scale features, not just surface roughness, the background noise was removed – only photons between 15th and 85th percentile of per-shot height distribution included
- Surface roughness, σ_h , is stdev of ATL07 sea ice heights within 25-km-long segments
- Pan-Arctic $\sigma_h = 0.18\text{m}$, with BG seasonal ice $\sigma_h = 0.15\text{m}$ and north of CAA $\sigma_h = 0.30\text{m}$
- UMD-RDA w/ATL03 used for ridge ID
 - UMD-RDA retains 99th percentile of photon height distribution for 5-shot aggregate
 - Ridge sails defined as any local maxima occurring 0.6m above local level ice surface
- Ridge width is along-track distance btw minima or point(s) at which elev drops below threshold height
- Avg sail height, h_s , of 1.5 m for 9 ridges north of CAA – OIB estimates ~1.6m so good agreement
- ATL07 can accurately ID ridges over MYI (struggles over smoother FYI), but h_s is underestimated considerably compared to UMD-RDA
- Ridges north of CAA 2.5X more frequent and on avg 0.28m (0.25m) taller in mean (modal) h_s

Melt ponds

- Small-scale pond features, ranging ~60–280m wide, aren't captured by ATL07
 - So, they develop University of Maryland-Melt Pond Detection Algorithm
- UMD-MPA estimates pond depth, h_{mp} , w/2D histogram → ponds occur where bimodal distribution exists w/primary mode close to mean segment elevation (i.e., pond surface) and secondary mode below water surface (i.e., ice surface) → h_{mp} calculated by estimating pond bottom elev from surface elev
 - Refraction correction applied to photons due to photons traveling through water

Melt pond depths ranged from 0.04–2.4m, w/modal (mean) depths of 0.35m (0.80m)

Floe Size Distribution and Lead Frequency

- IS2 over leads has a mean of zero and a stdev of 0.009m, a 50% improvement compared to IS which had precision of 0.02 over leads
- Leads defined as level ice surfaces w/≥15 contiguous retrievals within 0.1m of local reference surface and a stdev of ≤0.01m

- Average (median) lead width of 235 m (71m) and 75% if leads were <200 m wide
 - ~28% of IS2 data was leads, close w/Sentinel-2 open water fraction of ~25%
- Floes averaged 479m and 75% were <600 m wide

Discussion

- Sea ice features as narrow as 7.1m can be detected**
- Floe-scale freeboards can be retrieved w/IS2
- The ability to observe fine-scale features provides important information on deformational changes in ice that previous altimeters haven't been able to resolve → so now we get thermodynamic + dynamic changes
 - Essential for climate modelers (e.g., think surface drag)

Impressions

The methodology is the most useful part of this paper. Specifically, how they ID features like ridges, how they compute surface roughness, etc...

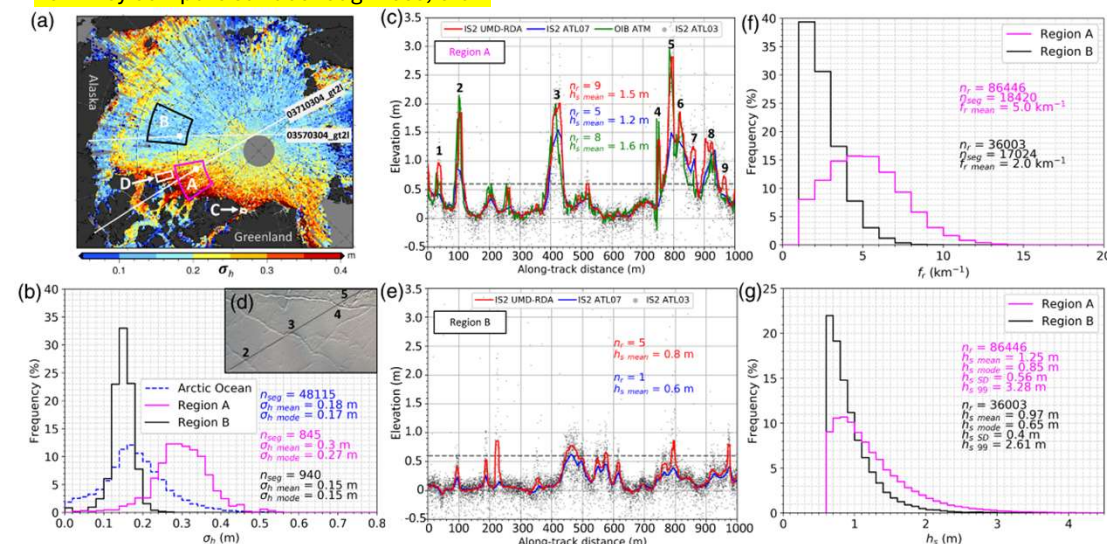


Figure 1. Arctic sea ice roughness and pressure ridge characteristics prior to melt. (a) Ice surface roughness (σ_h) in April 2019 derived from ICESat-2 ATL07, mapped at 1/8°. A–D indicate sites of detailed analyses described in the text. (b) Distributions of σ_h for the Arctic Ocean (blue dashed line) and Regions A (magenta line) and B (black line), as outlined in (a). (c) The 1-km-long transect of sea ice elevation within Region A (at white dot) on 22 April 2019, derived from the UMD-RDA (red line), ATL07 (blue line), and ATL03 (gray dots) ICESat-2 products and OIB ATM lidar data (green line). Distinct ridge sails are numbered. (d) Coincident OIB image of Region A transect, where numbered features correspond to sails detected in (c). (e) Same as in (c) but for transect in Region B (at white dot). Note that coincident OIB data were not acquired for this transect. (f) Ridge frequency (f_r) in Regions A (magenta line) and B (black line). (g) Same as in (f) but for sail height (h_s).

Lidar | IS2 | Surface topography | ATL03 | UMD-RDA

Detection of Melt Ponds on Arctic Summer Sea Ice from ICESat-2

Tilling et al. (2020)

Introduction

- At time of writing, melt ponds not classified in IS2 estimates of freeboard and melt ponds are separated by leads using a height filter

Data

- Each IS2 pulse emits $\sim 10^{14}$ photons and around 7 return to detector for a typical snow-covered surface w/clear skies
- After a photon is received at each independent timing channel, (16 for each strong beam, 4 for each weak beam), there is a dead time where ATLAS is effectively blind to additional incoming photons
 - Therefore, the ATLAS detector saturates if a pulse returns 16+ photons within a time less than the dead time interval which is generally around 3.2 ns (0.5m gap appears in height retrievals)
- IS2 ATL03, ATL07, and ATL10 Release 3 all used in this study
- IS2 ATL07 aggregates 150 consecutive signal photons, lowering measurement precision to $\sim 2\text{cm}$ over flat surfaces \rightarrow segment resolutions average $\sim 30\text{m}$ for strong beams and $\sim 75\text{m}$ for weak beams
- ATL07 and ATL10 segments classified based on backscatter signal, differing over summer/winter
- WorldView-2 scenes captured over Arctic Ocean ($\sim 2\text{m}$ res), Sentinel-2 scenes over CAA ($\sim 10\text{m}$ res)

Methods

- IS2 beams slightly off-nadir, so true specular returns will not occur (hence term “quasi-specular”)
- Number of photons returned per pulse (N_{photons}) for medium and high confidence photons used to quantify the reflectivity of IS2 returns
 - Quasi-specular returns defined as $N_{\text{photons}} \geq 16 \rightarrow$ full or near-full sensor saturation
 - Photons from diffuse pulses ($N_{\text{photons}} < 16$) grouped in 50-photon aggregates to represent sea ice surface

- Smooth leads filtered out using height filter along each image scene
 - Pond segments defined as specular segments where mean photon height is greater than the 20th percentile of all segment heights along-track, all other specular segments are leads

ICESat-2 Photon Scattering Behavior Over Melt Ponds

- Saturation of sensor evident by gap in ATL03 photon heights of $\sim 0.5\text{m}$
- Over 4 larger ponds (Sentinel-2), IS2 reflectivity increased in ¼, but pulses only specular across full length of one pond
 - Lower reflectivity attributed to higher water surface roughness from wind disturbance or a skim of new ice formation \rightarrow so algorithm has some limitations when not perfectly specular
- For 2 of 4 ponds, underlying ice bathymetry is detectable along w/surface \rightarrow there is inconsistency in which of these two dominate the IS2 return
- If there is any surface roughness or thin ice, then it will be hard for IS2 to get returns from the melt pond base
 - Two distinct surfaces also only visible when pond depth > the $\sim 20\text{cm}$ pulse width
- They note that melt pond depth can only be retrieved (Farrell et al. 2020) when water and underlying ice surfaces are both visible

Complications in ICESat-2 Melt Pond Height Retrievals

- Two main sources of bias in height retrievals over melt ponds: (a) small number of signal photons used compared to nominal 150-photons aggregated in ATL07, and (b) when detector is saturated, photons aren't recorded during the dead time and therefore heights will be biased high towards the leading edge of the return
 - They conclude that their height estimates for specular pulses are biased high
- ATL07 assumes a Gaussian surface height distribution of signal photons along a segment, so over melt ponds this fails and not ATL07 data are produced
 - Due to these inconsistencies in surface type classification, summer ATL10 data are also not likely to be representative of the true freeboard

Conclusions/Impressions

- This paper developed the first algorithm to detect individual melt ponds on summer sea ice from satellite altimetry \rightarrow Farrell et al. (2020) came out one month before w/UMD-MPDA
- Important to note that the algorithm here can only detect specular melt ponds, not diffuse
- Data/Methods description of IS2 was very informative

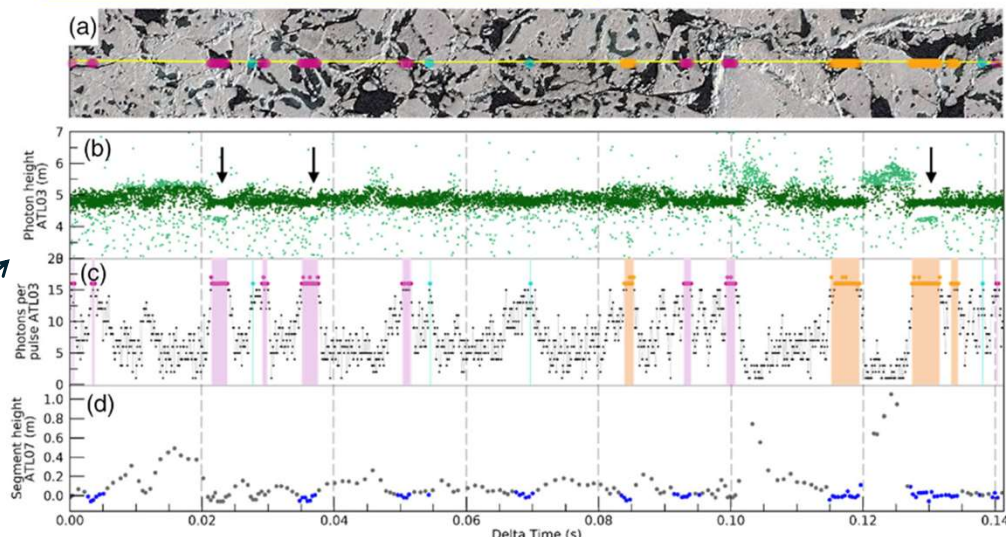


Fig. 1. (a) WorldView-2 images overlaid w/IS2 track and the location of specular pulses; melt pond (pink), drained pond/lead (orange), and ambiguous (turquoise). (b) IS2 photon heights, black arrows show effects of detector deadtime, (c) N_{photons} , (d) ATL03 heights for sea ice/pond mixture (grey) and leads/ponds (blue).

Lidar | IS2 | Melt ponds

Observing the evolution of summer melt on multiyear sea ice with ICESat-2 and Sentinel-2

Buckley et al. (2023)

Introduction

- Goal of paper is to build on studies like Perovich and Polashenski (2012) to look at melt pond evolution, but using altimetry to get pond evolution on a basin-scale

Study period and region

- Study period—2020 melt season where SATs were 2.1°C about 1981–2010 mean
 - Specifically, between 1 June and 15 September (begins pre-melt onset and ends at SIE min)
 - This led to second last September SIE on record
- Study region is north of CAA/Greenland → strong overlap w/the last ice area

Satellite imagery

- Sentinel-2 having two satellites, A and B, gives global revisit time of less than 5 days and 10m res
- WorldView-2 and WorldView-3 have resolutions of 1.85 and 1.24m, respectively → 18 images used
- Image classification: (1) near-IR band used to differentiate water/ice (NDWI), (2) pixels classified as water are further separated into open-water or melt pond pixels following approach of Buckley et al. (2020), (3) non-water pixels classified as ice if passing a threshold in red band

Satellite altimetry

- IS2 ATL03 → only strong beams used
- Two algorithms used to estimate melt ponds depth: UMD-MPA from Farrell et al. (2020) and density dimension algorithm (DDA) (Herzfeld et al. 2017, 2023)
 - Robust descriptions of these algorithms on page 6 – refer to if ever curious/necessary

Results

- MPF peaked at $16\% \pm 6\%$ on 24 June 2020 in Sentinel-2 imagery
 - By August, MPF < 5% for remainder of the season
- SIC >90% through June, but drops below 80% in late July as ice pack diverges from landfast ice
- Strong correlation ($r=0.77$) btw UMD-MPA and DDA derived pond depths
 - Stdev of residuals was 0.22m, which is substantial, despite mean residual diff of -0.4m
 - For both, median pond depths <50cm until mid-June when they slowly increase through July
- Freeze onset in August causes ponds to form ice lids which limit IS2 penetration
- ATL07 tracking over melted sea ice surface is very inconsistent compared to UMD-MPA and DDA
- Pond area is max in June (227 m^2) and min in early September (55 m^2)
- Image resolution strongly influence MPF calculations: Sentinel-2 MPF is 7.6% versus 25.5% from WorldView → also, SIC is 6.2% higher in Sentinel-2 than WorldView
- Approx ~73% of individual ponds not captured by Sentinel-2 due to spatial res, but this is only 38% of pond area in WorldView → i.e., Sentinel-2 is able to capture about 62% of total pond area
- As melt season progresses and more fine-scale features appear, Sentinel-2 performs worse compared to WorldView
- MPF can be biased low in Sentinel-2 results by up to 20.7% and averaging 7.2% when small ponds are widespread across the surface
- About 83% of total ponded area is made up of ponds w/area smaller than UMD-MPA minimum resolvable size (314 m^2), versus 14% for DDA minimum resolvable size (44 m^2)

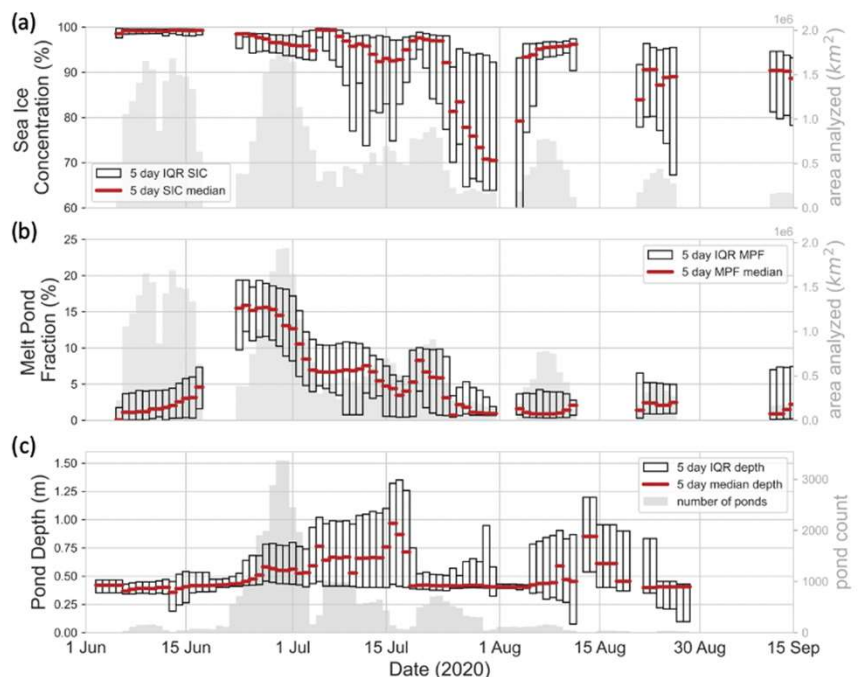
- DDA is automated, UMD-MPA is not → DDA gets more data bc it doesn't rely on cloud flag

Discussion

- Rapid increase in MPF in mid-June from 5%-20% in just a few days
- These algorithms are limited to min pond depths for observations, so estimates biased high
- Consistent w/MOSAiC and Polashenski et al. (2012), this study shows no simple relationship between pond depth and fraction → CESM uses a simple relationship to parameterize

Summary and Conclusions

- UMD-MPA biased high as it favors large pond (due to spatial res)
- DDA seems to be superior to UMD-MPA for a variety of reasons, including # of data, automation, and ability to resolve smaller ponds, etc..
- Pond classification strongly limited by spatial resolution of optical imagery
- Tracking pond evolution on FYI harder bc ponds are shallower and IS2 products limited by pulse width (0.2m)



Lidar | IS2 | Melt ponds | UMD-MPA | DDA

Linking scales of sea ice surface topography: Evaluation of ICESat-2 measurements with coincident helicopter laser scanning during MOSAiC

Introduction

- Paper goals: (1) validate ATL07 product, (2) see how surface roughness in ATL07 is related to height estimates, (3) quantify the degree to which true dimensions of sea ice surface topography, given by an airborne laser scanner (ALS) can be captured by IS2 products

Methods and Data

- ALS operating at 1064nm onboard helicopter that took off from RV Polarstern
 - Helicopter followed IS2 center-beam-pair ground track for ~130km achieving an overlap of 97km for strong beam and 117km for weak beam
- Elevations from ALS linearly interpolated to 0.50m (30 sec) grid
- IS2 center-beam pair used, ATL07 product, UMD-RDA w/ATL03 for ridge detection
 - For ATL07, 150-photon aggregates are (a) binned, (b) filtered to remove photons outside 2σ , and (c) then histogram is fit using dual-Gaussian mixture distribution and surface height is estimated from this fitted distribution
- Co-registration of IS2 and helicopter ALS: polygons created for each ATL07 segment w/13m width (conservative estimate of IS2 footprint size + geolocation uncertainties), ALS co-registration is completed every 30 sec (each 0.5m grid cell) w/correlation based drift correction
 - Drift correction – drift ~0.01-0.02 m/s, which can lead to max displacement of 70m over an hour → they correct based on correlation btw ATL07/ALS elevations
- “ATL07 seg” = co-registered ATL07; “ALS seg” = co-registered and segment-averaged ALS, and “ALS full” is the non-averaged, but co-registered ATL data

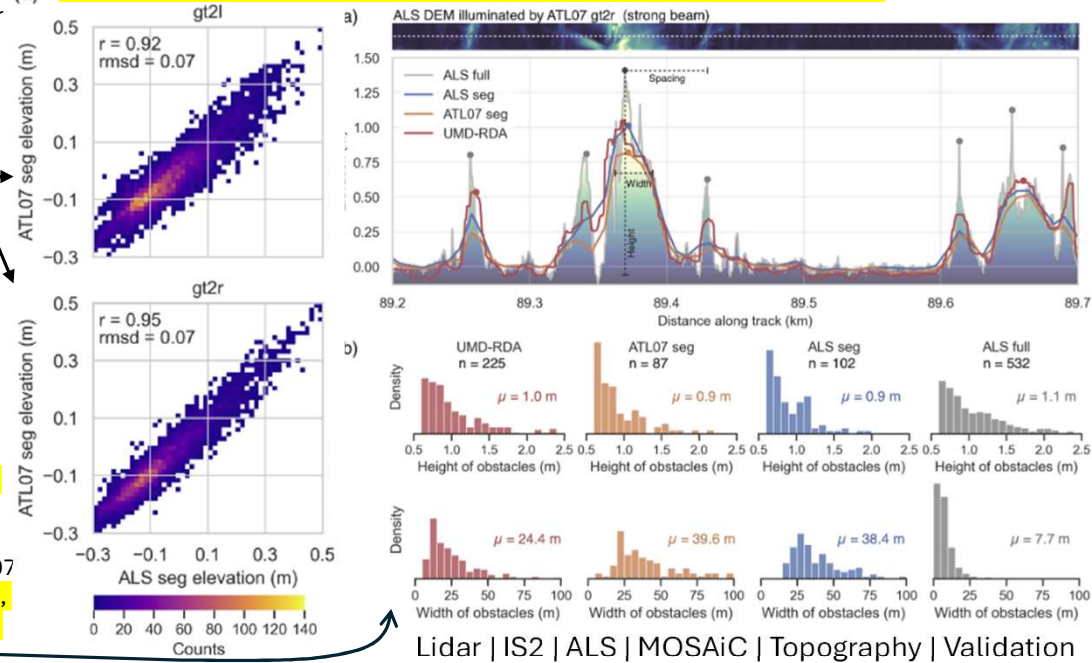
Results

- ATL07 and ALS elevations agree overall, however gt2r has higher dynamic range than gt2l
 - Correlations btw ALS and ATL07 gt2r (gt2l) are 0.95 (0.92), w/RMSEs of 0.07 for both
- ALS stdev compared w/ATL07 segment histogram width indicates how well individual photon heights can reproduce the surface roughness – correlations of 0.87 for gt2l and 0.88 for gt2r
- Over smooth ice, mean and stdev of ATL07 and ALS agree within ~1cm for both beams
- Over rough ice, mean within-segment differences are ~10cm (~30cm) for the strong (weak) beams and standard deviations differ by ~13cm (strong beam) and ~80cm (weak beam)
- Looking at distribution of roughness estimates in all segments, it is evident that using ATL07 heights to estimate roughness can miss extremely smooth (<10cm) and extremely rough (>40cm) ice, resulting in more moderate (10-30cm) roughness values
- Only one (zero) leads ID'd with strong (weak) beam in flight, while ALS detects 10 leads
- ALS detects 2X more topographic features (532) than UMD-RDA (225), 5X more than ATL07 seg (87), and 5X more ALS seg (102) → ATL07 strong beam here, weak beam detects even less
 - And ALS has a larger dynamic range → ridges are higher, troughs lower
 - Note: UMD-RDA requirement of 5-shot aggregates vs. 150-photon requirement for ATL07
- Strong beams, on average, capture magnitude of sail heights well w/means of 1.1m for ALS full, 1m for UMD-RDA, and 0.9m for ALS seg/ATL07 seg ... but they largely overestimate the width of topographic features (see Fig. 9)

Discussion

- Due to longer segment length, weak beam has smoother elevation profile than strong, but weak beam still have comparably high correlations w/ALS as the strong beam for elevation estimates
 - So weak beam can be used for elevation estimates, but probably not surf topography
- IS2 can detect leads, but not all of them → ATL07 limited by required 150-photon aggregate
 - Despite ~11m footprint, ATL07 segment res may be much longer bc of this^
 - In addition to resolution, omission of dark leads may explain why fewer are detected
- ATL07 processing, specifically omission of 2σ elevations, may explain part of disagreement btw ALS and ATL07 regarding surface roughness
- ATL07 tends to underestimate surface elevation over rougher sea ice compared to ALS
- Rough surfaces leads to more skew in weak beam than strong bc product smooths over large features, creating “longer” roughness segments → weak beam has longer tail than strong
- ATL07 captures 16% (4%) of ridges using strong (weak) beam; UMD-RDA captures 42% (30%)

Impressions – IS2 overall performs well w/elevation estimates but struggles with capturing full dimensionality of topographical features (and leads) due to limited spatial resolution. Robust examination of IS2 elevation accuracy (not thinking about freeboard or SIT here)



Lidar | IS2 | ALS | MOSAiC | Topography | Validation

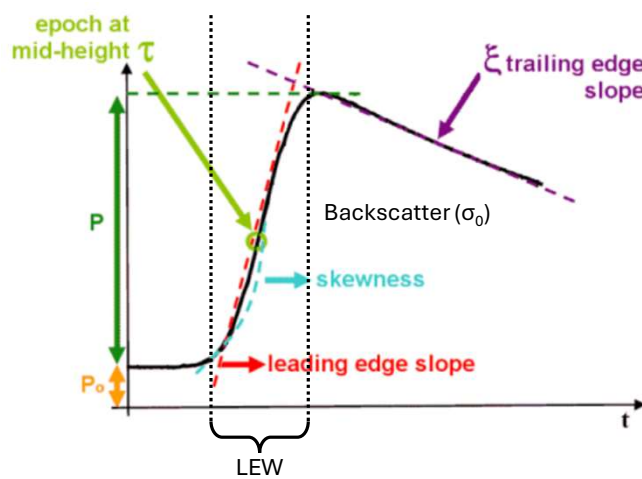
Ricker et al. (2023)

Radar Altimetry Tutorial

Rosmorduc et al. (2018)

Waveform characteristics

- Epoch at mid-height gives time delay of the expected return of radar pulse, and thus the time the radar pulse took to travel the range and back
- P = amplitude of useful signal
- P_0 = thermal noise
- Lead edge slope
- Skewness = leading edge curvature
- Leading edge width (LEW) → related to penetration into medium and surface roughness of target
- Trailing edge slope → gives information on antenna mispointing and signal penetration into medium (roughness as well)



Radar bands

- Ku – 13.6 GHz
- C – 5.3 GHz → more sensitive to Ku to ionospheric perturbation, less sensitive to liquid water in atmosphere
 - Often used w/Ku to correct for ionosphere delay
- S – 3.2 GHz → similar to C band, often used w/Ku
- Ka – 35 GHz → higher resolution due to higher frequency, high attenuation due to water vapor

Delay-Doppler (or SAR) Altimetry

- Unlike conventional radar altimeter, SAR exploits coherent processing of groups of transmitted pulses
 - Full Doppler bandwidth is exploited
- Along track processing greatly increases resolution

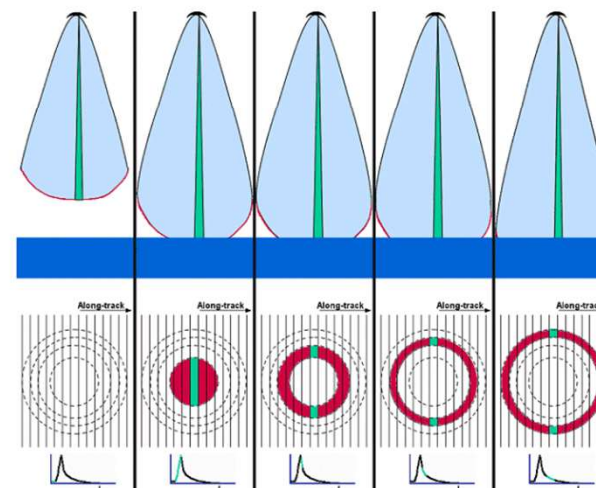
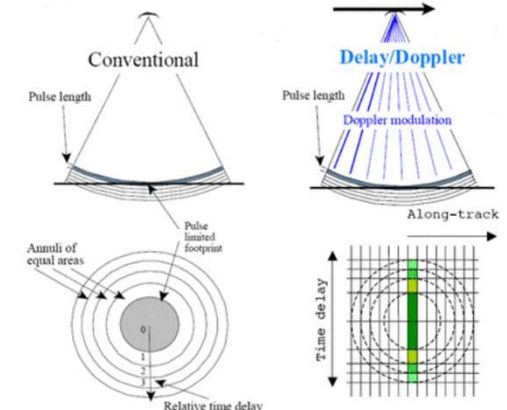


Figure 5.22. Theoretical “step-by-step” building of a SAR-altimetry waveform (for a single Doppler beam). Contrary to the classical altimeter, the lighted area is not a surface-constant ring, but only part of it, which explain the peakier shape of the echo. Several such beams are used at the same time (Using material from R.K. Raney, Johns Hopkins University Applied Physics Laboratory)

Radar | Altimetry tutorial
| SAR | Waveforms

Laboratory measurements of radar backscatter from bare and snow-covered saline ice sheets

Beaven et al. (1995)

Introduction

- Goal: examine backscattering characteristics of C (5.3 GHz) and Ku (13.4 GHz) radar over bare and snow-covered ice (smooth surfaces)

Step-frequency radar systems description

- They test all four linear polarizations w/both C and Ku band radars

CRREL experiment description

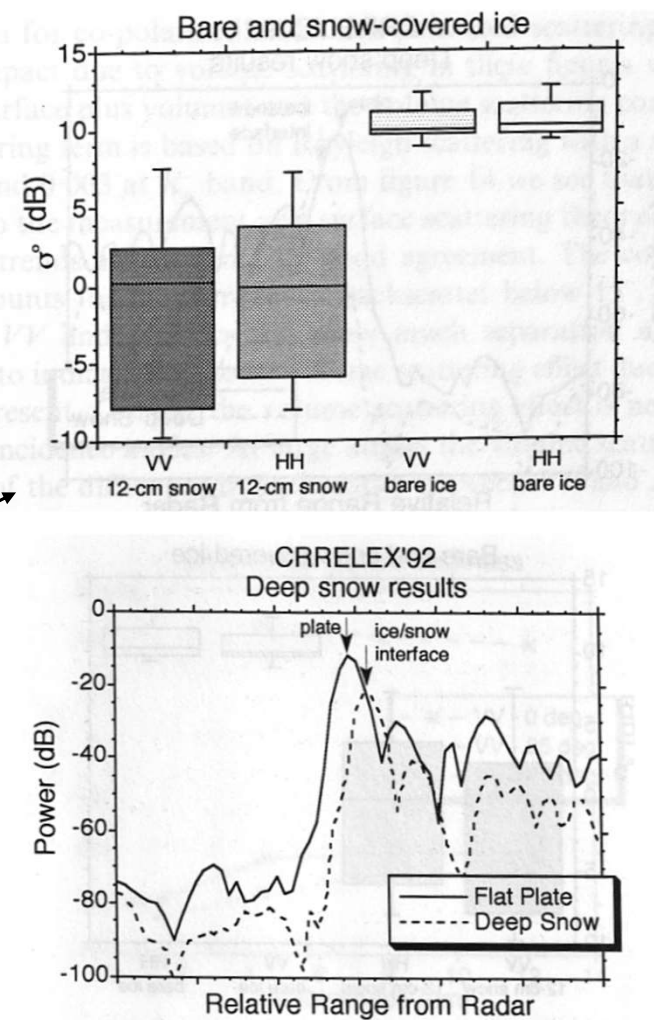
- The winter 1990 experiment created artificial sea ice by freezing water in an outdoor pond w/salinity of 24 parts per thousand
 - Measurements taken at incidence angles btw 0° and 60° w/all four linear polarizations
 - SIT was 20cm thick
- The 1992 experiment was in an indoor refrigerated facility (salinity = 24 ppt as well)
 - Early period (days 0-3): measurements taken over open water and ice; SIT reaches 12cm
 - Ku band measurements over snow covered ice occurred in 1992 experiments
 - Snow added in four layers to a height of 12 cm, then more added to reach 21cm depth → fresh, newly fallen snow
 - Range res through snow ~11 cm, hence min height of 12 cm used
- Other geophysical measurements: surface roughness, air temp, snow depth/density, and vertical temps of ice temp, salinity, brine volume, and crystal structure
 - Snow densities in 1992 experiment: 485 kg m⁻³, 277 kg m⁻³, 258 kg m⁻³, 288 kg m⁻³

Presentation of experimental results

- As ice grows, bulk dielectric constant decreases and surface roughness increases due to brine expulsion → both result in reduce back scatter at normal incidence angles
 - Increased surf roughness leads to increased backscatter off-nadir
- Introducing snow decreases backscatter at normal incidence angle, but increases the variation in backscatter
- At Ku-band, return from air-snow interface is negligible while return from snow-ice interface dominates
 - High volume scattering due to snow would broaden return pulse, but this isn't observed thus no evidence for volume scattering
- For smooth (rough) surfaces, coherent (incoherent) portion dominates the return signal
- Very good agreement btw measurements and predictions from radiative transfer model for both Ku and C band frequencies
- Volume scattering more prevalent at large incidence angles
- Brine wicking into the snow layer causes a roughening of surface at the snow-ice interface and this decreases (increases) backscatter at normal (large) incidence angle

Conclusions

- Surface scattering dominates with C and Ku band at low-to-moderate incidence angles, whereas volume scattering contributes more at high incidence angles
- Backscatter varies based on stage of ice growth over due to changing bulk dielectric constant
- Roughening at snow-ice interface due to brine wicking results in increased backscatter at most incidence angles, except nadir where it is significantly reduced
- After the addition of the first 2.5 cm layer of snow, the addition of subsequent snow layers did little to the backscatter
- Dominant Ku-band return is from the snow-ice interface



Radar | Snow-ice interface | Laboratory

CryoSat: A mission to determine the fluctuations in Earth's land and marine ice fields

Wingham et al. (2006)

Introduction

- Written in 2004 before the launch of CS in 2005, at time IS had recently been launched and the pre-existing radar altimeter was ERS-1 which had limited coverage due to 98.5° inclination

The CryoSat satellite

- SAR/Interferometric Radar Altimeter (SIRAL) → 13.6 GHz normal incidence
- 3 modes: (1) low resolution mode (LRM), (2) SAR mode (SARM), and (3) SAR interferometry mode (SARInM)
 - LRM is conventional pulse-limited altimetry w/single antenna
 - SARM provides along-track aperture synthesis using single antenna**
 - SARInM allows for along-track aperture synthesis using two antenna and for phase comparison btw those two antennas

- 92° inclination, altitude of ~717 km, and 369 day repeat period w/30 day subcycle over Arctic**
- Mask/switch btw LRM, SARM, SARInM automatically applied based on what surface the satellite is passing over → SARM over Arctic Ocean, SARInM GrIS margins, LRM over central GrIS

CryoSat level 1b data processing and products

- Point of closest approach (POCA)** → nadir point if surface has no inclination w/respect to sphere
- Following beam forming and slant range correction, echoes from beams directed at a particular location are gathered to form a “stack”
 - Variation in echo power across different looks indicates surface roughness → quantified using the metric stack standard deviation in sea ice literature

CryoSat level 2 data processing and products

- Freeboard, $f_{est}(y, t)$, estimated using: $f_{est}(y, t) = z_{ice}(y, t) - z_{mean}(y) - \sum_j \Omega_{ocean}(y, y_j) \times (z_{ocean}(y_j, t) - z_{mean}(y_j))$ where z_{ice} is surface elevation of ice, z_{mean} is mean sea surface, y is the position vector indicating a point on the ellipsoid, and Ω_{ocean} is a filter that acts on elevations z_{ocean} in the vicinity of y (eliminates long-scale errors)

Error budget and its validation

- Three types of errors: those that arise from (1) the measurement system, like radar speckle, (2) the processing of a signal to geophysical quantities like elevation, and (3) from forming local

Table 2
Nature and source of geophysical corrections

Correction	Source	Typical winter magnitude at 80°N, averaged over 1 month and 10 ⁴ km ² .	Reference
Ocean tide	FES 02	0.03 m	Le Provost et al. (1998)
Ocean loading tide	FES 02	0.002 m	Francis and Mazzega (1990)
Long-period tide	FES 02	0.0075 m	Le Provost et al. (1998)
Solid Earth	Cartwright Edden	0.015 m	Cartwright and Edden (1973)
Polar tide	Wahr	0.0025 m	Wahr, 1985
Dry troposphere	Meteo France/ECMWF	2.3 m ±0.02 m	Saastamoinen, 1972
Inverse barometric correction	Meteo France/ECMWF	0.03 m	Ponte (1991)
Wet troposphere	Meteo France/ECMWF	0.01 m	Saastamoinen (1972)
Ionosphere	Bent model	0.015 m	Llewellyn and Bent (1973)

averages w/higher level products due to sampling

- Errors that dominate in a point measurement may not have much of an impact when averaged over a large area, and vice versa
- Total SARM elevation error is 11.6 cm, w/6 cm due to orbit and 10 cm due to range error
- Since SIT is computed from freeboards which are a relative measurement, long-scale instrument system errors (particularly orbit error) are removed
- For SIT, errors due to density uncertainties are noted and the authors actually call for densities that are a function of SIT → they explicitly mention ridged ice
- A minimum error of 6.8 cm estimated for SIT**, but this doesn't factor in errors due to density uncertainties, returns from above s-i interface, etc...
- Also hard to determine errors for sea ice as there is so little in-situ data at time of writing

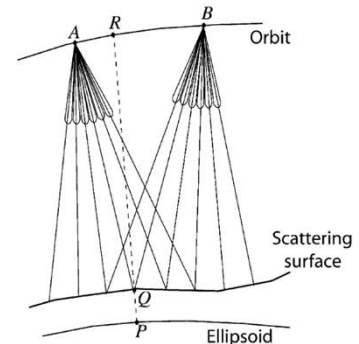


Fig. 9. The geometry of the multi-looking and slant range correction. A burst located at A on the orbit illuminates a set of 64 locations on the surface, approximately 294 m apart and lying approximately within $\pm 0.76^\circ$ of the nadir point at P . The beam rock angle directs the central beam at the nadir point P , which defines a set of points on the assumed surface. A little while later, a burst located at B also illuminates 64 locations. The beams of burst B are ‘rocked’ by up to a beam width to bring those of its beams that overlap beams from other bursts into exact coincidence on the points on the assumed surface. Q is such a point. Those points from the burst at B that do not overlap existing points define new points on the assumed surface at which beams from future bursts are directed. For clarity, only a few beams are shown, and the angles are grossly exaggerated.

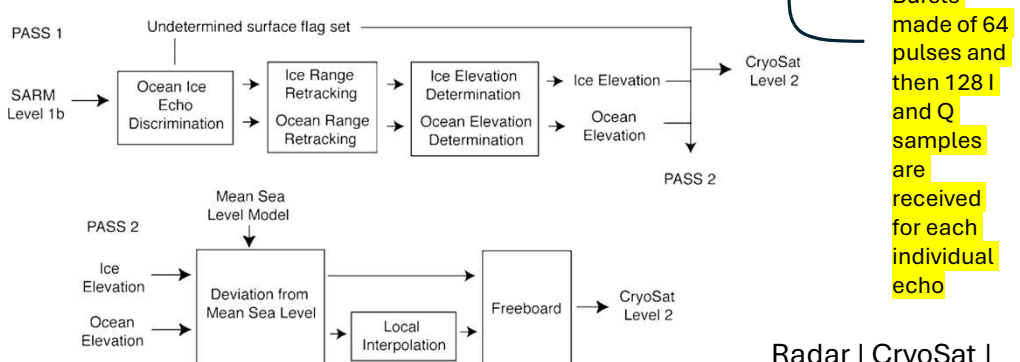


Fig. 18. The level 2 SARM processing chain.

Radar | CryoSat |
| SIRAL

Simulated effects of a snow layer on retrieval of CryoSat-2 sea ice freeboard

Introduction

- Focus of this paper is scattering at air-snow and how it impacts estimates of sea ice freeboard
- In presence of scattering within snow layer, corrections to the observed scattering surface, h_o , to obtain sea ice freeboard, h_f , are $h_f = h_o + (\delta h_p + \delta h_d)$
 - δh_p is the bias introduced by scattering at a-s interface and within snow layer
 - δh_p subtracts from h_f as the correction effectively moves retracking point closer to true s-i interface, which reduces estimated sea ice freeboard
 - δh_d is the bias due to the reduced propagation speed within snow layer
 - δh_d adds to h_f as refraction correction accounts for longer path length through dense medium, resulting in a larger sea ice freeboard
- Simulations w/CS2 radar parameters and snow scattering profiles of sea ice from OIB snow radar used to examine competing effects of δh_p and δh_d

Backscatter from IceBridge (OIB) radars

- Scattering within the snow layer (including form a-s interface) contributes to the radar returns, but the ratio of power (s-i/a-s in dB) indicates highest peak is usually from snow-ice interface
- OIB Ku-band radar returns suggest that observed ratios of detected s-i and a-s peaks show that strength of returns from two interfaces could be (comparable) within several decibels of each other when return power is low
 - If range resolution > snow depth, then you may not be able to resolve the two peaks from a-s and s-i-interface, as they'll be sort of blended as one
 - CS2 range resolution is ~47 cm, thus for most snow cover can't resolve two peaks

Simulations of δh_p and δh_d

- Three snow layers, L(r), simulated: (a) flat a-s and s-i interfaces, (b) 5cm roughness added to a-s interface, and (c) snow volume w/uniform scatterer
 - Snow varied from 5 cm to 50 cm
- Two retrackers: (a) half power of leading edge (TL) from Laxon et al. (2013) and (b) centroid location in leading half of the return (TC) → threshold leading/centroid = TL/TC (I think)

Case 1: Planar (flat) interfaces

- Over intermediate range of R_p , where $R_p = \frac{P_{s-i}}{P_{a-s}}$ (ratio of return power from each interface) and snow depth < 20 cm, required corrections are < 2cm
 - At higher snow depths, such as over MYI, required corrections are much larger
- Penetration bias, δh_p , using retracked points w/centroid approach (TC) is much less sensitive to return power and snow depth compared to the leading edge retracker (TL)

Case 2: Slightly rough air-snow interface

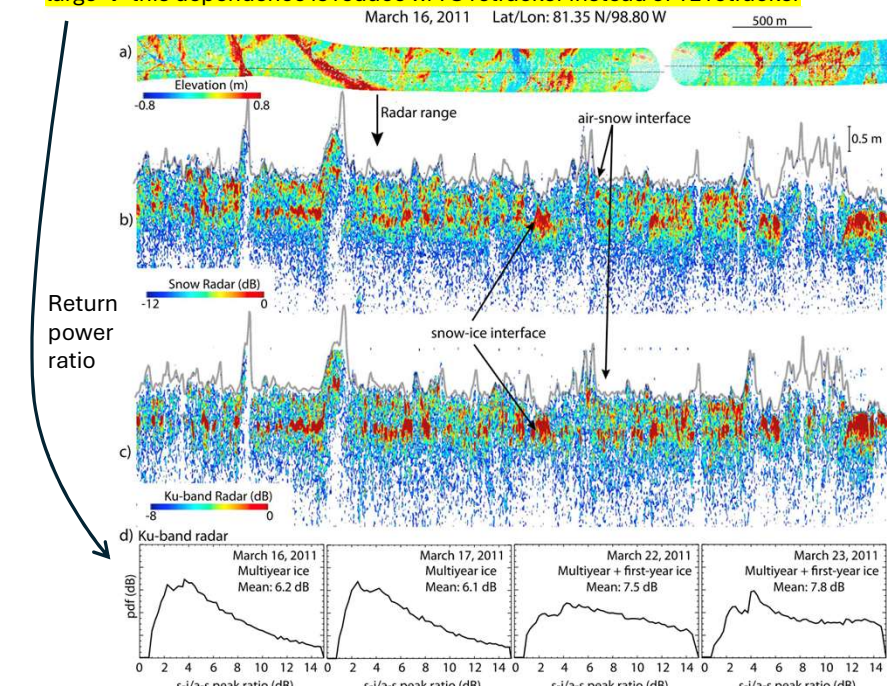
- Impacts of roughness are notable (widening of waveform) but small
- Main driver of penetration bias is the width of the radar pulse (~47cm) → determines range res
- As w/Case 1, sensitivity of penetration bias is reduced w/centroid retracker (TC) rather than TL

Case 3: Air-Snow Interface With Uniform Scattering Snow Layer

- As w/Case 1 and 2, higher sensitivity of TL than TC to the snow layer
- Unlikely that volume scattering plays a role in Arctic sea ice, more relevant for Southern Ocean

Conclusions

- The a-s interface contributes to returns at Ku-band frequencies → broadens response of the snow-ice interface and displaces retracking point toward the altimeter
- The a-s and s-i interfaces are not resolved by the limited bandwidth of CS2 (~47cm range res)
- δh_p highest when return power from a-s and s-i interfaces are comparable and snow depth is large → this dependence is reduce w/TC retracker instead of TL retracker



Clearly, scattering is coming from a-s interface here, but primarily from s-i interface

Figure 1. A 4 km segment of lidar elevations and returns from the snow and Ku-band radars acquired by an IceBridge (OIB) flight on 16 March 2011. (a) Elevations within Airborne Topographic Mapper lidar swath (~250 m; color-coded elevation) with the snow/Ku-band radar tracks (black dashed line) near the center of the lidar swath. (b) Range-varying radar returns along the track of the snow radar. The profile of lidar elevation (a-s interface) associated with each snow radar footprint of ~35 m is in black. (c) Same as in Figure 1b except for the Ku-band data. Uncalibrated radar returns (in dB) are relative to the highest values in this segment. The center location of segment is 81.35°N/98.80°W. Note the different ranges indicated by the color scale. (d) Ratio of the s-i to a-s peaks (in dB) for four OIB flights sampling a mix of multiyear and first-year sea ice. The range sample spacing of snow radar and Ku-band radar is ~3 cm (bandwidth: 4.5 GHz) and ~4 cm (bandwidth: 6 GHz), respectively.

An improved CryoSat-2 sea ice freeboard retrieval algorithm through the use of waveform fitting

Kurtz et al. (2014)

Introduction

- They discuss the biases introduced by using varying geophysical constants (e.g., ρ)
- They use the same density parameterizations in CS2 as in OIB to enable meaningful comparison**

Data sets

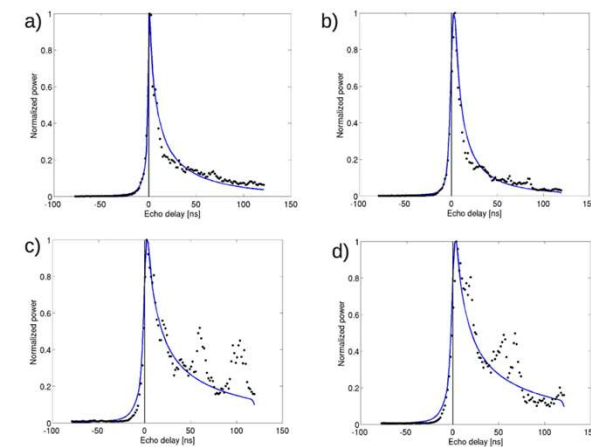
- CS2 L1b SAR and SARIn over March 2011, 2012, and 2013
 - Not using phase data in SARIn mode here, as focus is retracking return power waveform
- OIB sea ice freeboard, snow depth, and SIT products March 2011-2013 (40m sampling res)

CryoSat-2 multi-look echo phenomenology

- Assumptions:** surface scattering from s-i interface, Gaussian height deviations within radar footprint, perfectly nadir orientation, and some others (see conclusion for good summary)
- CS2 incidence angles over sea ice regions range from 0-0.76°
- Mean scattering occurs at roughly 85-95% of peak value, with some variation due to α (angular backscatter efficiency) and σ (stdev of surface height)

Surface elevation retrieval algorithm

- Physical model** is combined w/least-squares fitting procedure to estimate mean scattering point and mean surface roughness within CS2 echoes of different surface types
 - They use **lookup tables** for a discrete set of cases over Arctic sea ice to speed up the computation time
- Four free parameters are: (1) amplitude scale factor, (2) echo time shift factor (3) α and (4) σ
- Leads identified by computing pulse peakiness, $PP = \max(P_r) \sum_{i=1}^{128} \frac{1}{P_r(i)}$ where $PP > 0.18$ and a stack standard deviation < 4 → for all cases, RP near max peak of the return
- Sea ice floes defined as waveforms w/PP < 0.09 and ssd > 4 (3 for SARIn)



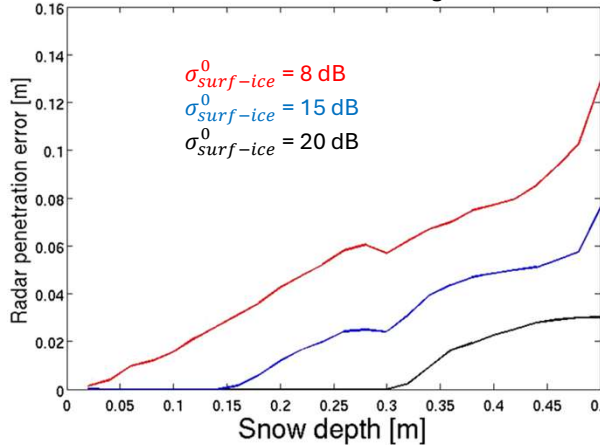
Black dots = CS2 points, blue line = model. Plots (c) and (d) are over a mixture of smooth/rough surfaces. Notice peaks in trailing edge do not impact fit as location of mean scattering surface is on the leading edge of the waveform.

CryoSat-2-derived sea ice properties

- They compare results using physical retracker (CS2WfF) w/results using a 50% TFMRA over floes and Giles et al. (2007) model over leads (referred to as ELTF method)
 - Leads from ELTF an average of 2.8 cm higher than CS2WfF, w/R=0.7
 - Mean freeboard differences are btw 11.5-12.7 cm over the three seasons between retrackers, corresponding to SIT differences btw 1.08-1.19 m → CS2WfF results thinner
 - Thus, threshold method (ELTF) leads to freeboard values being biased high
- All comparisons btw CS2 and OIB data are done w/gridded data
 - CS2 data effectively on 125 km grid, OIB on 25 km grid
- CS2-OIB w/CS2WfF method:** mean freeboard (SIT) differences range from 1-3cm (11-23cm)
- CS2-OIB w/ELTF method:** mean freeboard (SIT) differences range from 11.9-15.9cm (112-149cm)
 - Likely due to 50% threshold which is too low – should be closer to peak power
- CS2WfF correlation w/OIB >> than ELTF correlation w/OIB, but still not particularly high...**
 - This is subject of a future study, but likely due to sampling + off-nadir lead snagging

Estimation of errors due to radar penetration

- They model how radar penetration error changes w/snow depth for three cases: $\sigma_{surf-ice}^0 = 8$ dB, 15 dB, and 20 dB → comparable backscattering btw a-s and s-i interfaces, intermediate case, and case where scattering at s-i interface dominates
 - 20 dB case → error < 3cm even for deep snow
 - 15 dB case → error ~2 cm or less when snow depth < 20 cm
 - 8 dB case → error increases as a function of snow depth, but btw 4-8cm
- Overall, penetration error w/CS2WfF should be <4 cm for FYI and <8cm for MYI, but freeboard estimates will be biased high



- Unless snow is salty/wet, a significant portion of transmitted energy will penetrate to the snow-ice interface

Conclusions/Impressions

- Detailed CS2 processing and error propagation → refer to if needed
- Empirical approach w/this physical model results in thinner freeboards than threshold approach
- Penetration bias analysis similar to Kwok (2014) → all results are likely biased high to some extent
- Good summary of assumptions in Conclusion

Radar | CS2 | Physical retracker |
Penetration bias | OIB | Threshold retracker

Sensitivity of CryoSat-2 Arctic sea-ice freeboard and thickness on radar waveform interpretation

Ricker et al. (2014)

Introduction

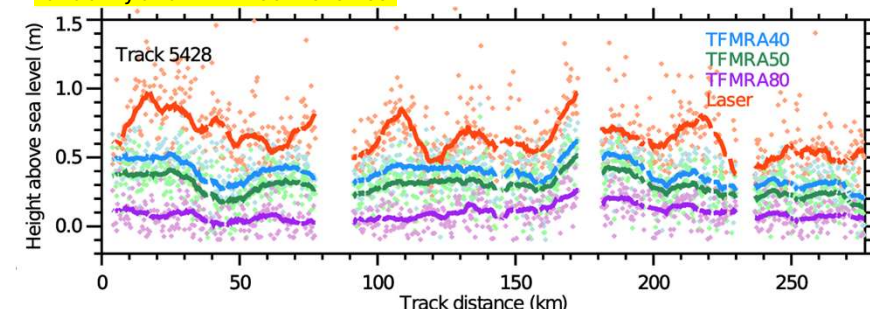
- Exploring the uncertainties introduced by 40%, 50%, and 80% TFMRA on freeboard estimates

Data and methodology

- They don't apply corrections to radar freeboard to get a consistent comparison throughout study
- CS2 L1b SAR and SARIn (in some areas), but SARIn phase information discarded
- Same retracker used over leads and sea ice to keep things consistent
- Pulse peakiness (PP), stack kurtosis (K), stack standard deviation (SSD), the PP of the 3 range bins to the left of the power max (PP_L), and the 3 to the right (PP_R), SIC from OSI SAF, and OCOG width (provides info on width of echo) → all used to discriminate sea ice and ocean surfaces
- Linear interpolation btw leads along ground tracks w/25 km running mean to get SSHA
- Radar freeboard (F_R) computed: $F_R = L - (MSS + SSH)$ where L is retracked surface elevation
 - Note, this is radar freeboard not sea ice freeboard as path length correction not applied
- mW99 snow depth, W99 ρ_s , FYI $\rho_i = 916.7 \text{ kg m}^3$ and MYI $\rho_i = 882.0 \text{ kg m}^3$
- Data averaged monthly on 25 km EASE-Grid 2.0 → freeboard/SIT averaged w/arithmetic mean
- Coincident ALS data from CryoVex campaign in Lincoln Sea 2003 (total length of 450km used)
 - Gridded to match CS2 spatial resolution using IDW (ALS footprint MUCH smaller)

Results

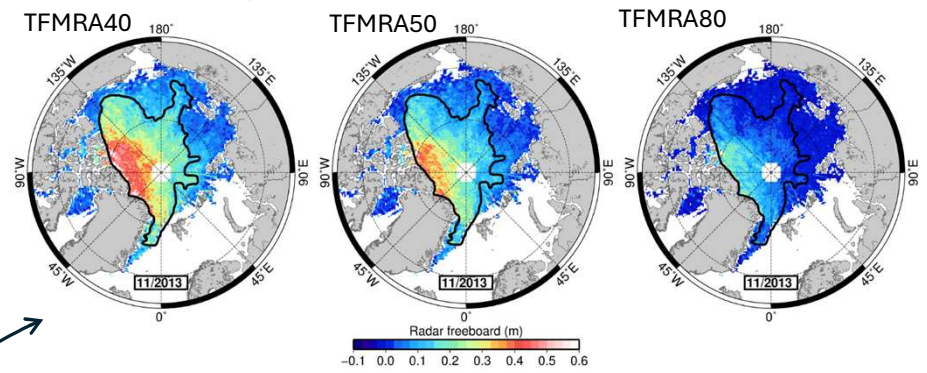
- Radar freeboards largest for TFMRA40 and lowest for TFMRA80 for both FYI and MYI
 - Differences between TFMRA's greater over MYI
 - Btw TFMRA40 and 80, deviations up to 0.35 m for MYI, but below 0.1 m for FYI
- ALS has stronger variability in surface elevations than CS2 data, w/TFMRA40 having the highest variability and TFMRA80 the lowest



- Bias that results from (a) interannual snow depth variability = 0.12 m (FYI), 0.21m MYI (b) interannual ρ_s variability = 0.10m (FYI) and 0.18 m (MYI), (c) $\rho_i = \pm 0.04\text{m}$ FYI/MYI
- Largest biases w/ice-type (which impacts snow depth, ice density) at margins btw FYI/MYI zones

Discussion

- Differencing ALS and CS2 estimates gives snow depths, or how far into snow layer radar wave propagates → 0.16 m, 0.24 m, and 0.4 m for TFMRA40, 50, and 80, respectively



- Mean snow depth along track from OIB snow radar was ~0.31 m
 - TFMRA40/50 underestimate (don't track) the s-i interface, whereas TFMRA80 too low
- Volume scattering through snow layer may impact lower portion of leading edge, leading to a shallower PDF for TFMRA40/50
- Flattened leading edge over MYI leads to larger range deviations when retracked compared to FYI which has a steeper leading edge → MYI differences are much larger
- Adaptive thresholding may be useful to accommodate regions where radar penetration is low
 - If minimal penetration, use low threshold and estimate total freeboard, if full penetration use a higher threshold and estimate the sea ice freeboard
- Uncertainties due to retracking/radar penetration roughly estimated to be 6 cm / 12 cm for FYI/MYI for freeboard, and 60 cm/120 cm for SIT → dominates total uncertainty

Conclusions

- TFMRA50/50 track above s-i interface, while TFMRA80 tracks below it
- Different TFMRA results in changing absolute magnitude of freeboard/SIT, but spatial distribution of these parameters are less affected
- TFMRA retracking deviations larger over MYI than FYI due to flattened leading edge
- Uncertainties in retracking/radar penetration dominate the uncertainty budget
 - Uncertainties in snow depth, ρ_i , and ρ_s are in range of 0.01m-0.2m for SIT

Impressions

Extremely thorough uncertainty propagation analysis in section 2.3 which is then described/commented on throughout the discussion. Refer to this when I need to do an uncertainty analysis myself. This study highlights challenges w/using TFMRA retrackers, suggesting that perhaps adaptive thresholding would be useful. Good discussion of random and systematic uncertainties.

Radar | CS2 | Retracker | TFMRA | Uncertainty budget

Variability of Arctic sea ice thickness and volume from CryoSat-2

Introduction

- Objective of paper is to look at seasonal/interannual variability of SIT/SIV from CS2

Data

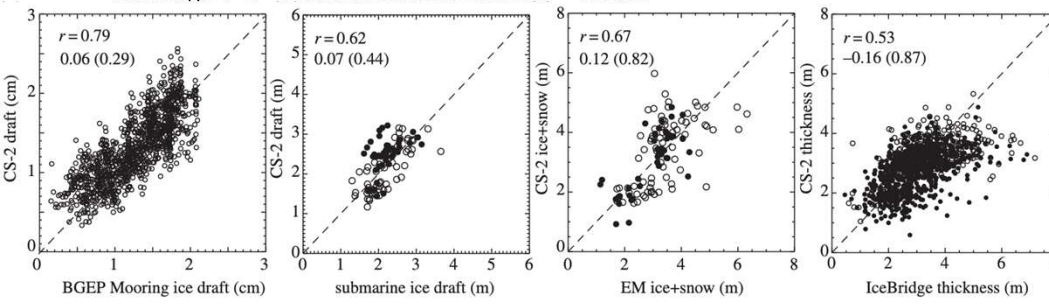
- CS2 L1B and L2 data products
- Ice draft from BGEP moorings, submarine ice draft from 2011, snow/ice thickness from AEM (2011/2012), SIT from OIB, MYI fraction from ASCAT, PMW sea ice motion

Estimates of ice thickness

- Motivated by Kwok (2014), they use **centroid retracking approach** instead of leading edge
 - Centroid is centermost point of waveform area, which is defined as interval btw the peak and half power point on leading edge of the peak → peak defined as first above 15 dBf
- Power of peak (P_c) and width of centroid (W_c) relative to range location of peak used for ice/water discrimination
 - Not using PP or SSD → these are relative measures of peak signal strength compared to strength of entire waveform
- Leads = $P_c > 40$ dBf and W_c to left of red slanted line:
 - Means/stddev of P_c/W_c in top right corner and fraction of obsv classified as leads in white
- Following Kwok (2014), $h_{fi} = h_o - h_{ssh} + (\delta h_p + \delta h_d)$, but they take $\delta h_p = 0$ (adjustment for penetration bias) as **they assume centroid retracker is tracking s-i interface correctly**
- mW99 snow depths using $\alpha = 0.5$ and 0.7 ; snow density from W99
- They used two ice densities: (a) $\rho_i = \rho_i^{FYI} = 917 \text{ kg m}^{-3}$ and (b) $\rho_i^{FYI} = 917 \text{ kg m}^{-3}$, $\rho_i^{MYI} = 882 \text{ kg m}^{-3}$ → where (a) is the upper bound and (b) is the lower bound of SIT/SIV estimates

Assessment of CS2 estimates

- Correlations and mean differences btw in-situ data and CS2 using $\alpha = 0.7$ and $\rho_i = 917 \text{ kg m}^{-3}$:
 - BGEP → $R = 0.79$ and mean difference = 0.06 m
 - Submarine → $R = 0.62$ and mean difference = 0.07 m
 - EM → $R = 0.67$ and mean difference = 0.12 m
 - IceBridge → $R = 0.53$ and mean difference = -0.16 m



Better overall agreement w/in situ data is shown using $\alpha = 0.7$ and $\rho_i = \rho_i^{FYI} = 917 \text{ kg m}^{-3}$

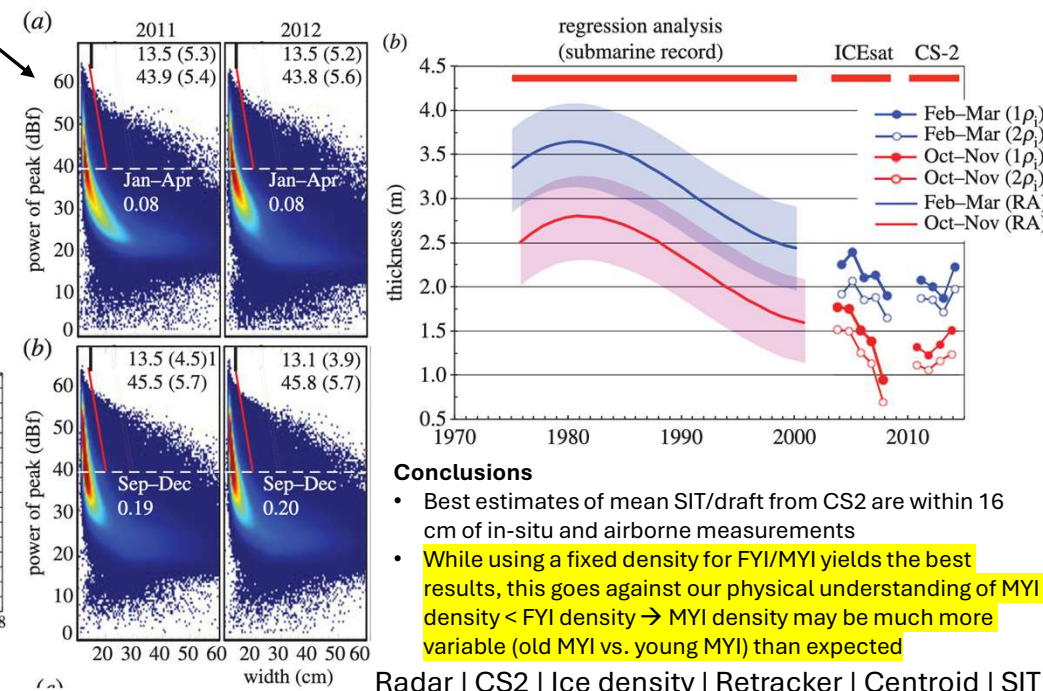
Kwok and Cunningham (2015)

Arctic Ocean CS2 ice thickness/volume

- using $\alpha = 0.7$ and the two ρ_i
- Mean SIT ranges from 1.27 m in October to 2.32 m in May (1 density case)**
 - FYI (MYI) increases from 0.95 to 2.15 m (1.83 to 3.73 m) → more MYI growth due to convergence
 - Mean SIV ranges from $6,819 \text{ km}^3$ in October to $16,369 \text{ km}^3$ in May (1 density case)
 - FYI (MYI) increases (decreases) from $3,203$ to $13,627 \text{ km}^3$ ($3,616$ to $2,769 \text{ km}^3$)
 - MYI SIV decline despite SIT increase indicates **SIV export > SIV production (growth) in MYI zone**
 - The ~2m increase in thickness is largely due to convergence, and they find a corresponding loss in MYI area over Oct-May → compression primarily north of Greenland and CAA coast
 - Two density results lead to reduction in MYI SIT by 0.25 m in October and 0.5 m in May**

Longer term records

- No trend over four years of study in this paper 2011-2014
- Btw IS and CS2 periods, trend is negative but far less than that over just the IS period (2003-08)
 - W/2 density case, trends are 10-13% lower btw IS and CS2 period



Conclusions

- Best estimates of mean SIT/draft from CS2 are within 16 cm of in-situ and airborne measurements
- While using a fixed density for FYI/MYI yields the best results, this goes against our physical understanding of MYI density < FYI density → MYI density may be much more variable (old MYI vs. young MYI) than expected

Radar | CS2 | Ice density | Retracker | Centroid | SIT

A Facet-Based Numerical Model for Simulating SAR Altimeter Echoes From Heterogeneous Sea Ice Surfaces

Landy et al. (2019)

Introduction

- Previous physical models of backscattered SAR altimeter echoes assume a Gaussian surface height distribution, whereas lognormal has been shown to better characterize surface roughness
 - They aim to create a numerical model based on this finding of lognormality

Numerical Echo Model

- Surface roughness (1-100s m scale) simulated using spectral analysis
 - They create a tetrahedral mesh that links vertices/nodes from the originally simulated surface and then they compute SAR waveform from integral of power backscattered from each triangular facet of the mesh
- They simulate CS2 waveforms → detailed derivations provided in this section
- Backscattering coefficient of snow, sea ice, and seawater, as well as volume scattering by snow all simulated to account for their individual contributions to total return power of waveform

Model sensitivity

Sensitivity to antenna parameters

- Realistic variations in satellite bench orientation (mispointing in pitch/roll) don't significantly impact the backscattered waveform shape

Sensitivity to snow-covered sea ice physical properties

- Surface backscatter coefficients at a-s and s-i interfaces have similar scattering signatures, but σ_{ssurf}^0 is significantly lower and drops off more rapidly than σ_{si}^0 bc the interface is smoother and dielectric contrast btw snow and sea ice is larger
- Small-scale ice surface roughness reduces the power of the waveform, but shape is the same
- Very low snow volume scattering and relatively constant over a variety of incidence angles

Model sensitivity to snow properties

- Backscattered echo is not sensitive to variations in snow surface roughness within realistic range of parameters tested in this study (0.5-2.0mm)
- When snow grain sizes > 1 mm, volume scattering is significant and leading edge of waveform becoming less concave
 - Similar effect w/ ρ_s when $\rho_s > 150 \text{ kg m}^{-3}$, but not to the same degree
- Even 10cm of snow results in reduced backscatter power, with fluctuations becoming enhanced bc the reduced wavespeed within snowpack emphasizes small variations in sea ice topography

Model sensitivity to sea ice surface roughness

- Overall, fitting an echo simulated from Gaussian surface rather than lognormal surface results in retracking point that overestimates range leading to an underestimate in sea ice surface height → this is for the same retracker threshold for both distributions, to be clear
 - This bias increases w/increasing surface roughness

- For lognormal case, retracking point is btw 60-80% threshold for when roughness is btw 0-50cm
- Model sensitivity to mixed surface types (leads)
 - Lead dominates the power return for 0-600m off-nadir, between 800-1000m the scattering from snow/ice become more noticeable, and by 1000m the lead is hardly detected
 - Lead snagging

Applications to sea ice observations

- CS2 echoes compared with modeled ones → surface topography observations from OIB ATM
- Sea ice surface topography (from OIB ATM) is fit well by lognormal model, and CS2 waveform is very similar to the modeled waveform
- Lognormal model performs well over mixed ice types where neither sea ice/leads are the dominant scatterer

Conclusion

- Sea ice roughness better characterized by a lognormal height distribution than a Gaussian one
- Echoes simulated from OIB ATM obs of lognormal sea ice compare well w/CS2 waveforms
- For ice surfaces w/typical roughness, retracking threshold is btw 60-80% of leading-edge power
 - But this varies non-linearly w/surface roughness

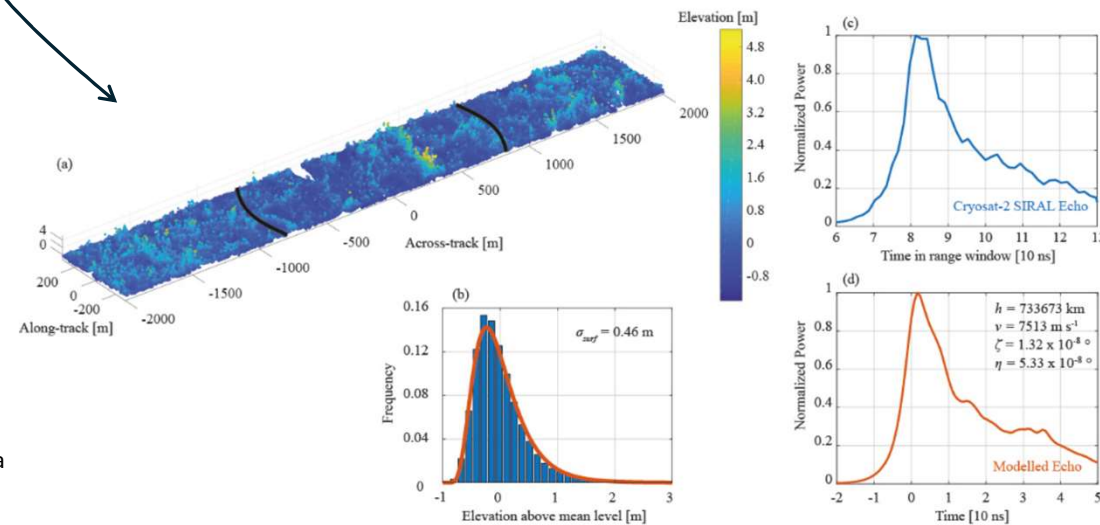


Fig. 12. Example of a Cryosat-2 echo modeled from real sea ice surface topography, including (a) ATM observations of the sea ice surface (with the extent of the pulse-limited footprint in black), (b) lognormal fit to the surface height PDF, (c) true Cryosat-2 SIRAL echo, and (d) modeled echo (using the inset, SIRAL antenna parameters).

Radar | Lognormal | Surface roughness | Retracking | CS2 | OIB ATM

Sea Ice Roughness Overlooked as a Key Source of Uncertainty in CryoSat-2 Ice Freeboard Retrievals

Landy et al. (2020)

Introduction

- This paper applies the simulations from Landy et al. (2019) to develop the LARM algorithm

Characterizing the sea ice surface roughness height distribution

- Airborne lidar/radar from OIB use to evaluate suitability of using Gaussian/lognormal assumptions for ice surface height PDFs when modeling SAR altimeter echoes from sea ice
 - ATM L1B Elevation and Return Strength V2 data collated within 1700m along-track sections
 - OIB Ku-Band Radar L1B geolocated Echo Strength Profiles V2 data → uses TFMRA50
- Normalized PDFs created using OIB lidar/radar data of surface height and then Gaussian/lognormal models are fit to the observed PDFs, finally KS test and RMSE used to determine which performs best
- Lognormal model has a superior fit to snow surface topography than the Gaussian model in 94% of cases (92% FYI, 95% MYI) and to s-i interface topography in 90% of cases (96% FYI, 88% MYI)
- Similar km-scale roughness statistics for a-s and s-i interfaces, with a-s roughness generally larger
 - Snow surface roughness is primarily controlled by ice surface roughness

Application of a Numerical SAR Altimeter Echo Model for Retracking CS2 Waveforms

- Building on Landy et al. (2019), they create a look-up table of 2,222 echoes to hasten fitting procedure by modifying large- and small-scale surface roughness parameters

Comparison of Physical-Model and Threshold-Based Retracking Algorithms

- Across typical range of surface roughness, 5-55cm, RP varies from 85-95% of lead-edge power for Gaussian echoes → approaches 100% w/o approaching zero (i.e., smooth leads)
 - For lognormal echoes, the range is much more variable from 60-95%
 - For heavily deformed ice, therefore, RP should be near 60%
- Lognormal and Gaussian retrackers produced elevations within 2cm over smooth FYI areas, but Gaussian elevations are over 6 cm lower than LARM
- TFMRA produce estimates for mean sea ice elevation that are higher than LARM
 - Largely influenced by TFMRA overestimating FYI surface elevation, as TFMRA70 (for example) assigns 70% threshold to this waveform when model indicates it should be ~90%
- Largest difference btw LARM and TFMRA is w/TFMRA50 → overestimates up to 30cm over MYI

Uncertainties in Sea Ice Freeboard Introduced by Ice Surface Roughness

- GSFC = Gaussian model, CPOM TFMRA70 = Threshold70+Peaks, and AWI TFMRA50 = Threshold50
- Threshold70+Peaks produces thinner freeboards than LARM, largely bc of the ~16cm bias deducted from all sea ice elevations to sea level (Tilling et al. 2018)
- Threshold50 produced freeboards within 2cm of LARM/Gaussian model over FYI, but over MYI freeboards are 2-12cm (5-25%) higher than the physical retrackers
- Between the 4 algorithms, with all steps of the processing chain equal except for the retracking method, March radar freeboards have an avg uncertainty of 15% FYI and 29% MYI

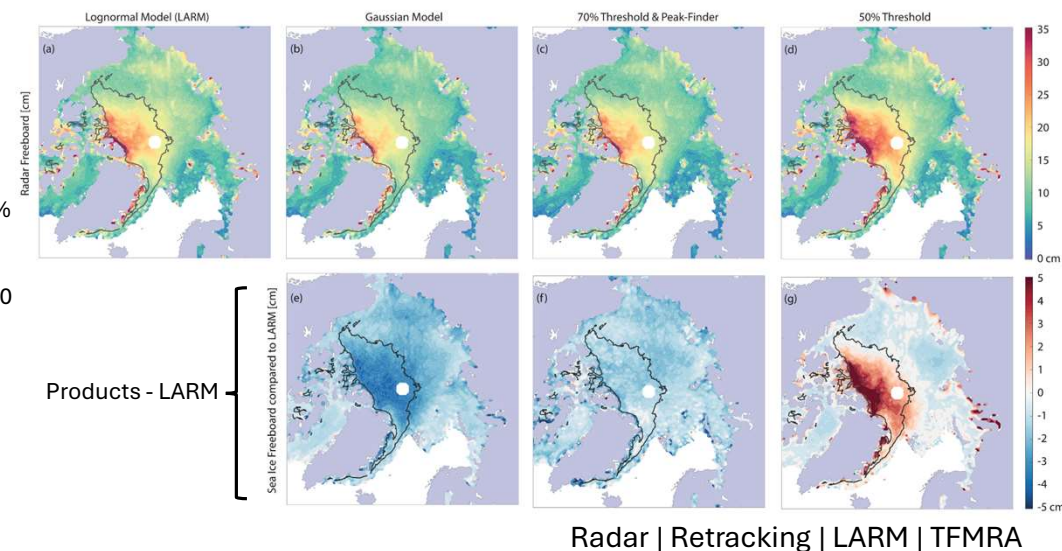
Independent Validation of Sea Ice Freeboard Retrievals

- Comparing 25km gridded averages w/OIB → CS2 sea ice fb computed w/OIB snow depths

- Mean sea ice freeboard differences (RMSEs) w/OIB:
 - LARM → -0.3 cm, 3.3 cm
 - Gaussian → -2.1 cm, 3.9 cm
 - Threshold70+Peaks → -2.0 cm, 4.1 cm
 - Threshold50 → 1.1 cm, 3.8 cm
- Variability in ice freeboards derived from each method is more than 3X larger over MYI than FYI

Discussion and Conclusions

- For TFMRA, there is a limit on how thin ice freeboard can be, but with LARM the RP can be >95% which allows ice freeboards of 2.5 cm (~25cm SIT) to be detected
 - This reduces the impact of a freeboard-floor, which can lead to + bias in estimates
- Mean SIT differences w/LARM:
 - Gaussian → 15 cm lower (FYI), 19 cm lower (MYI)
 - Threshold70+Peaks → 14 cm lower (FYI), 9 cm lower (MYI)
 - Threshold50 → 1 cm lower (FYI), 17 cm larger (MYI)
- Systematic uncertainties due to retracking can bias SIT estimates up to 20% (FYI) and 30% (MYI)
 - For FYI, this is the 2nd most dominant source of uncertainty behind basal salinity
 - For MYI, this is the most dominant source of uncertainty
- In general, winter sea ice freeboards are higher in the MYI zone and lower in FYI zone for LARM than the other products, and LARM SITs are larger → except w/Threshold50



Synoptic Variability in Satellite Altimeter-Derived Radar Freeboard of Arctic Sea Ice

Introduction

- Increasing snow mass → reduces freeboard → thus, if full Ku-band penetration to s-i interface, there should be a short-term negative correlation btw snow accumulation and freeboard
 - This is what they investigate w/CS2 (uncorrected) radar freeboards

Data and Methods

- CS2 CPOM product and CS2 LARM product → both over 2010-2020
- Combined CS2, Sentinel 3a/3b (CS2S3) radar freeboard datasets → to increase track density
 - CS2S3 w/CPOM retracker and CS2S3 w/LARM retracker
- All four radar freeboards binned to 25 km, then daily resolution datasets created from a 9-day moving window using optimal interpolation
- SMLG ERA5 snow depths, ERA5 snowfall, ERA5 2m air temps, and ERA5 h/v wind speeds
- Radar freeboards compared w/snow depth, snowfall, air temps, and wind speeds by producing daily mean and 31-day running mean of each dataset for each grid cell
 - Daily anomalies computed as difference between 31-day running mean and daily mean
 - Then, anomalies smoothed w/9-day running mean (i.e., *smoothed anomalies*)
- Slope of linear regression btw smoothed anomalies of radar freeboard and snow depth used to calculate fractional penetration (a) → α calculated by normalizing observed ratio of radar freeboard change to snow accumulation (i.e., the slope)**
 - Perfect penetration of $\alpha = 1$ means slope is $-0.54\text{m/m} \rightarrow R = -1$
 - No penetration of $\alpha = 0$ means slope is $+0.71\text{m/m} \rightarrow R = 1$

Results

Using CS2 CPOM

- Of grid cells w/statistically signif. correlations in central Arctic, 50% of correlations are positive** and mean ratio btw radar freeboard change and snow accumulation is 0.07m/m
 - Of the remaining 50% negatively correlated cells, mean ratio was -0.07m/m
 - In the marginal seas, 66% of statistically significant grid cells showed positive correlation**
 - Mean ratio of 0.20 m/m in pos cells; remaining neg cells had ratio of -0.26 m/m
- Magnitude of correlations and spatial patterns consistent btw CS2 CPOM and CS2S3 CPOM
- CS2 CPOM and CS2 LARM are overall consistent in correlation coefficients and spatial patterns, but more positive correlations w/LARM**
 - For both, no negative correlations were found in the Greenland Sea**

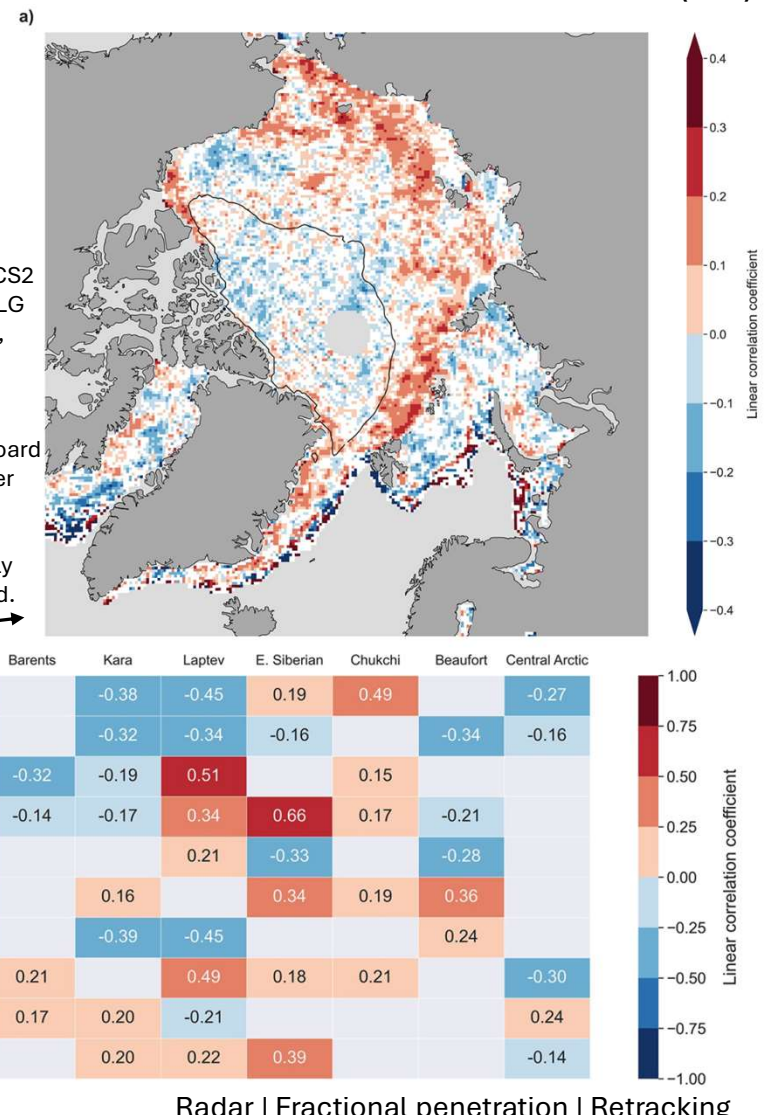
Discussion and Conclusions

- They generally find Ku-band radar penetrate deeper at low temps, in line w/Willatt et al. (2011)
- Correlations between radar freeboards and meteorological conditions cannot fully explain sensitivity of radar freeboard estimates to snow accumulation → snow properties (e.g., roughness, salinity, grain size) determine the variability in radar freeboard returns
- Varied response in radar freeboard to snow accumulation, → consistent, full Ku-band penetration to the snow-ice interface is unlikely**

- Short-term changes in freeboard likely reflect changing snow properties rather than changing height of s-i interface**

Fig. 1: Correlation btw smoothed anomalies of CS2 CPOM freeboard and SMLG snow depth over Oct-Apr, 2010 to 2020.
 (b) Regional correlation between smoothed anomalies of radar freeboard and snow depth per winter season.

For both, only statistically significant results colored.



Interdecadal changes in snow depth on Arctic sea ice

Webster et al. (2012)

Introduction

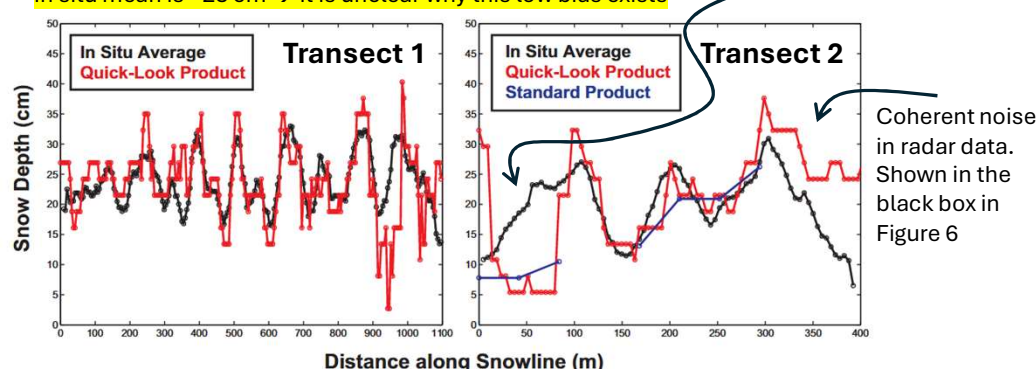
- ATOW: Interdecadal changes of snow depth on Arctic sea ice haven't been adequately addressed
 - Before this study, only W99 existed

Data

- Snow depth measured with University of Kansas ultrawideband frequency-modulated continuous wave (FMCW) snow radar using the 2-8 GHz frequency range (S and C band)
 - Footprint: 14.5m along track and 11m across track on level sea ice → processing (limiting speckle noise) reduces along-track resolution to 40m
 - Frequency changed over life of OIB, so range resolution varies from 5 cm (2009-2011) to 4cm (2012-2013)
- IceBridge standard product: 2009-2013, the Quicklook Product (2012-2013) slightly differs
- In situ data from BROMEX field campaign near Barrow, Alaska → two ground transects made underneath flight path in an area of level, undeformed FYI covered by drifted snow
 - Estimated error for an avg of 16 measurements per radar footprint was 1.4cm
- Analysis focuses on March – April, 2009-2013
- IMB buoy data also used and compared w/W99 climatology
- Snow depth interpolation method is same as W99 → 2D quadratic equation
- Analysis limited to western Arctic where OIB and Soviet drift stations overlap
- With all data combined, decadal change in snow depth can be estimated from 1950-2013
 - W99 (1950-1987), IMB (1993-2013), and OIB (2009-2013)
- PMW product used for freeze up over 1979-2012 from Goddard

Results – IceBridge Validation

- RMSE btw IceBridge quick-look and in situ averages was 5.8 cm, consistent w/estimated uncertainty of 5.7 cm for 2009-2011 IceBridge standard products → overall, OIB agrees w/in situ
- OIB product underestimates thin snow depths → in transect 2, OIB estimates are ~5-8cm whereas in situ mean is ~23 cm → it is unclear why this low bias exists



Results – Climatology

- Marked decrease in snow depth from 2009-2013 compared to the 1937, 1954-1991 climatology; average snow depth of $35.1 \pm 9.4\text{cm}$ observed in W99, while 2009-2013 average was $22.2 \pm 1.9\text{cm}$, suggesting a thinning of $37 \pm 29\%$
 - Most pronounced change in Beaufort/Chukchi Seas of $56 \pm 33\%$
 - Trend of -0.29cm/yr w/99% significance

Results – Accumulation Rates and Freezeup

- IMB buoys and Soviet Ice Station data compared to examine changes in accumulation rates
- Differences in accumulation rates were not large enough to explain observed decrease in snow depths across the western Arctic → annual snow accumulations comparable btw IMB/W99
- Correlation btw freeze up and snow depth is -0.68 over 2009-2013, versus -0.23 for 1979-1991 period, indicating that delayed freeze up may significantly contribute to decrease in snow depth
 - Since correlation is not -1, this indicates that other factors play a role, such as atm patterns /sea ice motion, deformation, and snow redistribution
- They estimate delay in freezeup results in $4.5 \pm 1.2\text{cm}$ total loss in western Arctic and $12.8 \pm 2.4\text{cm}$ in Beaufort/Chukchi Seas → results within the errors of differences btw W99 and IceBridge results
- Modeled surface heat flux through young ice over 2009-2013 is $79-85\text{ W m}^{-2}$, versus $43-49\text{ W m}^{-2}$ for young ice over 1954-1991 → sea ice can grow faster w/reduced snow insulation
 - Reduction in p_s in fall (less time for densification) has minimal effect ($\sim 1\text{ W m}^{-2}$)

Conclusions

- OIB agrees w/in situ snow depths, indicating it can measure snow accurately
- Marked reduction in snow depth, likely driven by delayed freeze up in fall
- Reduction in snow depth leads to 2X heat flux through young ice due to less insulation

Impressions

This is a good reference to cite when discussing interdecadal trends (decreases) in snow cover.

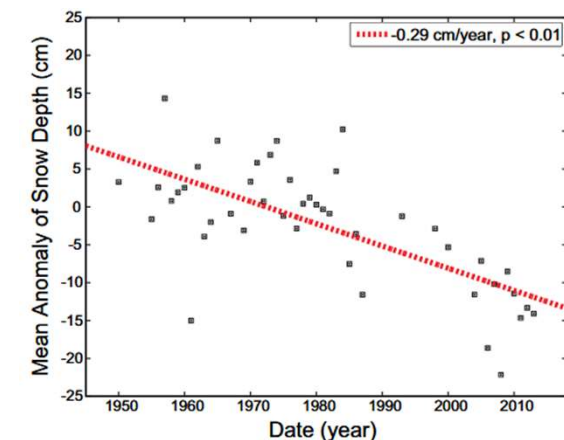


Figure 9. The decadal change in snow depth in spring. The anomalies were calculated using data from Soviet drifting ice stations (1950–1987), Ice Mass Balance buoys (1993–2013), and the Operation IceBridge snow depth products (2009–2013). The anomaly is the measurement minus the W99 multiyear average in spring at that location. The average of the anomalies for each year is shown by black squares, and the red line represents the trend in centimeters per year. For measurements within the western Arctic only, the trend was -0.27 cm/yr with 99% significance.

Radar | IceBridge | Snow depth | W99 | IMB |

Optimising Interannual Sea Ice Thickness Variability Retrieved From CryoSat-2

Introduction

- Follow on from synoptic variability paper, focusing on fractional depth of CS2 backscatter
- The focus is where the returned radar waves backscatter from, not where they penetrate to, as they may be absorbed or scattered w/o returning
 - $\alpha = 1 \rightarrow$ scattering from s-i interface; $\alpha = 0 \rightarrow$ scattering from a-s interface
- SIT retrievals generally have low bias due to competing biases canceling out in processing chain
 - They argue that instead of tuning to reduce bias, we should also be tuning to optimize the interannual variability in SIT

Data

- FSOO ULS moorings F11-F14 over 2010-2019; BGEP moorings 2010-2021 at A/B/D
 - Drafts converted to monthly averages
 - They use hydrostatic equilibrium equations rather than fixed conversion factor to estimate freeboard and SIT \rightarrow interesting...?
- SMLG for snow depth/density
- CS2 observations within 25 km of moorings are averaged monthly over Oct-Apr, 2010-2021
 - Retracker varied from 5-95% w/increments of 2.5% for sea ice surfaces
 - For leads, retracker kept to the 50% value specified by AWI processing
- Sea ice freeboard estimate: $F_t = F_r + (\alpha \frac{c}{c_s} - 1) h_s$

Methods and Results

- R^2 for CS2 products including interannual variability and ULS moorings are lower than the R^2 between CS2 products that are averaged across all years (i.e., no interannual variability) and ULS
 - When they replicate this[^] but just for a single month, R^2 is markedly reduced as the CS2 products fail to capture interannual variability
- Lowest mean bias values achieved using TFMRA 20-50% depending on α value
 - But you can tune to reduce bias at all TFMRA and α , indicating that the best combo of threshold and α can't be determined by an analysis of bias alone
 - Thus, assess how well CS2 captures interannual variability w/these two params
 - Thus, they do a comparison of monthly anomalies btw CS2 and ULS
- Lowest RMSEs (0.35–0.4 m) at TFMRA 70%–85% and $0.4 < \alpha < 0.75$
 - Optimal α is never 1 at any given threshold
- No combinations of α and TFMRA that effectively minimize bias lead to skillful estimate of variability \rightarrow a clear tension btw these two tuning techniques
- FYI \rightarrow lowest RMSEs are found at thresholds of 60%–85% when assuming $0.35 < \alpha < 0.8$
 - MYI \rightarrow lowest RMSEs are found at thresholds of 50%–75% and $0.25 < \alpha < 0.55$
 - Motivates usage of ice-type dependent retracking

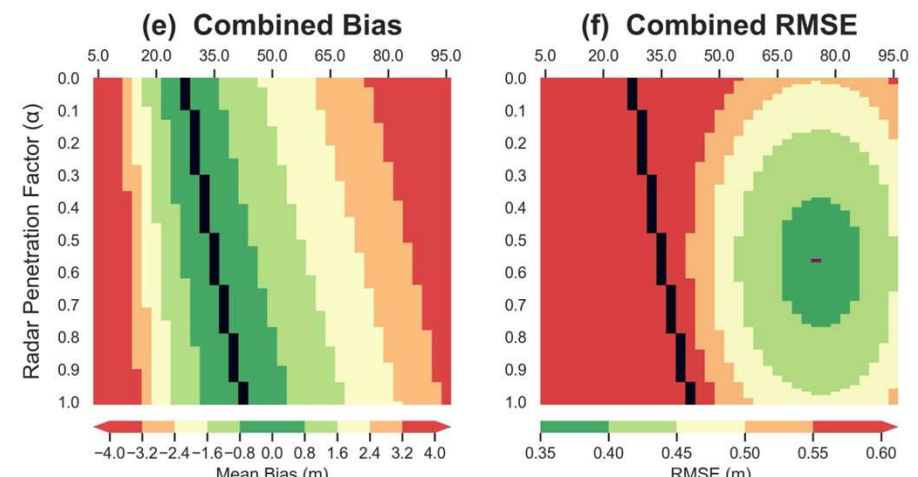
Discussion and Conclusions

- Higher interannual skill of α , with $0 < \alpha < 1$ indicates mean scattering horizon is neither s-i or a-s interface, but somewhere within the snow pack

- Optimal threshold/ α combo of 70-85% and $0.4 < \alpha < 0.8$,
 - But they find no perfect combination of threshold and α
- At optimal thresholds, however, there is generally a bias $> 2.5\text{m}$ and the skill in representing interannual variability is not statistically significant
- Perhaps choice of how to tune depends on purpose: for absolute values of SIT \rightarrow reduce bias, but you can also tune to best capture interannual variability if this is your focus
- Results suggest lower TFMRA better over MYI than FYI, in agreement w/LARM
- Changing ice density/snow depths had no appreciable impact on results \rightarrow bc of averaging?

Impressions

- Interesting study, but I have some issues/questions with it. First, there should have been a robust uncertainty analysis as they are, for example, assigning ice ages to monthly estimates over (at least) 25 km grid cells in regions like FS of varied ice types. I wonder why they convert draft to freeboard and SIT using hydrostatic equilibrium equations instead of Vinje and Finnekasa conversion factor \rightarrow what uncertainties does this introduce by having to assume parameter values like ice density?



Mean bias (left) and RMSE (right) between anomalies of SIT derived from CS2 and moorings. "Combined" refers to the fact that this is for BGEP and FSOO moorings. Black line shows threshold value where biases is minimized for a given value. Notice in (f), that the threshold/ α value that minimizes bias doesn't maximize skillfulness in capturing interannual variability

Radar | CS2 | ULS | Partial penetration | Interannual variability

Estimating Arctic sea ice thickness and volume using CryoSat-2 radar altimeter data – Part 1 (Methods)

Tilling et al. (2018)

Introduction

- End-to-end description of the processing steps to generate the CPOM CS2 product

The CryoSat-2 Satellite

- SAR: Across-track footprint is just the antenna-limited footprint, but the along-track footprint is pulse-limited and smaller than the antenna-limited footprint
- SAR: only uses one antenna for transmit/receive, but emits 64 phase coherent pulses in a burst as opposed to a single pulse w/LRM
 - Exploiting the slight frequency shifts due to Doppler effect allows the processor to separate the burst into separate beams along track with finer spatial resolution
- The beams from each burst are made to overlap with the beams from other bursts in exact coincidence by adjusting the look angle of the central beam (and in turn the other beams)
 - Over multiple bursts, each location is sensed multiple times giving us “multiple looks” at the same location which are then combined to form a “stack”
 - Standard deviation of multiple looks == stack standard deviation (SSD)
 - This takes advantage of different incidence angles w/each look
 - The waveforms from each stack are averaged into one composite 20 Hz waveform
 - Delay time and power of the individual “looks” has dependence on look angle, thus slant range correction applied, and power weighted depending on look angle

Data

- CS2 L1b data – instrument, but not geophysical, corrections applied automatically to L1b data
 - Range window is ~60 m, which corresponds to 256 range bins in the waveform data
 - SAR and SARIn data used, but phase info discarded for SARIn
- NASA GSFC SIC gridded 25km product and OSI SAF sea ice type
- Sever expedition in-situ data of freeboard, SIT, and snow depth from 1982-1988
- mW99 mean snow depths for each month in central Arctic applied to all sea ice observations

Sea Ice Thickness and Volume Processing Method

- Waveform discrimination: specular echoes defined as PP > 18 and SSD < 6.29 (<4.62) in SAR (SARIn) mode; diffuse echoes defined as PP < 9 and SSD > 6.29 (>4.62) in SAR (SARIn) mode
 - Echoes w/PP btw 9-18 are considered complex and are discarded
 - $PP = \frac{P_{max}}{P_{mean}}$
- Echoes over regions w/SIC > 75% considered ice floe regions, SIC=0% open ocean
 - Echoes from regions w/SIC between 0-75% are omitted (34% of data Oct-Apr)
- Processing only runs for October-April, so wintertime retrievals only
- Giles et al. (2007) retracking method for leads → two functions used to describe shape of specular echo (Gaussian func for leading edge, exponential decay for trailing edge)
- Diffuse echoes smoothed w/3pt moving avg before retracking using TFMRA70
 - Threshold applied to first peak (that's $\geq 20\%$ of max peak), not max peak to prevent off-nadir lead snagging

- Leading edge width, $W_{le} = (b_{70} - b_{30})$, used to ID complex leading edge rises → b_{70} and b_{30} are the range bins corresponding to TFMRA70/30
 - Waveforms w/leading edges larger than 3 bins are omitted
 - Likely due to off-nadir reflection from leads or heavily deformed ice
- Elevation, E, of lead/floe computed using: $E = A - R_0$, where E is elevation above WGS1984 ref ellipsoid, A is satellite altitude, and R_0 is range of satellite to surface
 - $R_0 = R_n + C_G + C_R$ where $R_n = \frac{ct_n}{2}$ and $C_R = (b_0 - b_n)\Delta_b$
 - R_n is range of satellite to surface presented by the nominal tracking bin
 - t_n is two-way travel time represented by nominal tracking bin
 - C_G represents geophysical corrections applied
 - dry tropospheric, wet tropospheric, inverse barometric, modelled ionospheric, ocean tide, long period equilibrium tide, ocean loading tide, solid earth tide, and geocentric polar tide.
 - C_R is the retracking correction → accounts for the fact that the bin returned by retracking differs from the nominal tracking bin of CS2 (bin 128 w/SAR I think)
 - b_0 is the bin number returned by the lead or floe retracker
 - b_n is the bin number of nominal tracking bin and Δ_b is bin width (0.2342m)
- 16.26 cm bias introduced by using different retrackers for diffuse/specular returns, so this is removed from all elevation measurements
- Ocean elevation determined by linearly interpolating leads over 100 km area and then this is subtracted from ice floe elevation to get uncorrected radar freeboard
- Sea ice freeboards outside -0.3m to 3m range discarded
- SIV is the product of SIT, fractional SIC, cell area, SIE mask, and fraction of cell that's ocean
- Cell fraction of FYI (F_f) and MYI (F_m) computed as $F_f = \frac{h_f}{h_f + h_m}$ and $F_m = \frac{h_m}{h_f + h_m}$ where h_f and h_m are total FYI/MYI thickness falling within a cell

Estimation of uncertainties

- p_i uncertainty estimated to be 7.6 kg m^{-3} → used in-situ estimates from Sever to solve hydrostatic eq. equations for p_i → seems far too low, although they say its likely an overestimate
- Freeboard uncertainty estimated to be primarily due to radar speckle, w/stdev of 9 cm
 - Not factoring in s-i interface uncertainty here
- After gridding monthly data, freeboard uncertainty is ~2cm, scaling to ~20 cm in SIT
- They focus on random errors w/freeboard retrievals, not discussing systematic errors

Impressions

- Excellent description of CS2 SAR – much more understandable than Wingham paper
- Uncertainty analysis is lacking → uncertainties seem to small and focus is on only random uncertainty and not systematic uncertainty. For example, they don't even consider the uncertainty introduce by partial penetration

Estimating Arctic sea ice thickness and volume using CryoSat-2 radar altimeter data – Part 2 (Results)

Tilling et al. (2018)

Table 1

The sea ice volume error budget. The October and April error columns give a value for the Arctic-wide error, with respect to the mean value, for each significant error source. The October volume error and April volume error columns show the contribution of each source to the total estimated sea ice volume error. These are then combined in a root-sum-square manner to give an estimate of the total monthly sea ice volume error.

Factor	October error	October volume error	April error	April volume error
Snow Depth	23.3%	10.3%	19.5%	9.0%
Snow Density	30.4%	6.9%	21.6%	5.5%
FYI Density	0.8%	6.1%	0.8%	6.7%
MYI Density	0.9%	6.1%	0.9%	6.7%
Sea ice concentration	5.0%	4.5%	5.0%	3.4%
Inter-annual ice extent	0.4%	0.25%	0.2%	0.15%
Seasonal ice extent	14.7%	8.4%	0.4%	0.25%
TOTAL (root-sum-square)		14.5%^a		13.0%^a

^a Excluding errors in seasonal ice extent.

Results and discussion

- Monthly gridded SIT estimates on 5 km grid from 2010-2017
- Average autumn SIT ~1.28 m, increasing to ~1.94 m in spring
- Validation of CS2 SIT estimates: comparison with OIB (2011-2014), EM from CryoVex campaign (2010-2012), and BGEP ULS estimates (2010-2013)
 - OIB and CryoVex EM data gridded to 0.4° by 0.4° grid
 - Monthly averages of CS2 draft estimates taken within 100km of BFEP moorings and compared w/monthly draft averages from moorings
- CS2 estimates agree w/OIB, CryoVEx, and BGEP measurements of SIT, ice + snow thickness, draft to within 0.5, 21.0, and 10.0 cm on average, respectively
- "When combined, the average difference between the OIB, CryoVEx, and BGEP estimates of ice thickness and those derived from CryoSat-2 is 2 mm."
 - "we conclude that there is no significant bias in the satellite data"
- MYI is the most variable ice type w/respect to SIV → drives interannual variability
 - FYI drives seasonal variability

Conclusions

- Main contributors to uncertainty in retrieval are snow depth and snow density, each monthly contributing an average of 10% and 6% to the total estimate SIV error, respectively
 - These contributions are likely an overestimate, they state
- Overall, CS2 SIT and draft estimates agree within 2 mm of in airborne/ocean-based platforms

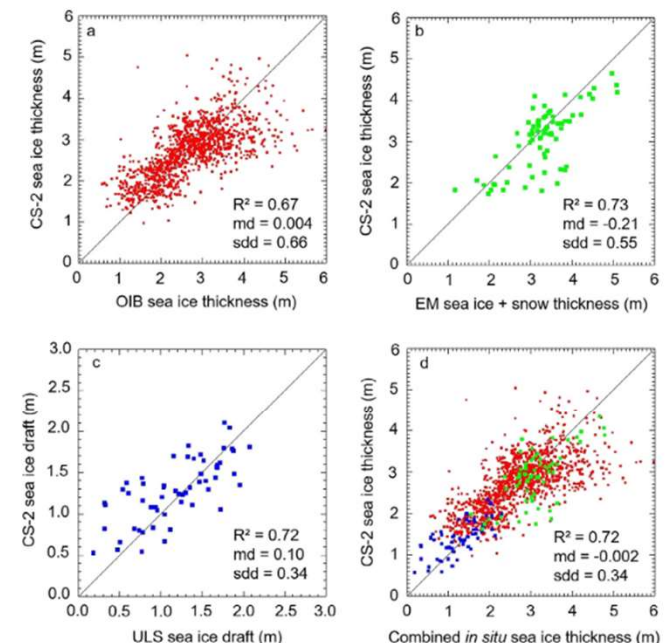


Fig. 16. Evaluation of CryoSat-2 (CS-2) sea ice thickness estimates. (a) Comparison of Operation IceBridge (OIB) and CryoSat-2 ice thickness for March and April 2011–2014. (b) Comparison of CryoVEx electromagnetic (EM) and CryoSat-2 ice plus snow thickness for March and April 2011 and 2012. (c) Comparison of monthly average ice draft from the Beaufort Gyre Exploration Project (BGEP) upward looking sonar (ULS) buoys with monthly average CryoSat-2 ice draft from within 100 km of each mooring, for October–April 2010/11–2012/13. (d) Comparison of ice thicknesses estimated from all three *in situ* datasets and from CryoSat-2. Values for the mean difference (md) and standard deviation of the difference (sdd) are expressed in metres.

Retrieval of Snow Depth on Arctic Sea Ice From Surface-Based, Polarimetric, Dual-Frequency Radar Altimetry

Willatt et al. (2023)

Introduction

- Investigating whether combo of KuKa polarimetric radar can be used to estimate snow depth, using the KuKa instrument from the MOSAiC expedition

Methods

- KuKa fully-polarimetric (VV, HH, HV, and VH) radar in nadir “stare” mode mounted on a sled-borne pedestal and towed at a rate of 1-3 m/s along transects ~800-1200m in length
- MagnaProbe used to estimate in-situ snow depth every 1-3m, collected within 1-2hr of KuKa
- Snow density derived from Snow Micro-penetrometer (SMP) and density-cutter measurements HH and VH used in this study, as HH is polarization used by SIRAL and SARAL AltiKa
 - VH means V receive, H transmit
- “Sub-banded data” is representative of CS2 SIRAL and ALtiKa → full bandwidth of KuKa not used
- For Ku and Ka w/HH polarization, primary scattering interface is the a-s interface**
- Comparison w/MagnaProbe snow depths suggests that peak VH scattering occurs at s-i interface**
- Range to a-s interface determined using full bandwidth HH, as the sub-banded data (which they used to match SIRAL bandwidth) is too coarse
 - Starting at 1m and increasing in range, once power > -50 dB (Ku) or >-55dB (Ka), highest amplitude peak within next 10 cm (Ku) or 6 cm (Ka) was taken as a-s interface
 - Averaging over all waveforms, highest amplitude peak (overall) was at a-s interface for 74.9% and 74% of HH echoes, and 1.1% (Ku) and 0.3% (Ka) of VH echoes
- Three techniques used to estimate snow depth:
 - (1) Polarization technique:** snow depth estimated as difference btw HH and VH ranges
 - Two differences computed: (a) diff in ranges of highest-power peaks of VH and HH btw 1-3m and (b) diff in waveform centroids btw VH and HH
 - (2) Frequency techniques:** using only HH data, they compute the differences in (a) highest amplitude peaks and (b) centroids from the Ku and Ka band HH
 - (3) Waveform shape techniques:** compute differences in ranges to highest amplitude peak and waveform centroid of each HH waveform, for both frequencies
 - Idea here is that deeper snow could lengthen trailing edge of the echo

Results

- Polarization : KuKa-derived snow depths agree overall, but Ka-derived are smaller than Ku-derived
 - KuKa has higher # of snow depths < 0.05m and longer tails than the MagnaProbe
- Polarization techniques provided the best estimates of snow depth, with R² values varying between 0.66 and 0.77 for full bandwidth data and between 0.62 and 0.67 for sub-banded data**
 - Mean MagnaProbe snow depths were ~20 cm in areas where Ku-band data were gathered, and Ku-band snow depths derived using polarization technique were 23 and 20 cm for polarization peaks and centroid approaches for full bandwidth data, respectively.
 - 27 cm and 23 cm for sub-banded data

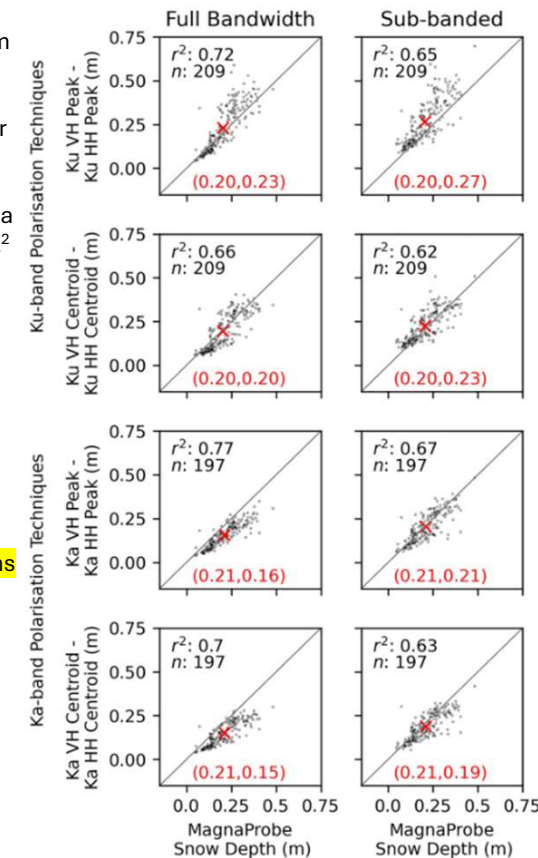
- Mean MagnaProbe snow depths were ~21 cm in areas where Ka-band data were gathered, and Ka-band snow depths derived using polarization technique were 16 and 15 cm for polarization peaks and centroid approaches for full bandwidth data, respectively.
 - 21 cm and 19 cm for sub-banded data
- Frequency techniques performed worst**, w/R² reaching 0.15 for Ku-Ka centroids w/sub-banded data and 0.01 for Ku-Ka peaks using full bandwidth data → snow depths at least 4X too small
- Waveform shape method better than frequency technique, but not as good as polarization**

Discussion

- Combining co-polarized w/cross-polarized data (“polarization technique”) provides a promising technique to estimate snow depths
 - Polarization technique w/Ka-band performed best in relation to MagnaProbe snow depths for either full-bandwidth or sub-banded data
- Primary scattering interface of Ku and Ka band was a-s, meaning the frequency differencing technique performed poorly → snow was cold, dry, and not saline as well
- “However, caution must be used when extrapolating to satellite scales”
 - Future work is needed on upscaling approaches to consider different footprint sizes and viewing geometries

Conclusions

- Polarimetric radar altimetry shows promise for estimating snow depth**, however there are no currently planned polarimetric satellite missions planned
- Simply differencing Ku and Ka band returns is unlikely to yield good snow depth measurements**



KuKa-derived snow depths (y axis) vs. MagnaProbe snow depths (x axis). Means provided in red text.

Effect of Snow Salinity on CryoSat-2 Arctic First-Year Sea Ice Freeboard Measurements

Nandan et al. (2017)

Introduction

- This is the first study to investigate the role of snow salinity on Ku-band radar penetration
- During formation of seasonal ice, some brine is expelled upward and then this is wicked into the first 6-8cm of the snowpack → this occurs primarily over FYI, not MYI
 - Ku-band through MYI generally has better penetration to s-i interface than FYI

Data and Methods

- CS2 AWI TFMRA50
- Field data from FYI collected over 9 campaigns in CAA from April-May, 2004-2017
- Brine volume (Ψ_{bs}), penetration depth (δ_p), and the main scattering horizon (S_H) are modeled
- Snow salinity correction factor, Δ_s , included in freeboard retrieval equation:

$$h_{fi} = h_{fi}^{CS2} + C_W + \Delta_s$$
 where C_W is the correction for reduced propagation speed through snow
 - $\Delta_s = H_s - S_H$ where H_s is snow height and S_H is the main scattering horizon
 - Thus, Δ_s is the expected vertical shift in scattering horizon due to snow salinity
- SMOS (L-band radiometer) used as complementary FYI SIT retrievals as CS2 limited to ice > 0.5m
- Relative error, E_R , expressed as ratio between SIT uncertainty and SIT

Results and Discussion

- Brine gradient → brine volume decreases away from s-i interface
- For snow depth ≤ 8 cm, the snow is usually found to be completely brine-wetted
 - For snow depth ≥ 8 cm, brine volume follows a gradient
- For $H_s \leq 8$ cm, Δ_s (shift in scattering horizon) is upwards, within 2 cm of snow surface
- For $10 \text{ cm} \leq H_s \leq 24$ cm, $\Delta_s = 7$ cm and for $H_s \geq 26$ cm, $\Delta_s = 6$ cm
 - Given the consistency in the shift of the scattering horizon above 10 cm, which is expected given brine wetted snow is generally within bottom 6-8 cm of the snowpack, they can compute an average adjustment factor of $\Delta_s = 7$ cm for $H_s \geq 8$ cm
- For 16cm snow layer, in cold, nearly brine-free conditions ($\Psi_{bs(-1\sigma)}$), TFMRA50 retracks to 15 cm
 - In highly brine-wetted snows ($\Psi_{bs(+1\sigma)}$), TFMRA50 retracks to 3-4 cm under a-s interface
- SMOS error is high when SIT > 0.35m, whereas CS2 error is high when SIT < 0.95m → limited confidence in SIT retrievals between 0.35-0.95m
- At SIT = 1.6m, relative error is the same regardless of whether snow-salinity correction is applied
 - As SIT decreases, though, retrievals with Δ_s adjustment have significantly reduced errors
 - 30% error vs. 19% error at SIT = 0.95 m (11% reduction)
 - 55% error vs. 30% error at SIT = 0.7 m (25% reduction)

Conclusions

- Important to know that these are modeling results → for example, the theoretically derived main scattering horizon for CS2
 - But, the thermophysical properties used in this study are from in-situ data
- Need for in-situ validation of modeled results, but they demonstrate huge impact of salinity
- Average adjustment factor of $\Delta_s = 7$ cm for $H_s \geq 8$ cm over FYI

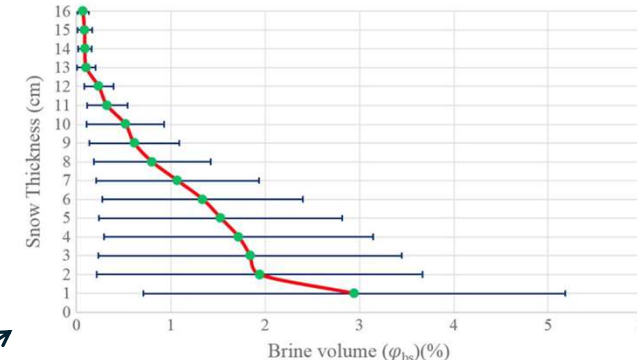


Figure 1. Mean brine volume (φ_{bs}) as a function of snow thickness for 16 cm snow covers on FYI. The error bars $\varphi_{bs(-1\sigma)}$ and $\varphi_{bs(+1\sigma)}$ represent one standard deviation ($\pm 1\sigma$) from the mean φ_{bs} . The snow/sea ice interface is located at 0 cm on the y axis.

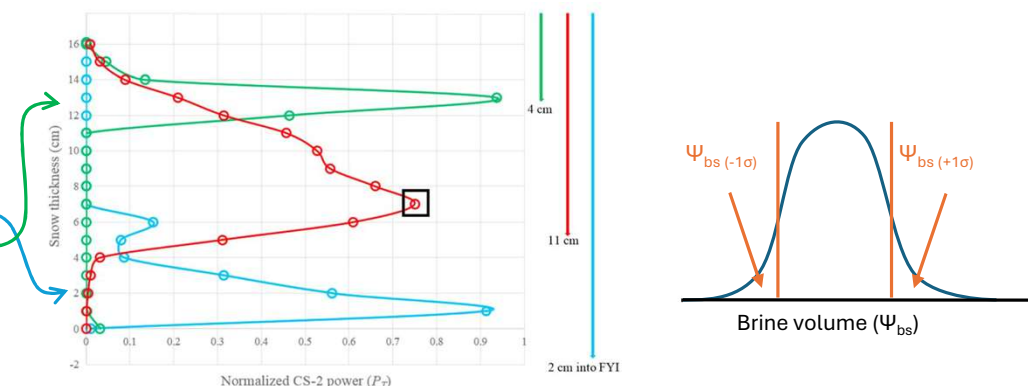


Figure 3. Simulated normalized echo power for 16 cm snow covers on FYI. The green, red, and blue lines represent power values for the distributions of $\varphi_{bs(+1\sigma)}$, φ_{bs} , and $\varphi_{bs(-1\sigma)}$, respectively. The downward green, red, and blue arrows indicate the maximum penetration depth for $\varphi_{bs(+1\sigma)}$, φ_{bs} , and $\varphi_{bs(-1\sigma)}$, respectively. The black square represents the S_H for φ_{bs} . The snow/sea ice interface is located at 0 cm on the y axis.

Snow Property Controls on Modeled Ku-Band Altimeter Estimates of First-Year Sea Ice Thickness: Case Studies From the Canadian and Norwegian Arctic

Introduction

- Builds on Nandan et al. (2017) by investigating the impacts of snow temperature, salinity, and density on Ku-band freeboard retrievals

Snow and Sea Ice Properties

- Ten case studies from CAA/Norwegian Arctic that all have estimates of snow density (ρ_s), snow salinity (S_s), and snow temperature (t_s)
- CAA samples span period May 1993–2015 and Norwegian samples from March 2015/2017
- Snow depth (H_s) group into thin (<10 cm), medium (10–30 cm), and thick (>30 cm) classes
- Temperatures classified as cold (C, mean $t_s \leq -10^\circ\text{C}$) and warm (W, mean $t_s \geq -10^\circ\text{C}$)
- All 3 thin snow cover cases were completely saline
- 8/10 cases had (a) top snow layer of fragmented precip particles, (b) wind slab layer, and (c) depth hoar layer
- Data → in-situ magnaprobe measurements, drill holes, EM device for SIT estimates, OIB snow radar and ATM, and then gridded monthly CS2 data from March 2015 over Norwegian sites
 - No airborne/satellite data over CAA, only Norwegian sites

Methods

- Same modeling of scattering horizon as Nandan et al. (2017)
- In this study, they use ∇ to represent the snow property correction factor which accounts for vertical shift caused by $\rho_s/t_s/S_s$, whereas Δ_s in previous 2017 study just accounts for S_s
- C_W = correction factor accounting for propagation delay through snow layer
- $T_{FYI(F_R)}$ = the predicted altimetry-derived SIT, $T_{FYI(M)}$ = measured SIT w/drill holes

Results and Discussion

- Local scale observations were representative of regional scale snow/ice properties
- Warmer snow temperatures shift scattering horizon up regardless of brine volume present
- SITs derived w/OIB data (snow radar + ATM) and simulated CS2 freeboards result in SIT overestimates of 95% and 47%, respectively
 - Largely due to the presence of a saline basal snow layer and 1/3 of the ice being flooded
- Errors in SIT are largest over warm, saline snow covers overlying thin FYI, with error decreasing with increases in FYI thickness and colder temperatures
- At $340 \text{ kg m}^{-3} \leq \rho_s \leq 440 \text{ kg m}^{-3}$, ∇ is 1 cm and 3 cm for -15°C and -5°C snowpack, respectively,
 - When $\rho_s \geq 440 \text{ kg m}^{-3}$, ∇ increases to 5 cm and 11 cm at -15°C and -5°C , respectively
 - SIT overestimated by 70% (30%) when $\rho_s \geq 440 \text{ kg m}^{-3}$ and $t_s = -5^\circ\text{C}$ ($t_s = -15^\circ\text{C}$)
- There is a need to have a propagation delay correction factor that is a function of snow depth and brine volume
 - 51% reduction in Ku-band propagation speed through saline snow covers than dry snow covers → largest reductions up to 70% for warm, saline snow covers
- With warmer snow, snow grains are enlarged and we move from a Rayleigh to Mie scattering regime, which results in significant volume scattering that is currently not accounted for
- Current retracking algorithms assume volume scattering to be negligible

Conclusions

- High snow salinity and warm snow temperatures leads to higher brine volume and greater dielectric loss, which induces considerable Ku-band microwave absorption within the snow
 - This shifts principle scattering horizon away from the snow-ice interface
 - Leads to overestimates in sea ice freeboard and SIT
- The combination of saline basal snow layers + flooding leads to massive errors in SIT estimates
- Salinity is the dominant snow property affecting the accuracy of Ku-band freeboards and SIT
- Snow density mostly influences Ku-band penetration when $\rho_s \geq 440 \text{ kg m}^{-3}$ and snow is warm
- “Compared to current operational retracker algorithms, which use a 25% propagation delay factor, a 39% delay in radar propagation is estimated here from the mean of ten snow cases”

Nandan et al. (2020)

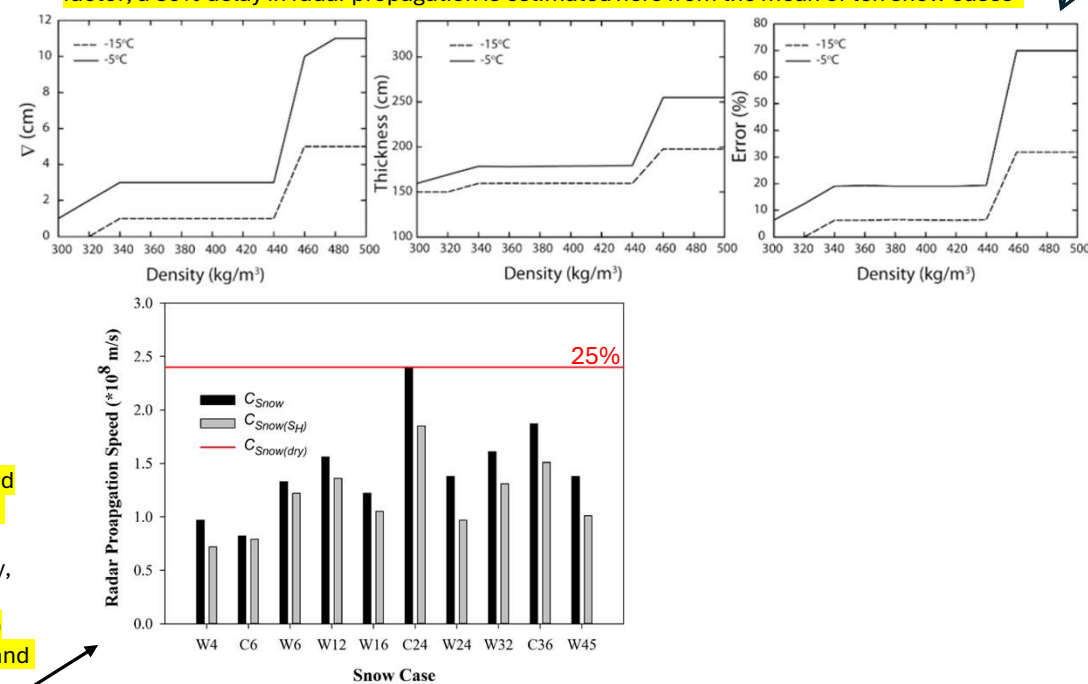


Fig. 11. Calculated speed of electromagnetic wave (C_{snow}) for the entire snow volume (black), and calculated speed ($C_{\text{snow}(S_H)}$) for the volume of snow between the air/snow interface and main scattering horizon S_H (grey), at $C_W = 0.25S_H$, for all snow Cases. The red line represents the reference speed of electromagnetic wave through a dry snow cover ($(C_{\text{snow(dry)}})$), after [59].

Radar | CS2 | Salinity | Temperature | Density | FYI

Wind redistribution of snow impacts the Ka- and Ku-band radar signatures of Arctic sea ice

Nandan et al. (2023)

Introduction

- This paper investigates how wind-induced changes to snow properties and topography affects Ku and Ka (KuKa) band radar signatures → KuKa deployed during the MOSAiC expedition
 - Radar is not satellite/airborne, but on the surface

Data and Methods

- KuKa range resolution of 1.5 cm (Ka) and 2.5 cm (Ku) due to large bandwidth
 - Scan angles: $\theta_{inc} = 0-59^\circ$, ~2.5min for a complete scan, footprints ~0.5-2m overall
- 10m meteorological tower captures temp, wind speed, humidity, etc... every 1 sec at 2m height
- Snow temps monitored w/thermal IR camera, other properties measured w/thermistors chains
- Snow surface roughness visualized using an optical camera within radar scan area and terrestrial laser scanner (TLS) data acquired a few times within/around the study period
- All KuKa waveforms overlaid w/TLS data to determine where radar backscatter came from
- Normalized radar cross section (NRCS) per unit area used as a metric to demonstrate radar backscatter variability during the two wind events (WE1 and WE2)
- They examine NRCS in 5° wide θ_{az} bins, called azimuth sectoring, to see how surface heterogeneity affects backscatter variability

Results

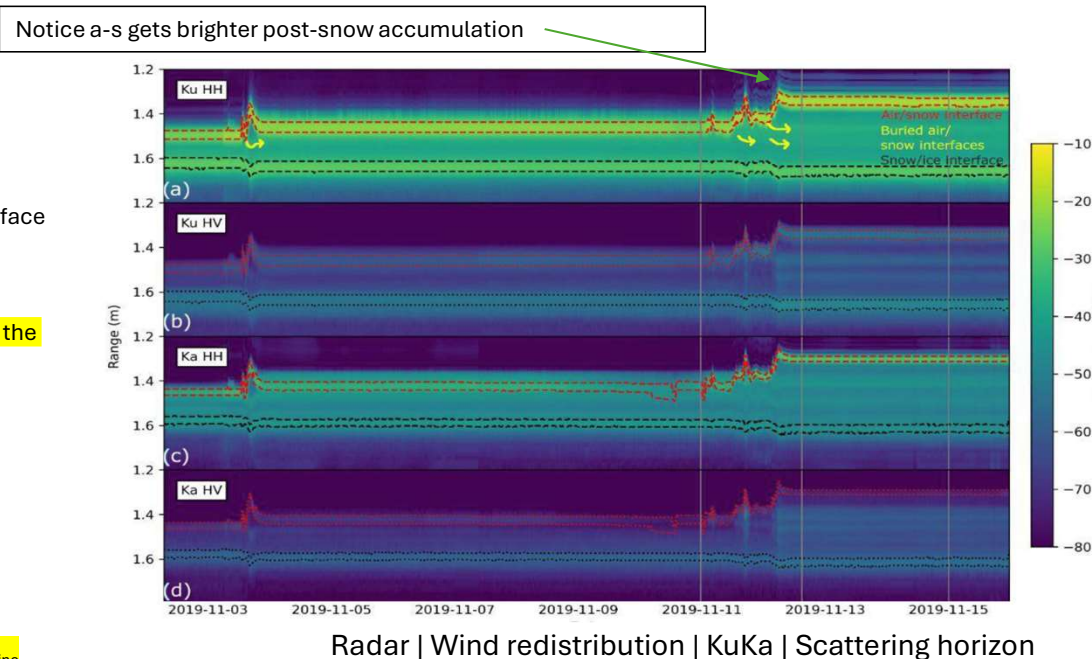
- WE1 → Nov 11-12, 12 m/s winds blowing SW to SE → temps from -32°C to -16°C
- WE2 → Nov 15-16, 15 m/s winds blowing SW to W → temps reached -4°C
- Temperature gradients indicate hoar metamorphism was occurring through the snowpack
 - This also played a role in increasing density of upper snow layers, but minimal
- Increased density in the upper 2cm of the snow layers over time**
 - Average ρ_s change at 3 sites: +31 kg m⁻³, +79 kg m⁻³, and +23 kg m⁻³
- Figure 5 shows images of how snow changed over Nov 9 -15 → significant changes in the surface topography in this area over just 6 days → this is also shown in Fig. 6 by the TLS plots
- Before wind events, radar backscattering quite stable for both Ku and Ka, w/peak power returning from a-s interface
- Despite snow being buried/redistributed, generally the previous a-s interface is still visible in the echograms for both Ku/Ka → indicates density contrasts within snow are important
- Quite evident that location of a-s interface changes over WE1 and WE2 → net upwards movement in response to snow deposition
- Prior to WE1, highest return power from mix of a-s and s-i interfaces for both Ku and Ka
 - During/after WE1/WE2, highest return power from a-s interface
- W/HH polarization the a-s interface is always the dominant scattering surface for Ku/Ka
 - W/HV polarization, it's the s-i interface for Ku/Ka but both are visible
- Peak power from interfaces much more evident at lower scan angles (e.g., nadir vs. 35°)
 - You get volume scattering at higher (more oblique) scan angles
- Overall, bulk of the peak power moves from the a-s to the s-i interface at all polarizations
- Spatial variability in backscatter in response to wind events evident at all polarizations and θ_{inc}

Discussion

- Pre-wind: dominant scattering at nadir for both Ku/Ka varies btw a-s and s-i based on local variations in snow surface roughness and density for HH/VV
 - For HV, dominant scattering interface varies w/snow depth
- Post WE1:** a-s scattering dominates at nadir for Ku/Ka at all polarizations due to smoothing of snow surface and increasing snow surface density
 - This could upwardly shift retracked elevation and bias sea ice freeboard
 - At larger incidence angles, s-i interface becomes more visible
- Retracking algorithms do not currently consider the leftward migration of the waveform leading edge due to the snow surface and buried (previous) a-s interfaces

Conclusions

- Air-snow and snow-ice interfaces visible in echograms for Ku/Ka frequencies at all polarizations
- Influence of buried a-s interfaces show that the historical snow conditions impact backscatter
- Wind action shifts primary scattering horizon from a mix of a-s/s-i to primarily a-s for KuKa
- The question is: what processes are also relevant at the scale of a satellite footprint?



The impact of snow depth, snow density and ice density on sea ice thickness retrieval from satellite radar altimetry: results from the ESA-CCI Sea Ice ECV Project Round Robin Exercise

Kern et al. (2015)

Introduction

- The main objectives of the Round Robin Exercise are (a) to select the best snow depth product for fb-to-SIT conversion and investigate influence of assumptions (e.g., ρ_i) on the SIT retrieval

Data

- Round Robin Data Package (RRDP) → ERS-1/2 and Envisat-2 sea ice freeboard, AMSR-E snow depth, W99 snow depth/density, BGEP ULS, US submarine ULS, UK submarine ULS, CryoVEx, and OIB
 - Radar altimetry measurements vary in spatial res from 2-10km based on surf properties
- Radar altimetry processing following method of Laxon et al. (2003) and Giles et al. (2008)
 - Radar freeboard gridded to 60km and averaged monthly
- They do not assess the uncertainty of radar freeboards here, but take them as accurate and investigate effects of different free parameters in SIT estimates**
- CryoVEx laser scanner (ALS) and radar altimeter data (ASIRAS) from DTU → airborne data
- Envisat RA-2 data collocated w/ALS using a 100 km radius centered at each ALS transect centre
 - Same collocation requirement for OIB
- ULS collocation is also a huge grid cell

Methods

- Standard set of densities: $\rho_i = 900 \text{ kg m}^{-3}$, $\rho_w = 1030 \text{ kg m}^{-3}$,
- They compare w/A10 densities $\rho_i = 882 \text{ kg m}^{-3}$ (MYI) and 917 kg m^{-3} (MYI)
 - They do this by varying results using each of the above ice densities while keeping snow densities fixed at $\rho_s = 240 \text{ kg m}^{-3}$ and 340 kg m^{-3}

Results

- W99 doesn't capture inter-annual variability in snow depth – largest disagreements over FYI compared to OIB and AMSR-E (which agree themselves within 2cm)
- Radar penetration into snow surface within Fram Strait during CryoVEx campaign was close to zero**
 - Radar sea ice freeboard and ALS lidar total freeboards agree w/ RMSD of 2cm, $R=0.99$, slope=1
 - Thus, if radar return was from s-i interface, these would not match this closely
- Mean OIB sea ice freeboard agrees well w/Envisat RA-2 when OIB snow depths are used (within 2cm)**
 - I.e., subtracting snow depth from OIB total freeboard, and using OIB snow depth for refraction calculation
- Envisat RA-2 draft agrees within 5cm w/BGEP ULS, however seasonal range is not captured by RA-2**
 - Radar altimetry gives much lower seasonal variation compared to ULS
 - A possible explanation is that during winter new ice forms causing the net ice density to increase which would result in a shrunk denominator in SIT equations causing larger SITs, but using a fixed density of say 900 kg m^{-3} will not capture this
- None of the four snow datasets (OIB, W99, mW99, and W99 over MYI w/AMSR-E over FYI) correlated w/OIB SITs more than 0.65 in 2009 → OIB snow data gives best agreement (which you'd expect)
 - In 2010, max correlation is $R = 0.38$

- OIB and RA-2 SIT agree well over FS ($R=0.80-0.84$ for 09/10), but only N=13 data pairs

Discussion

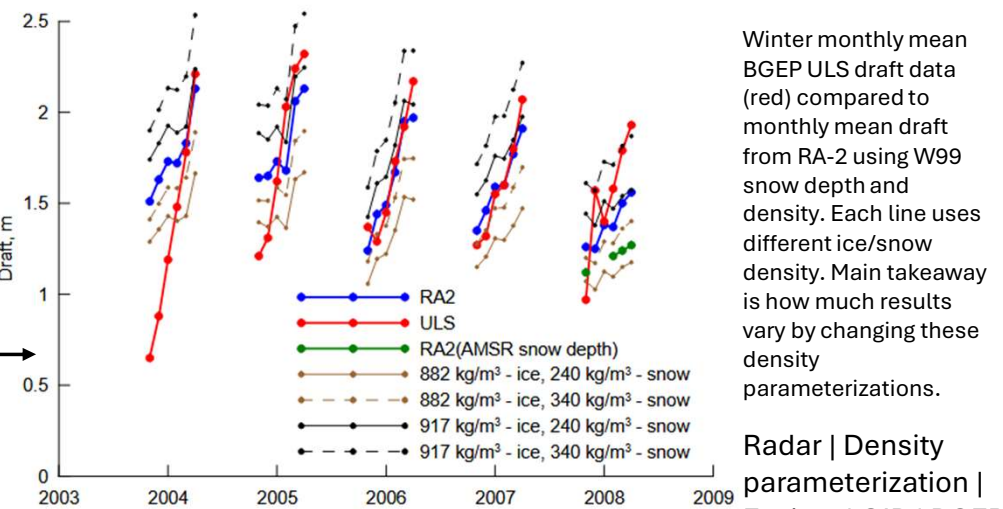
- Using constant $\rho_i = 882 \text{ kg m}^{-3}$ vs 900 kg m^{-3} results in negative bias of 20cm in draft
- Differences btw observed (ULS) and computed sea ice draft (from altimetry) differ month-to-month, limiting conclusions about what input parameters (densities) work best
 - RA-2 estimates are averaged over an area that is 10X larger than what ULS observes, and this may explain the lack of seasonal amplitude

- Variations in ρ_i cause variations in SIT that are as large as those caused by snow depth**
- For typical sea ice freeboard values, the range in ρ_i induces variations in SIT btw 0.4-0.8m**
- "We did not carry out a detailed investigation of the impact of snow density"

Conclusions/Impressions

- W99 is outdated – if used, accompany w/2nd product for FYI estimates
- It is important to consider the density differences btw ridged and level ice**

This paper is limited by (a) the number of collocated data and (b) the spatial radius which collocation is permitted (100km radius centered on 50km transects), and (c) differing temporal timescales – altimetry is averaged over a month, whereas campaigns/ULS are on order of seconds to hours



Implications of surface flooding on airborne estimates of snow depth on sea ice

Introduction

- First OIB validation study (w/in situ data from N-ICE2015) performed in the Atlantic sector

Data and methods

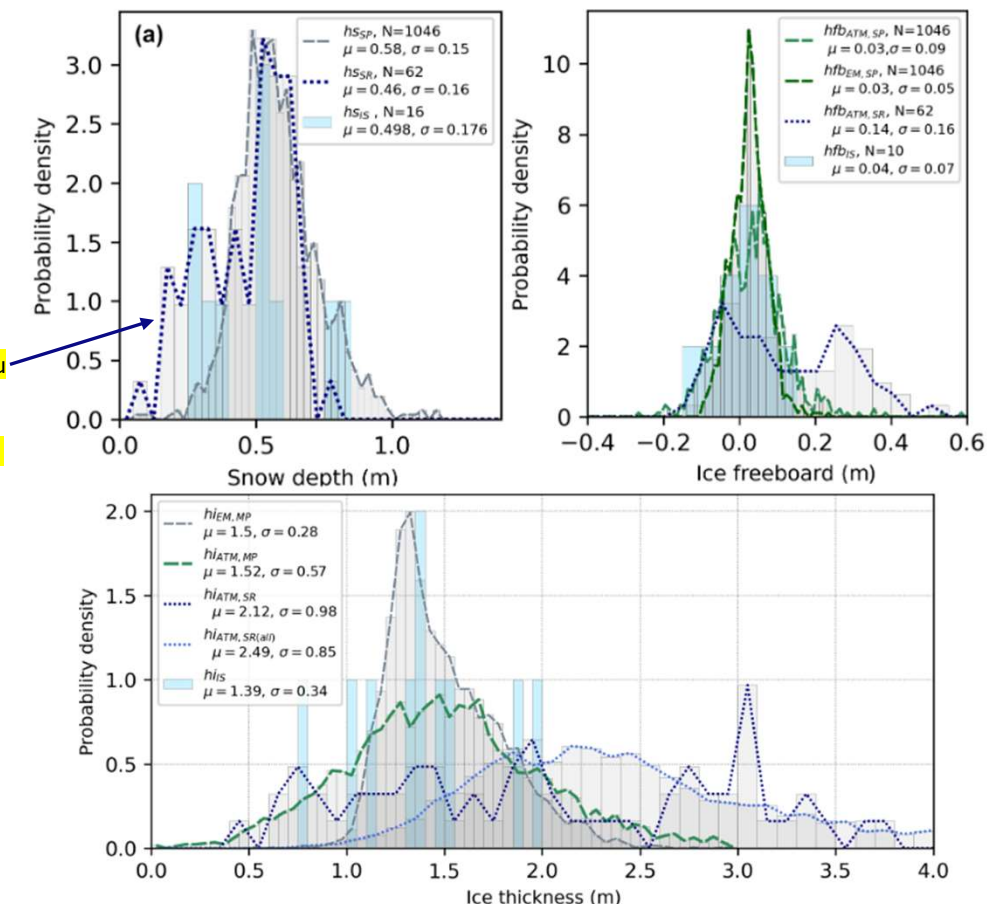
- In-situ samples from 24 Feb to 19 Mar 2015; OIB overflight on 19 Mar 2015
- Snow depth measurements from Snow-Hydro snow probe (SP)
- Total snow + ice thickness from EM31 electromagnetic device dragged on plastic sledge
- Drilled 10 drill holes, made a snow pit, and examined ice core to get ice geophysical properties
- OIB ATM, snow radar, and geolocated visible-band images
 - Drift correction applied to in-situ observations to maintain spatial coincidence w/OIB
- $\rho_w = 1027 \text{ kg m}^{-3}$, $\rho_s = 328 \text{ kg m}^{-3}$, and $\rho_i = 910 \text{ kg m}^{-3}$ → determined w/in-situ measurements
- Observations, both OIB and in-situ, averaged to 5m regular grid across the ice floe

Results

- OIB snow radar mean (mode) snow depth of 42 cm (40 cm); this is 16 cm (15 cm) less than in-situ
 - However, width and shape of distributions (stdev) agree well
 - Snow radar snow depth 8 cm lower than average at drill-hole locations
- Average freeboard in survey field site is close to 0 m based on drill-hole measurements, OIB ATM – snow probe measurements give a freeboard of 0.03 m, in good agreement
 - However, the average OIB ATM – OIB snow radar freeboard estimate is ~0.20 m
 - This difference indicates that the flooded layer is ~23 cm
- Average SITs from drill-holes, EM + snow probe, and ATM + snow probe are between 1.4-1.5m, whereas average SIT from ATM + snow radar is ~2.12 m

Discussion and conclusions

- Snow depths from OIB snow radar ~12 cm lower than in-situ probe measurements
 - Driven by saline, wet snow layers at s-i interface
- Salinity of ice core follows typical C shape w/high salinity of 11.3 psu near top and 5.8 psu at bottom → this indicates the floe is FYI
 - Snow salinity measurements show highly saline, 10 cm deep basal layers up to 10 psu
 - Further, 1/3 of drill holes had flooding, forming highly saline/slushy basal snow layers
- “we can report that the airborne snow radar is capable of measuring meaningful snow depth distributions even in challenging snow pack conditions” since the snow radar can reproduce the snow depth variability when compared to in-situ measurements, despite being biased high
- Flooding is not factored in as source of error in current retracker algorithms
- This paper highlights that radar altimetry in Atlantic sector is challenged by complex snow/ice conditions (temperature, salinity, flooding) and this can lead to significant underestimates in snow depth, overestimates in freeboard, and overestimates in SIT
 - As shown by the dark blue dashed lines in the PDFs to the right



PDFs of snow depth (top left), sea ice freeboard (top right), and SIT (bottom). μ and σ are mean/stdev. hs_{SP} , hs_{SR} , and hs_{IS} are snow height from snow probe (SP), snow radar, and in-situ drill holes (IS). $hfb_{ATM,SP}$, $hfb_{EM,SP}$, $hfb_{ATM,SR}$, and hfb_{IS} are freeboards from ATM and SP, EM induction and SP, ATM and snow radar (SR), and in-situ drill holes. Lastly, hi uses a combo of these abbreviations, but “MP” is a typo for “MP.” Focus on dashed dark blue line for OIB under/overestimates

Radar | OIB | Atlantic sector | Flooding

Airborne Investigation of Quasi-Specular Ku-Band Radar Scattering for Satellite Altimetry Over Snow-Covered Arctic Sea Ice

de Rijke-Thomas et al. (2023)

Introduction

- Propagation depth of Ku-band radar seems to be, in part, quite dependent on the spatial scale of observations, with surface-based approaches indicating minimal scattering from s-i interface but airborne observations indicating s-i interface is the dominant scattering horizon

Nadir Ku-band radar scattering theory over sea ice

- Less than 1% of radar spatial footprint needs to contain lead/smooth sea ice for the coherent (specular) reflection to dominate over the incoherent (diffuse) reflection
- This study aims to see whether the diffuse or quasi-specular component dominates the surface return and what their relative contributions are over different sea ice surface properties, snow cover, and geometry of sensing platform
 - Specifically looking at snow depth, roughness, and across-track footprint slope

Datasets

- NASA OIB Ku-band SAR L1b radar and ATM lidar to estimate snow depth and interface roughness
- OIB snow depth estimates compared w/in situ magnaprobe data from 2016 Environment and Climate Change Canada campaign near Eureka
- 8 OIB overflights of the “moderately” rough FYI ice floe and 7 overflights over MYI
- 23 snow pits dug to take measurements of temp, salinity, and density of snow

Methodology

- ATM lidar and Ku-band radar altitudes aligned by IDing footprints w/clear a-s and s-i interfaces, then adjusting radar-derived interface elevations to be aligned w/ATM
 - No leads to do this alignment as ice was landfast, so had to use this interface approach
- TFMRA70** used – echoes w/two-prominent peaks were assumed to be from a-s and s-i interfaces
 - Echoes w/one peak assumed to be from s-i interface → s-i appeared to be prominent in 91% of the double-peaked echoes over FYI, so they felt this was a safe assumption
 - Waveforms selected are quasi-specular, w/diffuse waveforms (e.g., 3 peaks) omitted
- Stdev of ATM within a 5m radius of footprint center used to estimate surface roughness
 - Footprint-scale roughness at s-i interface computed by subtracting in-situ snow depths from ATM laser spots within 0.5 m horizontal distance of each other, and then taking stdev of multiple s-i interface elevations within a footprint
- Return energy over varying topography estimated by normalizing the time taken for each part of the pulse to cross height variations (footprint-scale roughness) of an interface
 - Then, power of return from interface multiplied by time taken to pass over interface
- Across-track ATM laser data used to estimate surface slope

Results

- For FYI site, temps btw -23°C and -17°C, p_s decreased w/depth from 0.37 to 0.28 g cm⁻³, and main body of snow was not saline but bottom 20% had salinity of 11 ppt (MYI salinity <1ppt)
- Over FYI: airborne mean snow depth of 19.3 ± 8.2 cm, vs. in-situ mean snow depth of 21.1 ± 5.2
 - Mean absolute difference of 4.82 cm

- Over FYI, radar PP strongly correlates w/mean absolute error in snow depth, indicating that for peaky waveforms the s-i interface is clearly resolvable
- At MYI site, mean snow depth of 30.9 ± 34.5 cm, vs. in-situ mean snow depth of 31.1 ± 14.4 cm
 - Mean absolute difference of 21.7 cm
 - s-i interface retracked poorly w/TFMRA70 over complex, multipeaked waveforms
- At this point, they focus on FYI as they couldn't reliably estimate MYI snow depths^{^^}
- Errors in airborne-estimated snow depths closely related to surface roughness of snow/sea ice
- Footprints w/roughness > 10 cm, absolute errors >20 cm
- Footprints w/roughness < 7 cm, negligible bias, but snow depth underestimation increases w/surface roughness up to ~4cm
- 32% of footprints had stronger power return from a-s interface, 68% from s-i interface
 - Mean ratio of powers btw s-i and a-s was 4.8, indicating ~5x stronger backscatter from s-i than a-s over FYI site
- Return power doubled (tripled) over level ice compared to sloped surface for a-s (s-i) interface

Discussion

- Unable to assess impacts of snow layering, grain size, or snow density transitions
- Despite saline base of snowpack ~3cm above s-i interface, no evidence for limited penetration of Ku-band into snow over FYI

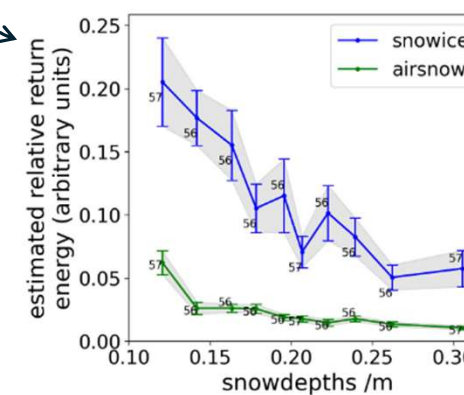
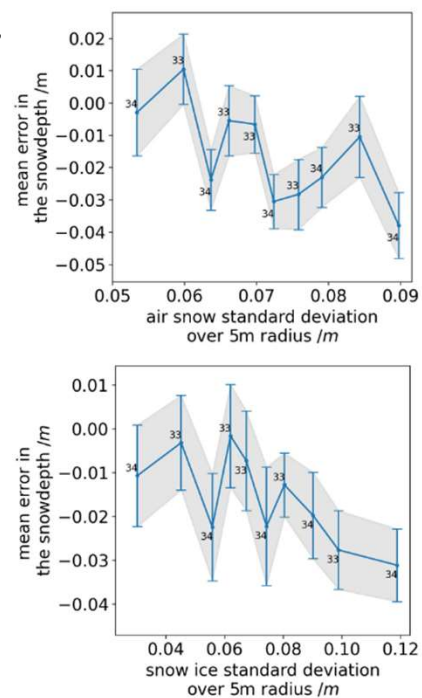


Fig. 4. Estimated relative return energies for both the air-snow and snow-ice interfaces for different snow depths over FYI.



Airborne Investigation of Quasi-Specular Ku-Band Radar Scattering for Satellite Altimetry Over Snow-Covered Arctic Sea Ice (continued)

de Rijke-Thomas et al. (2023)

- The results give strong evidence for probabilistic quasi-specular scattering of Ku-band radar from a-s and particularly the s-i interface over sea ice
 - As surface roughness increases, radar return is less likely to be dominated by specular scattering and error in retrieved snow depth increases
 - Perhaps this is why the radar freeboard doesn't vary by the expected amount in Nab et al. (2023) → snowfall/redistribution changes prominence of a-s interface
- Using CS2 SARIn, they find strong phase coherence in initial backscatter respond at waveform leading edge for all sea ice surfaces, and that this gets stronger w/smooth surfaces
 - Which makes sense, things get more specular
- Quasi-specular scattering appears to start contributing to Ku-band backscattering somewhere between the surface-based and airborne-based scales, as there has been no compelling evidence for quasi-specular scattering w/surface-based Ku-band radar
 - Coherent backscatter from slightly-rough radar surface can be expressed as:
$$\sigma_{coh}^0 \approx 4|R_0(\theta)|^2 \frac{H}{\tau} e^{-4(k^2 \sigma^2 + \frac{\theta^2 H}{\tau})}$$

σ is rms of surface height, k is wavenumber ($k = 1/\lambda$), $R_0(\theta)$ is Fresnel reflection coefficient, τ is pulse width, and H is height of sensor above surface → larger H for satellites leads to more coherent returns and more quasi-specular scattering which enables better identification of the s-i interface

 - But there is a competing reduction due to θ as drop-off in backscatter with angle I stepper than at airborne scales
- Effects of volume scattering unable to be investigated in this study

Conclusion

- Over FYI, Ku-band backscatter from both a-s and s-i interfaces are primarily controlled by quasi-specular scattering, with the specular component of the return being stronger for s-i interface
- In waveforms w/o quasi-specular backscatter, a-s and s-i interfaces have similar return power
 - Without fine range resolution like OIB, empirical retracking methods would measure height of a-s, s-i, or somewhere in-between leading to significant biases
- Based on the coherence seen in CS2 SIRAL returns, as well as relationship btw specular scattering and footprint slope at aircraft scale (lower slope=stronger specular reflection), majority of backscatter at Ku-band for satellite platforms is likely to originate from specular scattering (and thus the s-i interface) rather than diffuse scattering
 - Slope over CS2 footprint likely smaller than OIB footprint
- Despite surface-based studies showing Ku-band returns well above the s-i interface, this bias is not seen in satellite retrievals when compared w/in-situ estimates from sensors like ULS
 - "Our results present an explanation for this apparent contradiction because the geometries and length scales of the surface-based investigations do not necessarily reflect the situation for satellites."

- Only 1.8cm underestimation of FYI snow depths despite high basal salinity indicates that at the airborne scale, even if radar penetration through the snowpack is reduced by higher absorption from brine-wetted snow grains, the snow-ice interface can still be prominent if it produces a strong, quasi-specular reflection
- Their results indicate that Ku-band satellite radar altimetry return is more likely to sense s-i than a-s interface over FYI w/similar properties to the study site here
 - As Arctic shifts to a predominantly FYI regime, perhaps Ku-band radar retrievals of freeboard will be improved

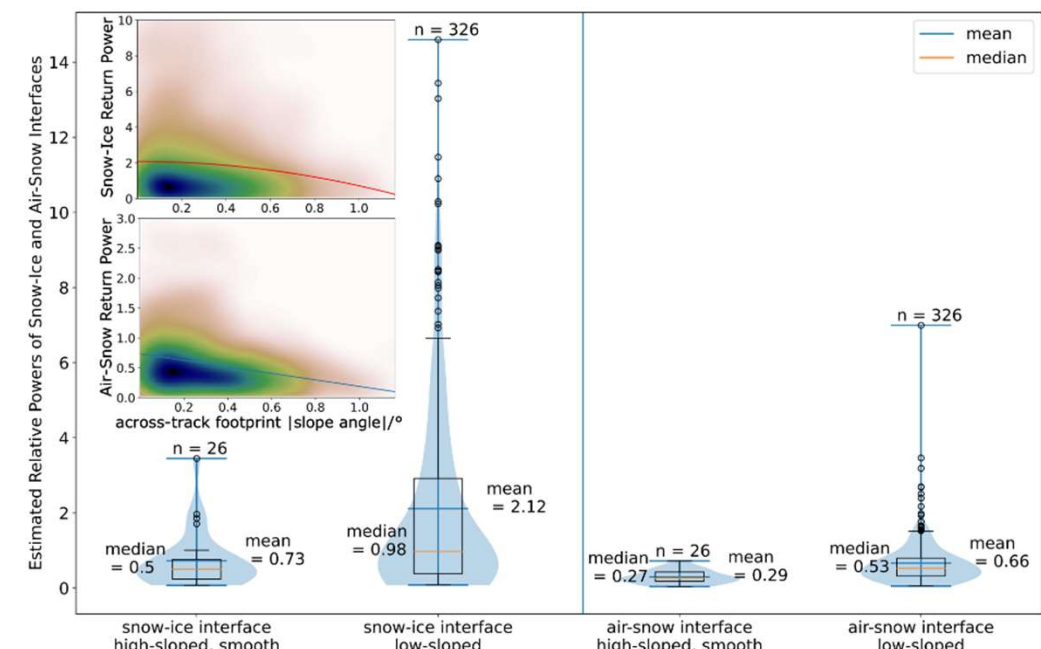


Fig. 10. Comparison between the power returns of the (left) snow-ice and (right) air-snow interfaces for first-year sea ice, comparing level (<0.2°) footprints with smooth, sloped footprints (>0.8°, with values no higher than 1.3°). (Inline left) Probability distribution functions of the linear return powers from (top) snow-ice and (bottom) air-snow interfaces, against footprint slope angle, using a Gaussian kernel-density estimate. The fit equation for the snow-ice interface is $y = 1887.2 - 1885.1e^{0.000724x^2}$ and, for the air-snow interface, is $y = 0.734 - 0.544x$.

Return power doubles (triples) over level ice compared to sloped surface for a-s (s-i) interface

Radar | OIB | Quasi-specular | Retracking | a-s s-i interfaces

Multi-frequency altimetry snow depth estimates over heterogeneous snow-covered Antarctic summer sea ice – Part 1: C/S-, Ku-, and Ka-band airborne observations

Introduction

- First evaluation of airborne coincident Ka, Ku, and C/S radar w/lidar obs over Antarctic sea ice
- Great summary of what airborne missions have happened recently in N/S hemispheres

Data

- CRYO2ICEANT22 summer airborne campaign 29 Nov – 20 Dec 2022 → airborne cryo2ice underflights in Weddell Sea carrying Ka, Ku, and C/S band radars along with laser scanner (ALS)
 - No in-situ observations, so ERA5 used for precip/air temp/snowfall estimates
 - Ka/Ku band range res ~4cm, C/S band range res ~2-4 cm; radar footprints ~5m diameter
 - ALS operates in NIR w/ $\lambda=904\text{nm}$; 1 observation per m^2 and 0.7m diameter footprint

Methodology

- FMCW snow radars generally use multiple retrackers to track peaks in return waveform, whereas conventional Ka/Ku radars use one and assume return is from one dominant scattering interface
 - TFMRA40/50/80 used when assuming single scattering horizon
 - Continuous wavelet transform (CWT) and peakiness (PEAK) retrackers for multiple
- Nadir lidar profile as avg of ALS observations within 2.5m radius of center location of radar obs
- ALS and radars calibrated by lining up returns over specular leads and determining mean offset
- PP used to discriminate btw surfaces, w/similar values as Tilling et al. (2018)/Ricker et al. (2014)
- Sensitivity to p_s analysis showed max difference ~3cm, so results insensitive to choice of p_s

Results

Microwave penetration into snow

- They use one retracker for airborne Ka/Ku, but multiple retrackers for C/S band
- Maximum power reflected within 10 cm from a-s interface for ~33% and ~43% of observations for Ku-band and Ka-band, respectively
- ~60% (~46%) of Ku-band (Ka-band) obs were scattered within snowpack btw 0.1–1.5 m
 - This suggests that Ka-band radar is penetrating through the snow
- In several instances, Ka-band is reflected below Ku-band, suggesting a greater sensitivity to retracking threshold at Ka-band → also indicates volume scattering may play a role
- Max reflection from depth of 57 cm, 44 cm, and 42 cm below ALS (a-s interface) with C/S band, Ku-band, and Ka-band radars, respectively

Tracking a-s and s-i interfaces

- Between 52–55% of observations are within 10 cm of ALS interface at both Ku and Ka-band using TFMRA for all retracker thresholds → i.e., the first significant peak in the waveforms is likely a-s
- PEAK retracker seems to track s-i interface well with C/S band radar
- Snow depths derived w/ALS–KuTFMRA50 or ALS–KaTFMRA50 yield snow depths < 5 cm, and similar results for Ka-Ku whether TFMRA50 is used or if max power threshold is used
 - Lidar-radar w/TFMRA & Ka-Ku radar both can't accurately measure snow depth (Fig. 7d)
- Max power return within 5cm of a-s interface 46% of time w/Ka, 31% w/Ku, and 17% w/C and S

Fredensborg Hansen et al. (2025)

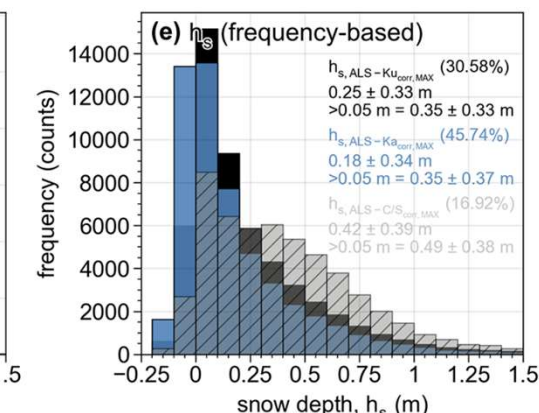
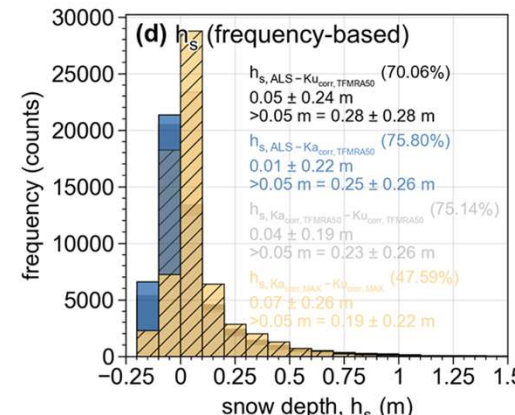
- Ku and Ka seem to returning from within the snowpack but not all the way to the s-i interface when compared w/ALS – C/S max power threshold
- Even ALS-C/S band snow depths vary greatly based on whether PEAKS or CWT retracking is used

Discussion and outlook

- Assumption of full Ku-band penetration to s-i interface over Antarctic sea ice doesn't hold
- C/S band max return occurs ~60 cm below a-s interface, indicating this may be the s-i interface and C/S band is less sensitive to geophysical properties that impact dielectric properties of snow
- Avg temp up until campaign was ~5°C → thus, very well could have s-i interface temps >-5°C and liquid water present in the snow
- It is assumed that C/S band doesn't scatter within the ice → I wonder if this is 100% true always

Conclusions/Impressions

- a-s interface contributes to scattering at both Ka and Ku-band frequencies
- Several instances show primary backscatter at a-s and weaker peak also s-i interface for Ku-band, so it's possible that a retracking method could be used to get snow depth from just Ku
 - But... not likely w/spaceborne radar due to higher range res (~47 cm)
- They weren't able to determine whether any of the frequency-retracking approaches accurately captured snow depths, as there were no in-situ observations
- The lack of info about snow geophysical properties, weather conditions, and no in-situ measurements of snow depth, the evaluation of microwave penetration depths are not particularly meaningful



Snow depth distributions for different frequencies/retracker combos. 2nd line is the means, 3rd line is means for snow depths >5cm. Percentage in parentheses gives % of obs w/snow depths >5cm

A 10-year record of Arctic summer sea ice freeboard from CryoSat-2

Dawson et al. (2022)

Introduction

- They collate optical and CS2 observations, use along-track local variations in echo parameters instead of absolute values, and include local elevation variation as a classification variable to distinguish melt ponds from leads, creating the first CS2 summertime product w/a CNN

Methods

- CS2 L1b and L2 SAR and SARIn w/SAMOSA+ retracker for May-September 2011-2020
- Landsat-8, Sentinel-2A, and Sentinel-2B optical satellites for overlapping scenes w/CS2
 - RADARSAT-2, Sentinel-1A, and Sentinel-1B SAR imagery as well
- Overlapping scenes were within 15m of CS2 acquisition so no drift correction was needed
- Leads classified manually using true color w/optical satellites and HH/HV polarizations w/SAR
- Leads only recorded when there was a corresponding change in CS2 elevation and it could be visually identified, thus the minimum lead size observed was ~300m
- Three classification categories: leads (N=170), good floes (N=236), and noisy floes (N=193)
- Elevation, σ^0 , PP, and range integrate power (RIP) peakiness were the 4 best classifiers for leads
 - These four parameters[^] over an 11-point (3km) window used within a 1D CNN
 - The CNN correctly classified 80% of testing data, w/only 5% of floes classified as leads
- Leads can be obscured by noise in CS2 data due to strong reflections from melt ponds masking the lead signal, but these “errors of omission” shouldn’t impact estimated sea ice freeboard
- Interpolating over lead tie points works in winter, but in summer when lead detection is sparse this can lead to averaging over long distances (>100s km)
 - Instead, freeboard elevation on good/noisy floes are interpolated within a 7 km window centered over each lead, resulting in one radar freeboard per lead
 - They adjust the interpolation by reducing influence of outliers to prevent the influence of lead snagging, as the floes are centered around the lead
- Radar freeboards gridded w/IDW to produce 15-day freeboard fields on 80km grid
 - 2-3X larger than standard 25km res for CS2 gridded products → limitation of the method

Results

- Product struggles to ID leads in MIZ, so no data common in these regions
- Product can capture the seasonal evolution of radar freeboard quite well
 - Comparison btw Apr/Oct from winter processor (Landy et al. 2020) and May/Sep from this product shows good agreement in spatial patterns
- May radar freeboards > April for most years, before declining afterwards → likely explanation is that scattering horizon shifts upwards from April to May as more moisture is in the snowpack
 - But this could also be due in part to the summer processing
- Summer processor significantly overestimates radar freeboards over edges of central Arctic ice pack compared to winter processed data

Validation

- CS2 radar freeboards compared directly w/OIB ATM as all snow is assumed to have melted
 - For 2016 campaign, difference is $2 \pm 6\text{cm}$, but OIB much thicker in 2017 campaign

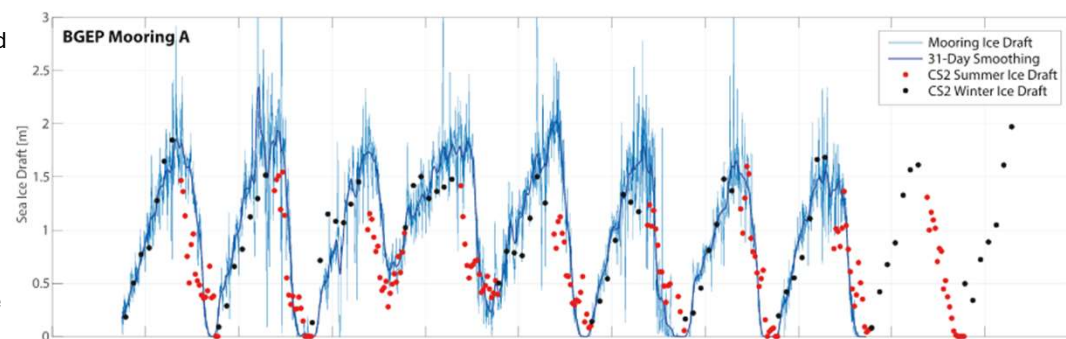
- For 2017, CS2 underestimates freeboards by $10 \pm 6\text{cm}$ ($20 \pm 10\text{cm}$) for smoother (rougher) ice
- Compared to EM surveys, CS2 observations near N Greenland/Lincoln Sea underestimate SIT by $1.0 \pm 0.4\text{m}$, by $0.76 \pm 0.4\text{m}$ in Fram Strait, and by $0.28 \pm 0.2\text{m}$ in central Arctic
 - Clearly, based on EM and OIB, this product struggles more over rougher sea ice (MYI)
- CS2 estimates, when compared w/ULS, capture the timing of growth/melt cycles quite well
- Despite assuming high p_i (930 kg m^{-3}), CS2 drafts underestimate compared to ULS from May-Jun
 - This indicates that snow loading is still important to account for in these months
- Correlation btw CS2 and ULS for May-Sep are btw 0.62-0.76 for the 3 BGEP moorings, with mean biases of $-13 \pm 0.45\text{m}$, $-0.33 \pm 0.52\text{m}$, and $-0.29 \pm 0.51\text{m}$

Discussion

- Summer processing scheme cannot estimate radar freeboards thinner than 4cm
- Summer processing scheme performs most poorly over rough, MYI
- 3 categories of uncertainty: classification, elevation retrieval, and freeboard to SIT conversion
 - Misclassification not thought to strongly contribute to freeboard underestimation
 - Elevation retrieval likely contributes strongly to underestimation, as if melt ponds surface is below ice surface, range will be biased higher and freeboard biased low
 - They intentionally use a high p_i , which would bias SIT high, thus they conclude that the freeboard to SIT conversion is unlikely leading to freeboard underestimation
 - Not accounting for snow load also unlikely as comparison vs. EM was in July
- Regional and seasonal patterns of freeboard variability captured well by CS2
- The conservative classification for leads limits number of freeboard observations

Conclusions

- The first pan-Arctic summer sea ice freeboard estimates from a satellite radar/laser altimeter
- Key source of bias is radar overestimating range as melt ponds lie below ice floes mean level



Radar | CS2 | Summer radar freeboards

A year-round satellite sea-ice thickness record from CryoSat-2

Introduction

- This is the first year-round satellite-derived SIT dataset covering 2011-2020

Methods

- Foundation of the algorithm is the Dawson et al. (2022) approach using the 1D CNN
- EM range bias correction applied to 80-km gridded CS2 obs by simulating CS2 backscatter from sea ice surfaces w/varying surface roughness (σ) and melt pond coverage (f_p)
 - Correction is diff btw SAMOSA+ and “true” retracked point on simulated waveform
- Pan-Arctic σ estimates from std dev of s-i interface obtain using LARM dataset in winter and then doing Lagrangian forward/backward propagation of the floes for the summer months
- f_p from Sentinel-3 OCLI; snow depth from SMLG w/MERRA2 forcing
- Dawson et al. (2022) found larger radar freeboards in May than April → scattering above s-i interface → this study assumes Ku-band penetrates 90% of snow when present from May-Sep
- LARM SITs from Oct-Apr, the modified Dawson et al. (2022) approach for summer months
- Validation data/results:
 - Icebird AEM averaged to 80km grid: $R^2 = 0.8$ w/mean diff CS2-AEM = -16 cm in 2011
 - Median bias of 28 cm over N. Greenland, Lincoln Sea, and Fram Strait in 2016-18
 - BGEP ULS: mean bias for moorings A-D are -16 ± 32 cm, -19 ± 34 cm, and -27 ± 42 cm
 - Correlations (R) btw 0.84-0.87
 - Laptev sea moorings: mean draft bias -6 ± 40 cm w/ $R=0.74$
 - Fram Strait moorings: +11cm draft bias (CS2-ULS) during winter

Summer SIT from CS2

- Simulated EM range bias shows that it increases over rougher sea ice, leading to underestimated radar freeboards – see Dawson and Landy (2023) for empirical evidence of this
- Thickest pan-Arctic mean summer SIT of 2.01 m in May 2015, thinnest of 0.52 m in Oct 2011
 - Highest interannual variability in July (18 cm), lowest in January (8 cm)
- Seamless transition from winter LARM estimates to summer estimates, w/same spatial patterns

Seasonal Variability in SIV

- The contribution of SIT anomalies to SIV anomalies is 5X that of SIC anomalies
 - Correlation btw SIV and SIT anomalies is 0.97, vs. 0.27 for SIV and SIC anomalies
- CS2 and PIOMAS SIV have R^2 of 0.96 (FYI=0.96, MYI=0.83) and RMSE of $2,350 \text{ km}^3$ (FYI = $1,190 \text{ km}^3$, MYI = $1,200 \text{ km}^3$), respectively

Covariance between SIV and SIE

- Statistically significant ($P < 0.1$) positive correlation btw Jun-Sep SIE and earlier SIV/SIE, starting from lead times between May-July
 - Lead times for significant correlations increase over the summer
- Results indicate the presence of a spring predictability barrier, consistent w/modeling studies
- Spring predictability barrier → defined as a springtime date such that predictions initialized on/after (prior to) the date can (cannot) skillfully predict summer sea ice
 - Intense dynamics/growth in late winter prevents link btw winter SIT anomalies and SIE

Future implications for forecasting

- SIE covaries w/future SIE at short lead times around 0-45 days, whereas SIV becomes dominant for predicting SIE btw Aug-Dec over lead times of 45-300 days
 - This means that Oct-Dec SIE can be accurately forecasted from SIV estimates as early as the preceding Jan-Feb → but after Jul-Aug, SIE becomes more important predictor

Next steps

- Need to better understand EM range bias – airborne campaigns would help w/this
- FYI/MYI density evolution during the summer is poorly constrained
- Improved estimates of σ and f_p is key, and need more summertime SIT validation data in Arctic

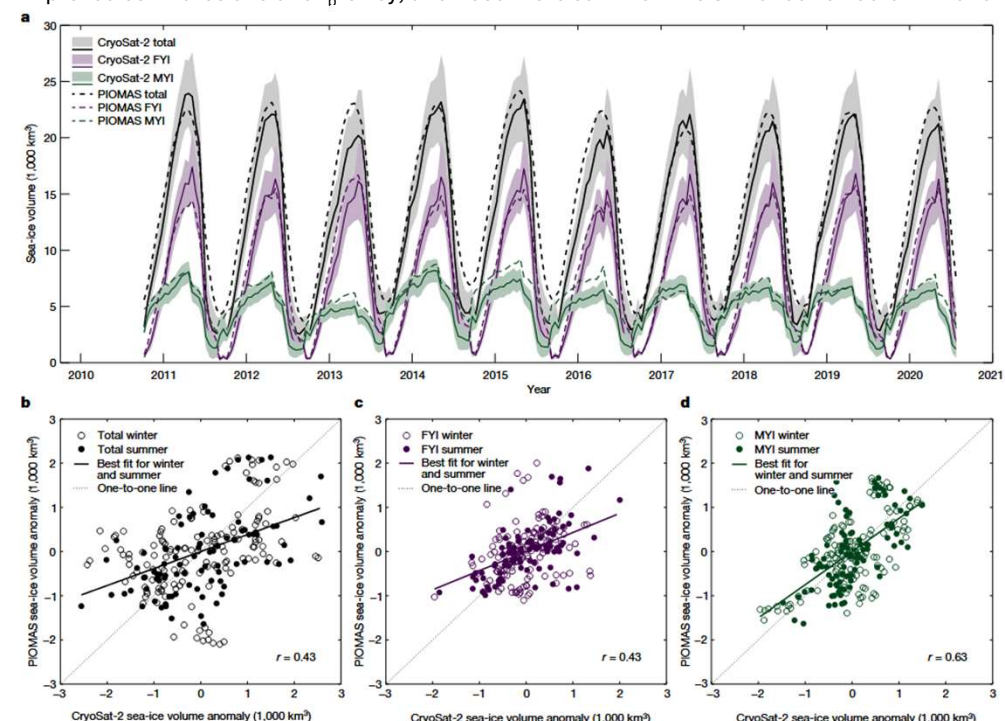


Fig. 2 | Time series of SIV derived from CryoSat-2 compared with reanalysed predictions of ice volume from PIOMAS. a, SIV from CryoSat-2 is presented with uncertainty envelopes for the entire Arctic and separated into zones of predominantly FYI and MYI (using the NSIDC sea-ice-age dataset⁴). The CryoSat-2 SIV uncertainties are derived from the total ice thickness uncertainty

(Methods) multiplied by the ice area. b–d, Scatterplots of the SIV anomalies, for total (b), first-year (c) and multi-year (d) ice after removing the climatological seasonal cycle of ice volume from the CryoSat-2 and the PIOMAS time series.

Radar | CS2 | Summer | SIV | Predictability | EM range bias

Comparing elevation and backscatter retrievals from CryoSat-2 and ICESat-2 over Arctic summer sea ice

Dawson and Landy (2023)

Introduction

- The first study to compare IS2 and CS2 elevations over summer sea ice
- IS2 doesn't have the EM range bias (returns from melt pond below ice surface) that CS2 does, so comparing the backscatter retrievals can provide some indication of the magnitude of this bias
 - Any differences btw IS2 and CS2 will have some contribution from unknown height biases in the respective products

Data and methods

- CS2 L1b and L2 baseline D w/CPOM retracker, TFMRA50, and SAMOSA+ and IS2 ATL07 v5
 - Only July-Sept obs, to make sure there was no snow loading, from 2018-2021 ($N \sim 61k$)
- Surface reflectance compared using IS2 N_{photons} and CS2 σ^0
- CS2 and IS2 lead detection the same, using Dawson et al. (2022) approach
- Melt pond fractions (f_p) from Sentinel-3 OLCI dataset, daily 12.5 km grid
- NSIDC sea ice age and Polar Pathfinder products
- IS2 and CS2 elevations compared by averaging IS2 points within 150m radius of CS2 footprint
 - IS2 had to have a minimum of 50 points for a comparison to be made
 - Observations must be within 3 hr of each other and have drifted <300m

Results

- CS2 elevations for all retrackers are lower than IS2 by median diff of 7.1, 1.6, and 2.4 cm for CPOM/TFMRA50/SAMOSA+, respectively
 - After this, they only use SAMOSA+ as it's been used in Dawson et al. (2022) and Landy et al. (2022)
- Median difference btw IS2 and CS2 was 1.3 cm (FYI) and 2.5 cm (MYI), and CS2 leads are lower than IS2 by a median difference of 3.5 cm
- Photon rate and CS2 backscatter increases throughout the summer as f_p rises
- Low photon rates and backscatter from rougher surfaces (see b and c in figure to the right →)
- No significant relationship btw N_{photons} and σ^0 at CS2 footprint scale
- IS2-CS2 elevation vs. surface roughness (σ_{IS2}) has slope of $0.659 \pm 0.007 \text{ cm/cm}$, meaning EM range bias increases by 3.2 cm for every 5 cm the sea ice roughness increases
 - At min σ_{IS2} (~3cm), range bias is 1.9 cm → EM range bias is quite small for smooth floes
 - Also, CS2 underestimates elevation more over MYI than FYI (Dawson et al. 2022), supporting this finding
- Largest elevation differences occur over rough surfaces w/low N_{photons} and σ^0 , indicating that floes w/lower coverage of surface water produce larger height differences (larger EM bias)
- When f_p is high (20-30%), elev difference is ~5-10cm regardless of surface roughness, but when f_p is low (<20%) the elev differences increase from 0-30+ cm as σ_{IS2} increases

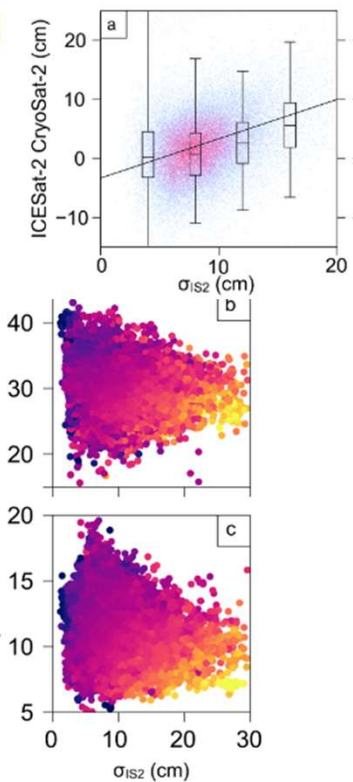
Discussion

- Negligible median height differences btw IS2 and CS2 (~2.4 cm), compared to the larger differences shown w/OIB in Dawson et al. (2022), indicate IS2 may also underestimate surf elev

- Observed and theoretical EM bias agree, w/EM biases increasing w/higher surface roughness and reduced f_p
- Coincident data resulted in few f_p below 0.1, thus hard to compare theoretical and observed EM biases as low melt pond fractions
 - Nevertheless, EM bias increases as surfaces get rougher, and for a given roughness it increases w/lower reflectivity
- Observations show larger biases (5-10cm) for low σ_{IS2} (<10cm) than simulations (0-5cm)

Summary

- Median EM range bias using SAMOSA+ is between 1-3.5 cm
- EM range bias larger over MYI than FYI
- Gridded f_p from S3 OLCI too coarse resolution to interpret height biases at individual crossover locations, but despite this limitation the observed EM biases agree w/theoretical simulations



Elevation difference between IS2 and CS2 as a function of (a) melt pond fraction (f_p) and surface roughness (σ_{IS2}), (b) CS2 backscatter rate (σ^0) and σ_{IS2} , and (c) photon rate (N_{photons}) and σ_{IS2} . Contours indicate theoretical radar EM bias from (Landy et al. 2022)

Radar | CS2 | IS2 | Summer | Backscatter | Melt ponds | EM range bias

Retrieving Sea Level and Freeboard in the Arctic: A Review of Current Radar Altimetry Methodologies and Future Perspectives (Part 1)

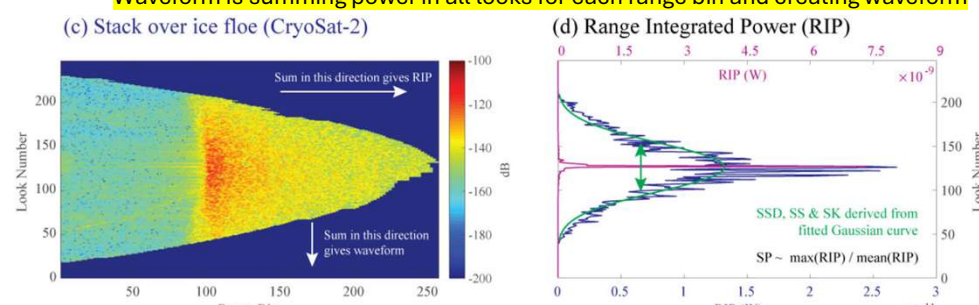
Quarly et al. (2019)

Introduction

- Traditional low-resolution measurement altimeters = LRM; SAR = delay-Doppler altimeters (DDA)
- DDA describes specific implementation used for CS2/S3, "SAR altimetry" is the common phrase
- SAR = beam-limited, LRM = pulse-limited

Waveform discrimination

- Classical techniques include setting empirical thresholds on parameters derived from the waveforms, such as PP, SSD, LEW, TEL, and σ^0
- Statistical techniques – supervised (neural networks) and unsupervised (partitional clustering)
- Incoherent sum over all look directions gives a SAR waveform
- SAR range integrated power** is a derived waveform created by summing power across Doppler beams in range direction → sum range for all bins for each look and create distribution
 - Waveform is summing power in all looks for each range bin and creating waveform

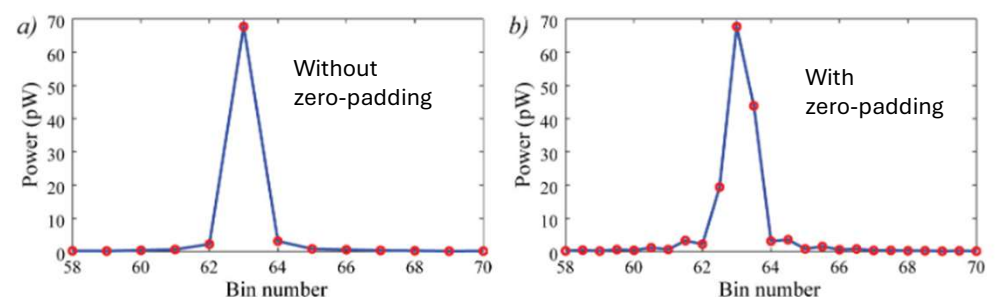


- SAR waveform discrimination can be separated into 3 categories: power-based methods, RIP and waveform shape-based methods, and statistical techniques
 - Power-based → thresholding based on max (or relative max) power return
 - RIP/waveform shape → fitting waveform shape to RIP (e.g., Gaussian/ lognormal) w/ automatically defined PP/SSD/etc... or Ricker approach of estimating PP/SSD/etc... in certain range bins before/after peaks
 - Statistical → machine learning techniques
- Using/not using Hamming window in Fourier analysis to reduce sidelobes impacts performance of thresholds in SAR waveform classifiers → thus, Level 0 to Level 1 processing is important
- Key methods to validate waveform discrimination: optical/SAR imagery and aircraft campaigns

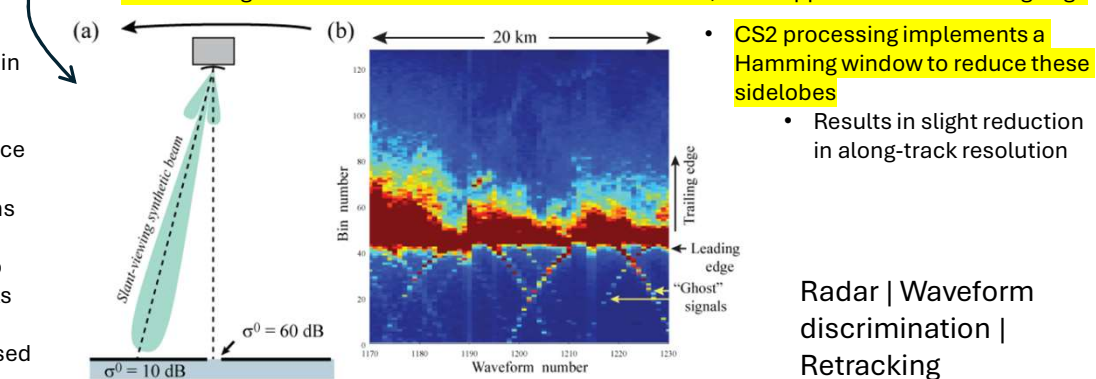
Waveform retracking

- Empirical retracking** → TFMRA common because (a) it's simple/efficient, (b) it matches well to validation data, and (c) tracking the first max eliminates the possibility of retracking max peaks created by off-nadir lead snagging
- Physical retracking** → return waveform fit with a model that best matches its shape and is based on physics of EM interaction b/w transmitted pulse and scattering surface

- Zero-padding** is important for lead detection as it avoids the loss of info that occurs upon squaring voltages → it allows FFT to produce more frequent samples within waveform shape
 - Longer FFT = more range bins = easier to resolve peak of single, isolated frequency
 - No change in range res, but more finer sampling of the signal/spectrum



- For empirical algorithms, there can be a relative bias in retracking due to diff waveform shape from floes/leads → similarly, if 2 physical retrackers are used for floes/leads, a bias may exist
 - Thus, it is advantageous to have one unified retracker for all surfaces
 - SAMOSA+ and Kurtz et al. (2012) model are examples of these unified models
- Lead, or off-nadir, snagging impacts trailing edge, but azimuth ambiguity (side-lobe effect) can result in spurious power before the leading edge of the nadir backscatter**
- Azimuth ambiguity → when a synthetic Doppler beam is looking off-nadir in a slant view, and there is a bright/specular source near nadir, the weighting provided by the synthetic beam's antenna pattern can't fully compensate for the highly contrasting backscatter strengths
 - Since strong return is closer than the intended slant view, it will appear ahead of leading edge



Radar | Waveform discrimination | Retracking

Retrieving Sea Level and Freeboard in the Arctic: A Review of Current Radar Altimetry Methodologies and Future Perspectives (Part 2)

Quarly et al. (2019)

Corrections and References Needed for Inferring Precise Geophysical Values

Atmospheric corrections

- Three corrections for atmospheric components altering propagation speed of radar waves:
 - Ionospheric correction → account for free e^- in propagation path, minor at polar latitudes
 - Dry tropospheric correction → account for delay in wave propagation due to mass of air and, thus, surface pressure
 - Wet tropospheric correction → account for delay due to water vapor in atmosphere
- Dynamic atmospheric correction → modeling of sea surface response of preceding time series of pressure and wind
 - Comprises a “static” response to atmospheric pressure → inverse barometer correction; and the high-frequency dynamic response to the history of changes in atm pressure/winds
 - For sea level under floes, only the “static” IBC correction is applied

Tides and Mean Sea Surface

- MSS is the largest correction, ranging over more than 40m across the Arctic Ocean
 - SSH is inferred by interpolating lead heights relative to the MSS
- Magnitude of atmospheric/ocean corrections provided in Table 3, page 26

Freeboards and converting to SIT

- Steps to calculate freeboard: (1) surface elevations of ice floes/water in leads retrieved relative to ellipsoid describing approximate shape of the Earth, (2) geophysical corrections applied, (3) lead elevations interpolated to retrieve SLA (difference btw instantaneous sea surface height and MSS), and (4) SLA is subtracted from sea ice elevations to get freeboard
 - Since freeboard is a relative quantity, geophysical corrections shouldn't impact the retrieval
 - But spatial variations in SSH between leads causes interpolation errors, which geophysical corrections can help to minimize

Comparison with in-situ and airborne measurements

- Mean dynamic topography = height signature consistent w/mean surface geostrophic currents
 - MDT can be estimated by MSS-geoid

Future prospects: expectations and hopes

- Further knowledge of surface scattering from snow on ice floes, melt ponds, etc.. needed
- Improved retracking techniques
- SARIn phase information can be used to correct off-nadir lead snagging

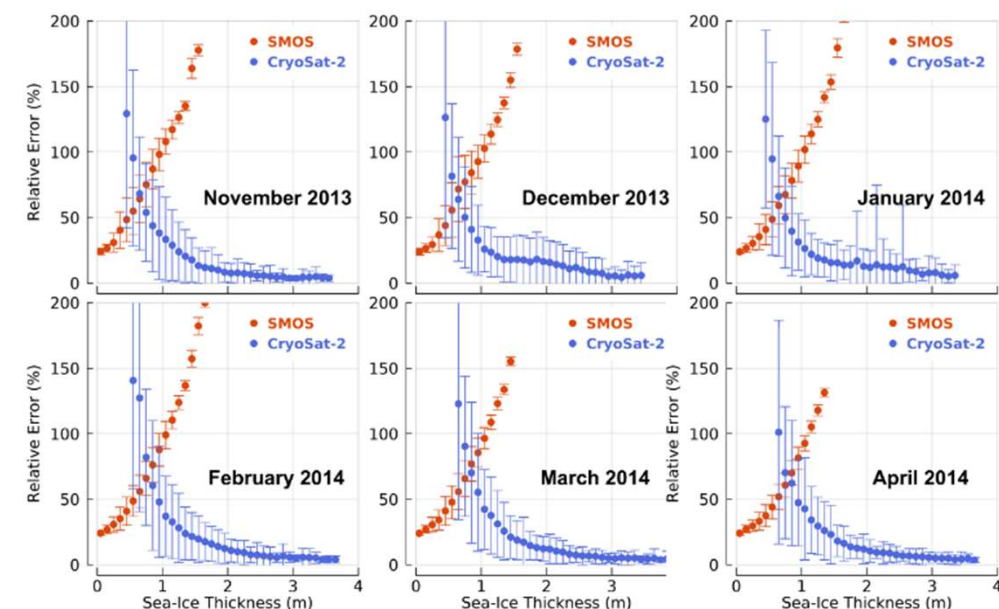


Figure 22. The relative uncertainties for CryoSat-2 and SMOS (Soil Moisture and Ocean Salinity) Arctic ice thickness estimates during one winter season, November-April, 2013/2014. Relative uncertainties are binned in steps of 0.25 m of sea-ice thickness. The error bars represent the standard deviation of the mean relative uncertainty for each bin.

Methods of satellite remote sensing of sea ice

Measurement principles and methods

- PMW measure emissivity in microwave range, in part, bc it's more variable than physical temp
 - Microwave brightness temperature: $T_B = \varepsilon T$
- ε is a function of the dielectric properties of a material, and for sea ice the salinity, temperature, and porosity largely determine its dielectric properties
- Microwaves penetrates snow and sea ice → radiation at 89 GHz penetrates less into sea ice than at 19 GHz, so diff frequencies/polarizations can be used to estimate snow/sea ice properties
- Higher salinity FYI = small penetration depth and high ε , the opposite for MYI
- Optimal frequency for minimal atm influence is < 10 GHz, but this results in large spatial footprints → AMSR2 is at 36.5 GHz which gives better spatial resolution, but more attenuation
- $\sigma^0 = \frac{\sigma}{A} \rightarrow$ radar backscatter coefficient is equal to radar backscatter divided by unit area
 - σ^0 of deformed or porous ice is higher for cross-pol than co-pol channels
 - Polarized radiation depolarizes when it is scattered by rough features
- SAR: along-track (azimuth) resolution is proportional to antenna length and independent of λ and R , whereas w/traditional altimeter it would be equal to: $\alpha = R \lambda l$
 - R is distance btw satellite/observed surface, λ is wavelength, and l is antenna length
- SAR: across-track (slant range) resolution depends on incidence angle and pulse length, and pulse length depends on λ
- If x is a geophysical quantity and F is a radiative transfer model, then satellite measurements y can be expressed as $y = F(x)$ and this can be theoretically inverted to solve for x
 - This has been done in the visual domain, but is hard in microwave domain given snow/ice microwave emission depends on many variables: e.g., salinity, snow grain size/shape
- ML/AI relies on in-situ training data, which we have very little of in the Arctic and is often constrained to certain regions and time of year
 - Further, we need consistently updated in-situ data as past observations may no longer hold in the current state of climate warming, which would lead to biases in ML/AI outputs

Sea ice parameters

- SIC computed by PMW by examining differences in T_b from sea ice and open water
- Polarization difference $P = TB_v - TB_H$ can be used to discriminate btw sea ice/water
- Polarization ratio $PR = \frac{TB_v - TB_H}{TB_v + TB_H}$ is used to remove dependence on physical temperature
- Algorithms combine TB from two diff polarizations (group 1), from two diff frequencies (group 2), or both (group 3) → group 4 combines two algorithms or products, e.g., EUMETSAT OSI SAF
 - Group 1 (2) → Comiso bootstrap algorithm polarization (frequency) mode
 - Group 3 → NT and NT2 algorithms
- Sea ice age determined via PMW as coarse-grained snow on rougher MYI has higher TB because of larger volume scattering contribution than saline, less porous FYI
- Gradient ratio used to estimate MYI fraction: $GR(37,19) = \frac{TB_{37v} - TB_{19v}}{TB_{37v} + TB_{19v}}$ as FYI GR ~0, MYI GR < 0

- SIT is estimated using microwave approaches by taking advantage of the change in salinity w/SIT
- SAR ice drift/dynamics use a sequence of two images, separated by a time short enough so they don't decorrelate, and then the features are identified in each using cross-correlation
- Maximum cross-correlation feature tracking w//microwave TB or scatterometry → box of image pixels e.g., 5x5 is selected in first image, then moved within a search window around the position of the original box in the second image → for each location of the box, cross-correlation btw radar backscatter or TB distribution is computed
- Location w/max cross-correlation gives best match, and distance (relative locations) btw centers of two boxes is the magnitude (direction) of the displacement vector
 - Drift speeds = displacement / time diff btw scenes

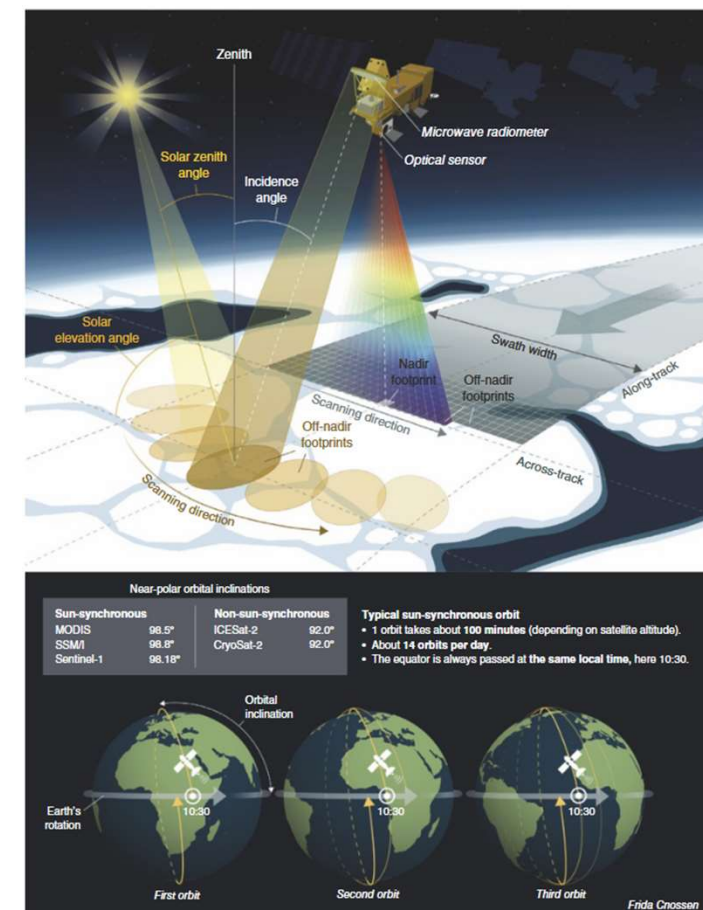
Uncertainties

- Key sources of uncertainty identified: (a) sensor onboard the satellite, (b) conversion from raw measurement to geophysical quantity, and (c) variability of features within satellite footprints

Impressions

- Great overview of all sea ice remote sensing, explaining basic like what is/determines microwave brightness temp, how SAR works, etc... a first-look if idk an answer to a remote sensing Q that's not about altimetry

Foundations | Sea ice remote sensing



Potential basin-scale estimates of Arctic snow depth with sea ice freeboards from CryoSat-2 and ICESat-2: An exploratory analysis

Introduction

- This was written when IS2 was in development and preparing for launch
- "Presently, there are no direct measurements of time-variable snow depth at the spatial scale needed for thickness calculations"
- This is the first study to explore the potential for freeboard differencing, with the goal to motivate NASA and ESA to collaborate and get near-coincident observations of IS2 and CS2

Data

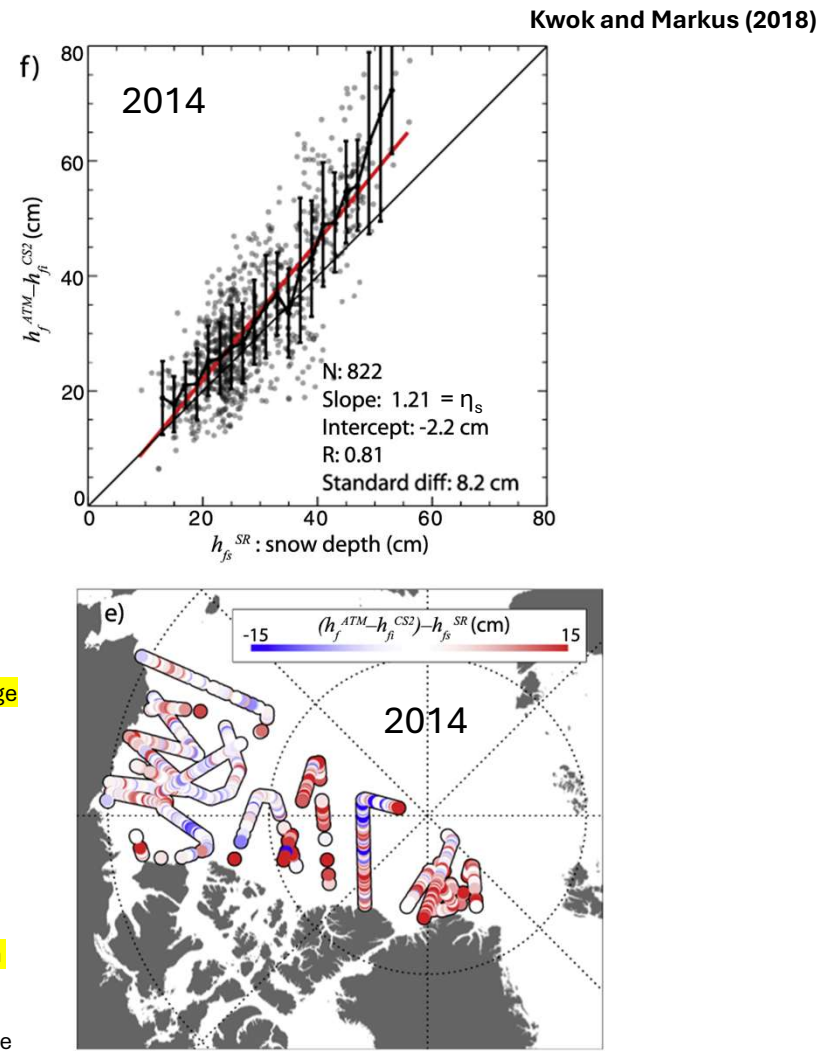
- Data from spring 2014-2015
- CryoSat-2 → gridded (12.5km) 30-day fields of freeboards from Kwok and Cunningham (2015)
- IceBridge ATM freeboard → 1-2m footprint, across-track swath of 45m → total freeboard
- IceBridge snow radar → ~6GHz bandwidth (C-band), avg footprint spacing ~5m, footprint size ~5-10m
 - η_s computed using snow density of 320 kg m^{-3}

Results/Data Analysis

- Derivation of freeboard differencing provided in section 3.1
 - $h_f^{ATM} - h_{f_i}^{CS2} = \eta_s h_{f_i}^{SR} + \varepsilon$ where $h_{f_i}^{SR}$ is OIB snow radar depth and ε is error in that estimate (Eq. (4))
- Regressing $h_f^{ATM} - h_{f_i}^{CS2}$ vs. $h_{f_i}^{SR}$ gives correlation, but slope of line also gives estimate of η_s
 - For 2014, $R=0.81$ and slope = 1.21
 - 2015 data has similar results as 2014, with $R=0.80$, slope = 1.22
 - For both 2014 and 2015, η_s is close to ~ 1.25 , which is expected for a $\rho_s = 320 \pm 60 \text{ kg m}^{-3}$
- ATM freeboards and snow depths are mapped to 12.5 km averages to make comparable w/CS2
 - CS2 averages are 30-day gridded fields centered on day of OIB flight
- $h_f^{ATM} - h_{f_i}^{CS2} > h_{f_i}^{SR}$ in general
 - "since Eq. (4) is expected to be valid when η_s is expected to be greater than unity."
- Regression slopes of 1.21 and 1.22 correspond to a snow density of $\sim 260 \text{ kg m}^{-3}$ which is lower end of expected range
- If they had chosen to compute snow depth using $\eta_s = 1.25$, results would have differed from OIB by $\sim 3\%$
 - So, results are relatively insensitive to choice of η_s , but it does introduce some uncertainty
- Some mention on whether radar return comes from s-i interface, but they reference simulations from Kwok (2014) stating that this is largely due to retracking approach and surface roughness
- Standard error is $\sim 8\text{cm}$, some of which they attribute to not perfect coincidence (both spatially and temporally)

Conclusions

- Here, ATM is used as a proxy for IS2 to explore potential of freeboard differencing
- Two years of ATM-CS2 vs. OIB snow radar snow depths have R of ~ 0.80 and η_s of ~ 1.21
- "[O]ur results suggest that it is possible to obtain time-varying estimates of snow depth over the entire Arctic Ocean (potentially bi-weekly timescales) from freeboard differences"
- "Adjusting the orbits to provide nearcoincident space-time sampling of the surface, to minimize aliasing of geophysical processes (snowfall and snow mass redistribution in this case), is obviously of significant interest to the science community."



Cryo2Ice | CS2 | OIB ATM | Snow depth

Arctic Snow Depth and Sea Ice Thickness From ICESat-2 and CryoSat-2 Freeboards: A First Examination

Kwok et al. (2020)

Introduction

- First examination of IS2 and CS2 freeboard differencing over 14 Oct 2018 to 30 April 2019

Data

- CS2 freeboards processed following Kwok and Cunningham (2015)
- IS2 ATL10 lidar freeboards → strong beam only
- Daily fields of reconstructed snow depths from ERA-I and ERA-5 – 100 x 100 km grid
 - Lagrangian parcels tracked and snow accumulated on each parcel
 - Snow allowed to accumulate when SIC > 50% and T < 0°C
- OIB ATM and snow radar data from 12 and 22 April 2019

Estimation of snow depth from freeboards

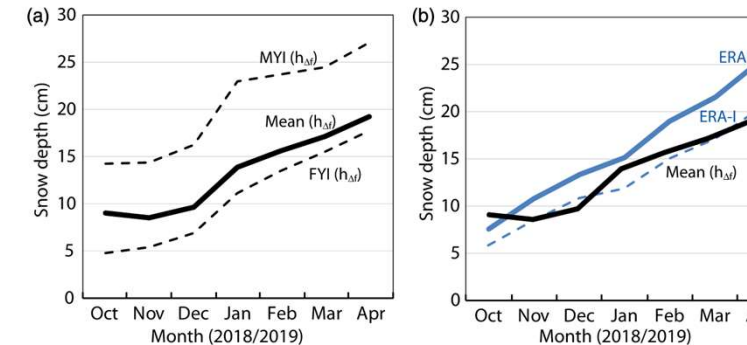
- Freeboard differences computed using 25 km gridded IS2 and CS2 data
- At each IS2 gridcell, CS2 observations within a 75 km box and $|\Delta T| < 15$ days
- Snow depth relatively insensitive to uncertainties in bulk snow density
 - Uncertainty in snow depth accounts for ~4% of difference in freeboard, vs. uncertainty in SIT accounts is ~70% of the freeboard difference

Snow depth estimates

- Qualitative agreement in snow depths between $h_{\Delta f}$, h_{ERA-I} , and h_{ERA5} from Oct-Dec
 - Although spatial pattern similar after Dec, magnitude of h_{ERA-I} and h_{ERA5} is much larger
 - Expected as no loss terms in reanalysis reconstructions (e.g., no wind blown snow)
- Bimodal $h_{\Delta f}$ plots, reflecting snow on FYI and MYI
- Chukchi Sea shows strong snow growth starting in Jan → associated w/strong cyclones that winter
- Snow depth evolution: ~9 cm (~5 FYI, ~14 MYI) in late Oct to ~19 cm (~18 cm FYI, ~27 cm MYI) in April
- Freeboard explains >80% of variance in snow depth → roughly 50% of total freeboard is snow

Comparison with snow depths from OIB data

- FB differences w/IS2-CS2 and ATM-CS2 highly correlated and differ by less than 1 cm
- $h_{\Delta f}$ compared w/OIB SR: differences of 4.7 cm (12 April) and -2.3 cm (22 April)



Notice that snow depth increases in the ERA-I and ERA5 are more monotonic

Sources of uncertainty

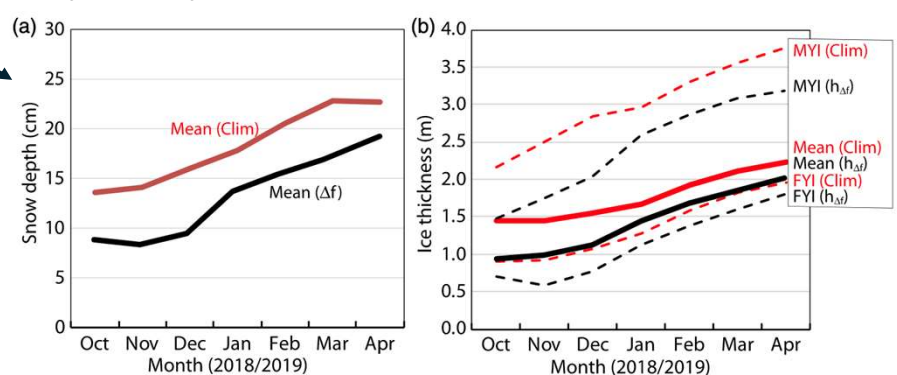
- They examine sampling w/combinations of $|\Delta T| < 1, < 10, < 15$ days and grid sizes of 25 and 75 km
 - Stdev in calculated snow depths are all < 1cm → low spatial variability in CS2 freeboards
 - To be expected, as in absence of deformation the spatial variation of ice floes governed by basal growth and snow loading
 - ~10% of growth in SIT adds to h_{f_i} , ~3% of change in snow depth changes h_{f_i}
 - Variability of IS2 h_f is more than double that of CS2
 - The limited variability of ice freeboards allows them to bin over such large regions
 - This indicates that effect of ice dynamics is small in this study
- They acknowledge Nandan et al. (2017, 2020) studies, but state that “[w]hile the physical basis of a displacement of the RP due to brine wicking is sound, we do not believe that we understand the prevalence of this process ... to warrant implementation at this time.”

SIT using satellite snow depth and a modified climatology

- $h_{\Delta f}$ ranges from 8.1 cm in Oct to 18.6 cm in Apr, while climatology range is 13.6 to 22.6 cm
 - Largest disagreements over MYI north of CAA/Greenland
- Over the 6.5-month growth season, the average difference in monthly mean SIT is 0.33 m (FYI: 0.23 m; MYI: 0.58 m).
 - Largest differences in Oct/Dec, but increased snow depths gives closer agreement in Jan-Apr

Conclusions

- Overall, the area-averaged snow depth and SIT from the modified climatology are higher by ~5 cm and 0.33 m
- Discussion of sampling interesting and worth revisiting w/my own study; a foundational Cryo2ice study



The Antarctic sea ice cover from ICESat-2 and CryoSat-2: freeboard, snow depth, and ice thickness

Kacimi and Kwok (2020)

Introduction

- Before this paper, SIT estimate relied on assumptions (1) independent snow depth measurements, (2) snow depth being equal to h_f , or (3) empirical relationships btw h_f and SIT from field data
- This paper is the Southern Ocean companion of Kwok et al. (2020)

Data (Apr-Nov 2019)

- IS2 ATL10 freeboards from strong beams only
- CS2 freeboards processed using Kwok and Cunningham (2015) procedure → gridded to 25 km
- Sampling is $|\Delta T| < 10$ d and within 75 km box → as w/Kwok et al. (2020), stdev < 1cm for all sampling combos

IS2 and CS2 freeboards

- Five key processes that contribute to modification of h_f in Antarctic winter

$$\Delta h_{fs}(t) = \delta h_{snow} + \delta h_{\Phi} + \delta h_{sti} + \delta h_{def}^s \text{ and } \Delta h_i(t) = -\alpha(\delta h_{snow} + \delta h_{\Phi}) + \beta \delta h_{sti} + \delta h_{def}^i + \delta h_{gm}$$

- Snowfall (δh_{snow}) → P-E; snow load depresses freeboard by $-\alpha(\delta h_{snow})$ → α is based on ρ_i, ρ_s and ρ_w
- Spatial redistribution of snow including loss to leads (δh_{Φ}) → freeboard adjusts hydrostatically by $-\alpha \delta h_{\Phi}$
- Snow ice formation (δh_{sti}) → freeboard gains $\beta \delta h_{sti}$, β is fraction of snow converted to ice freeboard
- Ice deformation → changes snow layer (δh_{def}^s) and ice freeboard (δh_{def}^i)
- Basal ice growth and melt (δh_{gm})

Persistent wind-driven convergence along coastal A-B seas → highest freeboard variability and R^2 btw IS2 and CS2 is 0.90, highest of any region → anomalous onshore winds perpendicular to coast in 2019 due to deep ASL

Thickest fb in W. Wedd (~36-41cm range), lowest average freeboards found in E. Wedd (~15-25cm range)

Ross Sea: ice production occurs in the Ross Shelf polynya, Terra Nova Bay, and McMurdo Sound polynya

- Long tong of thin ice extends seaward and west from Ross Embayment, consistent w/CW drift due to ASL
- Inflow of thick coastal A-B sea ice replenishes some of the new ice that is exported here

Pacific and Indian Ocean sectors primarily seasonal ice, fed by coastal polynyas and Ross Sea outflow

- Behind E. Wedd, lowest freeboard/SIT in Southern Ocean

Snow depth estimates

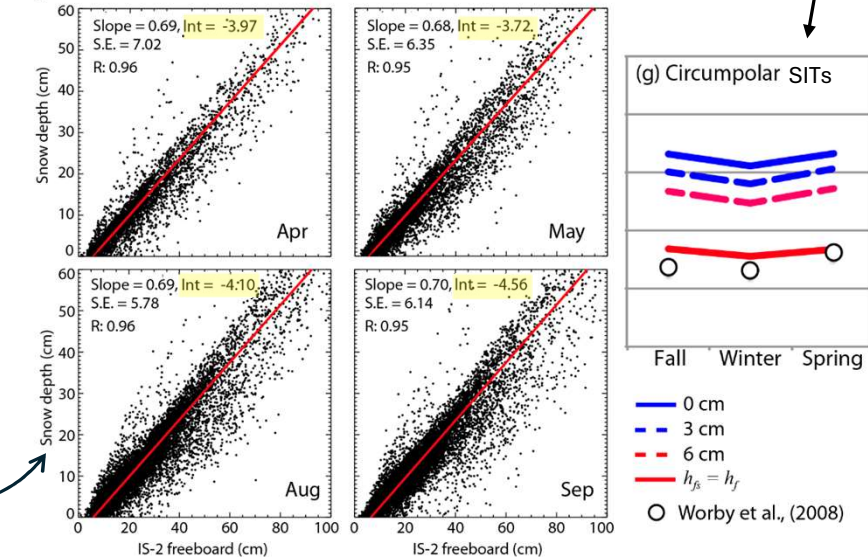
- Snow-ice assumed to have same density of sea ice
- "There is no generally accepted value for bulk density of snow in the Antarctic" → they use 320 kg m^{-3}
- As w/Kwok et al. (2020), uncertainty in snow depth (SIT) is ~4% (70%) of difference in freeboards
 - For $h_f^{IS2} - h_f^{CS2} = 30\text{cm}$, this translates to 20cm uncertainty in SIT due to thickness, and ~1cm due to snow
- Thickest (thinnest) snow in W. Wedd/coastal AB (Ross/E. Wedd) → only AB and coastal AB show seasonal increases
 - This indicates that processes that remove snow overwhelm all precipitation signals in all months
- Between ~66-70% of the IS2 freeboard is snow, compared to ~50-55% in the Arctic
 - Consistent negative intercepts in IS2 freeboard vs. snow depth plots indicate a retrieval is biased, resulting in Δh_{fs} overestimate of +3.4-4.5cm
 - Attributed to RP > snow-ice interface

Ice thickness and volume

- Thickest ice in W. Wedd (~2.50m) and coastal AB (~3.25m), thinnest in Ross (~0.90m) and E. Wedd (~<1.5m all months)
- Weak seasonal cycle of SIT in all sectors except AB and coastal AB
- SIT in sectors of seasonal ice seem to be too high (~1.5m) → points to CS2 biases
 - They apply 3cm and 6cm adjustments (resulting in reduced SIT), saying that these large-scale adjustments likely provide better estimates
- SIV has consistent seasonal growth, driven by changes in areal production as SIT has little seasonal variability
- With adjustments of 3-6cm, estimates of circumpolar SIV are 17,900-15,600 km^3 in Oct w/SIT of ~1.29-1.13m

Conclusions

- In 2019, observed seasonality in sector-averaged freeboards, snow depth, and SIT are surprisingly weak, unlike the Arctic, due to many competing processes (e.g., snow redistribution, snow-ice formation, etc.)
- Evidence points to biases in CS2 freeboards due to RP above s-i interface
 - Sector-scale adjustment of 3-6cm gives more credible results
- Very little validation data in the Antarctic for snow/freeboard/SIT estimates



Cryo2Ice | Antarctic | RP bias

Arctic Snow Depth, Ice Thickness, and Volume From ICESat-2 and CryoSat-2: 2018–2021

Kacimi and Kwok (2022)

Introduction

- This paper builds on Kwok et al. (2020) by examining interannual variability in freeboard-derived snow depths, SIT, and SIV over 2018–2021 → Kwok et al. (2020) was a first examination over a single winter season

Data

- IS2 ATL10 → variable along track res of ~27–200m; estimates from 3 strong beams gridded to 25km
 - 3 strong beams have higher resolution than weak → better representation of spatial mean
- CS2 freeboards processed using procedure from Kwok and Cunningham (2015) → also gridded to 25km

Snow depth estimates

- mW99 from Kwok and Cunningham (2008, 2015) → adjusted for FYI fraction + shifting curve to earlier in season
- Δf_s computed using CS2 observations within 75 km box and $|\Delta t| < 10$ days
- Decrease in snow depth from 2018–2019 through the next 2 seasons from ~12.6cm to ~11.7cm in October
- Mean April decrease of ~2.5cm of Arctic, largely due to -3cm change over MYI
- Average seasonal growth is from around 12 cm to 20 cm over October–April
- $\Delta f_s < mW99$; range of Δf_s differences over 3 seasons are within annual variability ~3–6cm reported in Warren et al. (1999)

Ice thickness and volume

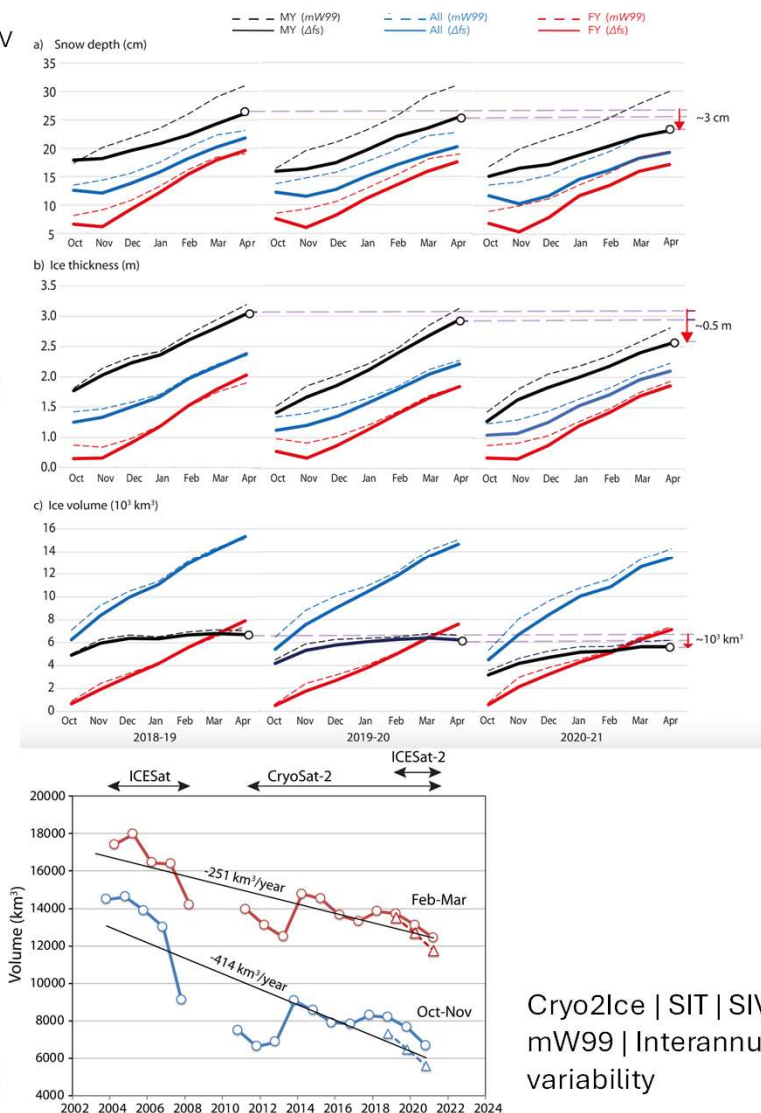
- In this paper, h_{IS2} is SIT derived w/IS2 and Δf_s , while h_{CS2} is SIT derived w/CS2 and mW99
- h_{IS2} decreased over the three seasons
 - Differences over 2020–2021 relative to 2018–2019 range from -0.28 m (Apr) and -0.14 m (Jan), largely due to MYI reductions in CAA and region north of Greenland
- "In April 2021, the MY-ice is thinner by ~0.50 m, accounting for a ~16.1% loss relative to 2019."**
 - Seasonal ice varies similarly across the winter over all years, growing from 0.71 m (Oct) to 1.91 m (April)
- $h_{CS2} > h_{IS2}$ for both ice types, w/larger differences over FYI**
 - Differences between estimates are greatest in fall and decrease by mid-winter
- h_{CS2} also shows declining SIT over the three seasons, driven by MYI losses and little interannual variability in FYI
- Magnitude of thinning is much larger w/ h_{IS2} than h_{CS2} → 16.1% loss vs. 12% loss between April 2019–2021
- h_{IS2} mean SIV change of ~700 km³ btw April 2019–2020, ~1,214 km³ btw April 2020–2021
 - Net SIV decline of -12.5% (MYI 16.3%, FYI 10%)
 - Changes in MYI volume largely due to thinning, as MYI area is somewhat consistent across the 3 years
- FYI SIV changes are insignificant, while MYI changes drive SIV decline

Volume estimates during the satellite altimetry period

- Placing results from this study in context of CS2 record (2010–2021) and IS record (2003–2008)
 - Trend is loss of -251 km³/year and -414 km³/year in winter (Feb–Mar) and fall (Oct–Nov), respectively
- Since beginning of century, Arctic has lost 1/3 of its winter SIV (~6,000 km³)

Conclusions

- Observed thinning and SIV decline due to MYI losses, as FYI end of season variability is insignificant
- Using mW99 leads to larger SITs by up to ~22m, especially during fall where prescribed snow loading is higher
- SIV changes are -12.5% overall and -16.3% for MYI using freeboard-differencing, versus -5.9% and -12.1% using mW99
- For the 3 years, decrease in mean April snow depth (~2.50 cm) and SIT (~0.28 m) are equivalent to an SIV loss of ~12.5%



Cryo2Ice | SIT | SIV |
mW99 | Interannual
variability

Arctic Freeboard and Snow Depth From Near-Coincident CryoSat-2 and ICESat-2 (CRYO2ICE) Observations: A First Examination of Winter Sea Ice During 2020–2022

Fredensborg Hansen et al. (2024)

Introduction

- First examination of feasibility of along-track Cryo2Ice snow depth estimates

Data and Methods

- IS2 ATL10 w/all six beams, and ATL20 to make monthly composites of snow depths
- CS2 ESA-E, AWI, and LARM
- Snow depths compared w/AMSR-2 over FYI (5 day avg), SMLG, mW99
- Avg Cryo2Ice timelag of 2.03-2.71 hours over 2020–2022
- 3500m radius provides comparable results to smaller search radii w/o compromising # data
 - Distance from IS2 samples to CS2 nadir point is around ~2400m for both years
- Ice motion per Cryo2Ice timelag computed w/Medium Res OSI SAF product
 - Avg drift of 2 km over 2020–2021, w/only ~14% of obs drifting > 2.5km
 - Uncertainty statistics at 3 hrs similar to 6 and 12 hr, so assumed these statistics are representative from 0-3hr
- Comparisons w/SIMBA and AWI buoys within ±50km and 2 days
- Random errors → RMSD of along-track freeboards; systematic errors → max absolute height difference btw 3 CS2 retrackers per Cryo2Ice point (i.e., retracker bias as first approx. for systematic uncertainty)

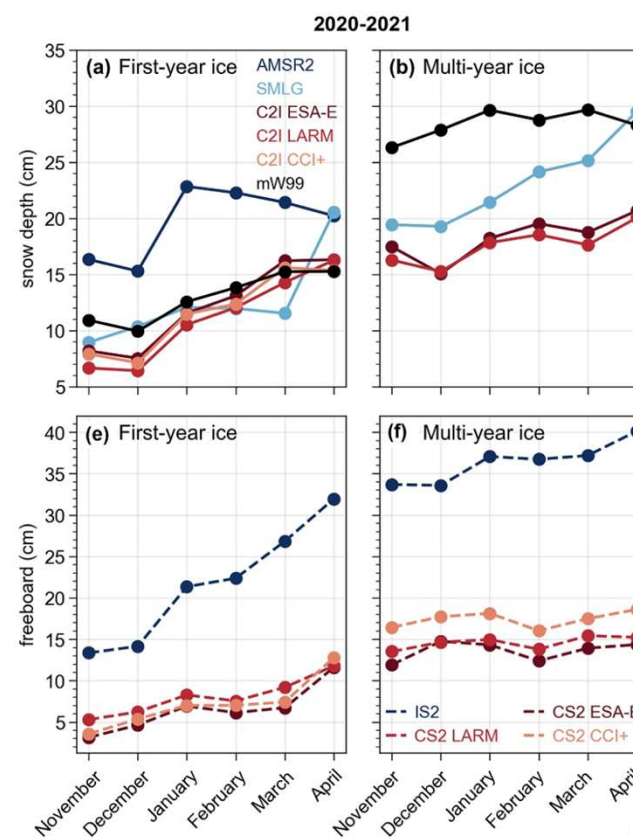
Results

- Consistently thicker snow depths from AMSR2 than Cryo2Ice over FYI
- SMLG snow depths also larger than Cryo2Ice snow depths over both ice types
- Largest SMLG-Cryo2Ice disagreements occur in Atlantic sector and Pacific Arctic regions near storm tracks/large open water areas → Cryo2Ice snow thinner in these regions
 - Hard to determine whether Cryo2Ice underestimate snow depth of SMLG overestimates
- Comparisons with buoys show inconsistent results and conclusions are difficult to derive
 - Weak R w/acoustic buoys (AWI), moderate R w/thermistors string buoys (SIMBA)
- ~9cm of seasonal accumulation over FYI, in agreement w/mW99 and SMLG
- Cryo2Ice obs close to SMLG at beginning of season, but ~10cm less at end over MYI
- Average uncertainty of 11 ± 3 cm over 2020–2021, and 10 ± 2 cm for 2021–2022
 - Min estimate, as systematic biases in IS2 not estimated
- Preferable to only use IS2 strong beams, but limitations on number of data makes this hard
- Choice of snow density is not impactful for snow depth estimates, but gets magnified in freeboard-to-SIT conversion

Conclusions/Impressions

- No statements made about which radar retracker performs best or any real conclusive statements about Ku-band radar wave propagation
- This is important to refer to for the uncertainty analysis and to get some basic ranges for snow depths, but the figures are quite hard to understand

- Cryo2Ice snow depths thinner than SMLG/AMSR-2 snow depths, with differences being most pronounced in the Atlantic and Pacific Arctic.
- Along-track snow depth uncertainty of $10-11 \pm 2-3$ cm for 7-km segments w/random (precision of freeboard/snow depth obs) and systematic (re-tracker biases) contributions of 7 and 4 cm, respectively
- Poor correlation w/buoys overall, better to compare w/non-point measurements
- The value of this paper lies largely in the methods and discussion, not in the results



Cryo2Ice | Snow depth |
Freeboards | pan-Arctic

Snow depth estimation on leadless landfast ice using Cryo2Ice satellite observations

Introduction

- This is the first comparison of Cryo2Ice snow depths to in-situ estimates over landfast ice, which is leadless, so they use tidal variations to account for differences in ssh btw IS2/CS2 obs

Data and methods

- Uncorrected ATL07 heights → 25km coastal buffer not applied
 - Strong beam 2l used, as closest of all three to in-situ obs (~1500m)
- Hourly tidal corrections applied, ranging from -62 to +62cm → larger than over open ocean
 - Corrections from Global Ocean Tide Model 4.8
- CS2 L2 Baseline-E data** → tidal corrections from Finite Element Solution 2004 Ocean Tide Model
- Field measurements → **75 km transect across Dease Strait**; snow depths using magnaprobe from four sites ranging from smooth, rough, and mixed sea ice roughness zones → 1 May 2022
- Cryo2Ice tracks had 77 min time lag and were ~1.5 km apart on 29 April 2022
- High SLP system lead to negligible surface winds over the area
- Difference in tides over Cryo2Ice time lag was 7.9 cm from the IS2/CS2 tidal corrections (models), whereas tide gauge had the difference at 6 cm → so the in-between Cryo2Ice heights adjusted by 1.9 cm before computing snow depth
- Sentinel-1 SAR used to compare the σ_0 profiles of IS2/CS2 to see whether they are “seeing” the same snow → diff in $\sigma_0 < 1$ stdev of backscatter of each track → observing the same snow

Results

- Mean snow depth varied btw 9-17cm across the four in-situ sites
- Mean snow salinity varied btw 1.5-2ppt, w/one site having 6.78 ppt salinity
- Mean snow bulk density varied btw 358-374 kg m⁻³ w/one site having 248 kg m⁻³
 - Wind slab layer 4-7cm above s-i interface increases ρ_s
- Snow density (salinity) decreases (increases) as you get closer to s-i interface**
- Adjusted mean Cryo2Ice snow depths are 7.4 cm, w/max of 39.4 cm → significantly lower than the in-situ max of > 90 cm**

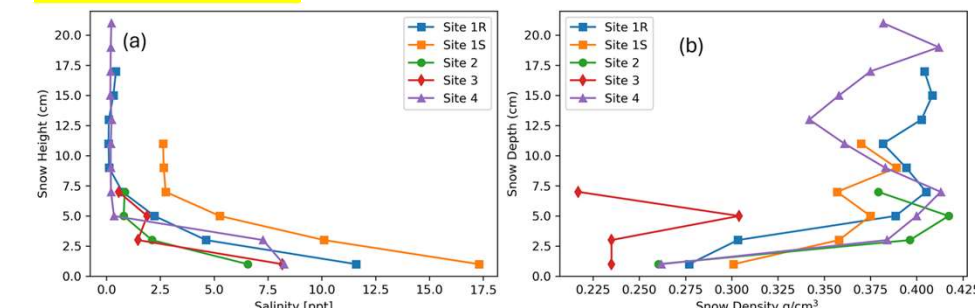


Figure 6. (a) Snow salinity and (b) snow density change by snowpack depth at the four snow sampling sites. Zero snow depth in both plots represents the snow–ice interface.

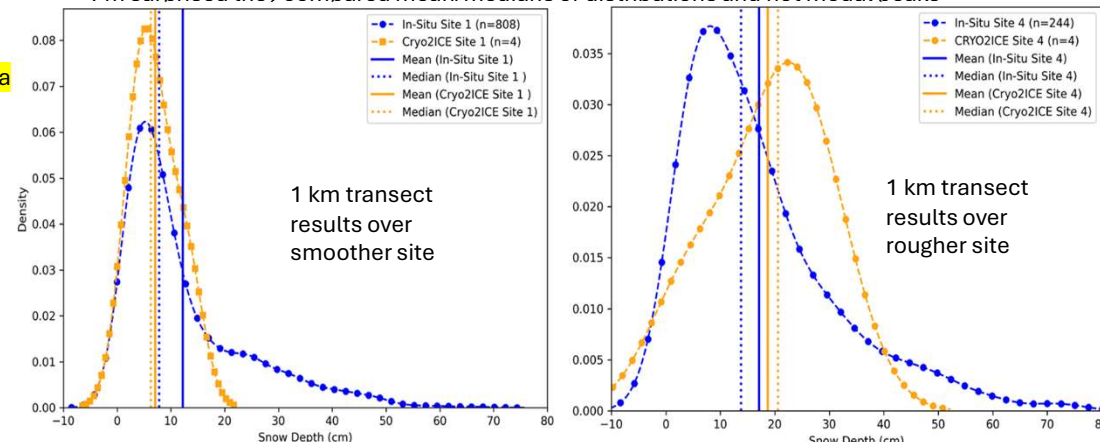
- 20% of Cryo2Ice observations were negative snow depths which led to widening of distribution

Discussion

- Cryo2Ice snow depths underestimate the observed snow depths (mean of 7.4 cm vs. 11.9 cm)**
- Cryo2Ice underestimates attributed to coarse resolution of CS2 → distributions truncated at the tail w/the thicker portions of in-situ snow depths unresolvable from space
- Averaging IS2/CS2 over a 1km transect rather than 300m transect makes results more comparable with in-situ estimates, but you lose some distinct morphological features
- The snow depth distributions themselves are similar, but mean/median/mode differ greatly
- Cryo2Ice performs worse at site with roughest surface
- Higher snow depths coincided w/the site with the least saline snow
- “The chance of snow bulk density impacting on the Cryo2Ice retrievals was less likely”
- Difference in IS2 and CS2 heights increased by 7.9cm due to ocean tide adjustment, but tide gauge indicates it should be 6cm → 1.9 cm diff introduces a ~26% bias in retrieved snow depth
 - More broadly, overall uncertainty is 15-40% due to tidal diff in btw satellite passes
 - Effects absolute magnitude, but not relative variations in retrieved snow depths

Conclusions

- Cryo2Ice performs well over regions w/thin and smooth snow, while struggling to capture snow depths > 30cm irrespective of roughness characteristics
- They can't conclude whether the several cm of disagreement btw in-situ and Cryo2Ice snow depths are due to snow geophysical processes, surf roughness, and/or errors in tidal corrections
- I wonder how results would change w/non-fixed retracker product like LARM
- I'm surprised they compared mean/medians of distributions and not modal peaks



Cryo2Ice | Leadless | Landfast | Snow depth | CAA

Multi-frequency altimetry snow depth estimates over heterogeneous snow-covered Antarctic summer sea ice – Part 2: Comparing airborne estimates with near-coincident CryoSat-2 and ICESat-2 (CRYO2ICE)

Fredensborg Hansen et al. (2025)

Introduction

- The first Cryo2Ice validation underflight carried out w/full suite of instruments to evaluate penetration into snow

Data

- IS2 ATL07 used for visualization purposes, ATL10 is used for processing
- CS2 L1b w/3 different processing chains: ESA-E, CryoTEMPO, and FF-SAR
 - CryoTEMPO surface elevations derived using SAR Altimetry Mode Studeis and Applications over ocean (SAMOSA+) algorithm
 - FF-SAR → coherent processing of radar echoes, physical retracker
- Airborne campaign observations within 60m of CS2 observations, w/80% within 20 m
- CREESIS Ka, Ku, and C/S-band radar altimeters as described in Part 1 w/retrackers TFMRA40, 50, 80 for assumed single scattering horizons, CWT and PEAKS for multiple scattering horizons
 - MAX refers to location of maximum power of waveform that's extracted to represent dominant scattering interface
- AS w/Part 1, no in-situ or other reference observations (e.g., buoys) available
- AMSR2 PMW-derived and CPOM Antarctic Snow on Sea Ice Simulation (CASSIS) snow depths

Methodology

- Fredensborg Hansen et al. (2024) method for processing Cryo2Ice data
- Airborne data first averaged into 1km segments, then smoothed w/search radius of 3.5km to make comparable w/Cryo2Ice, then both airborne and Cryo2Ice segmented to 25 km

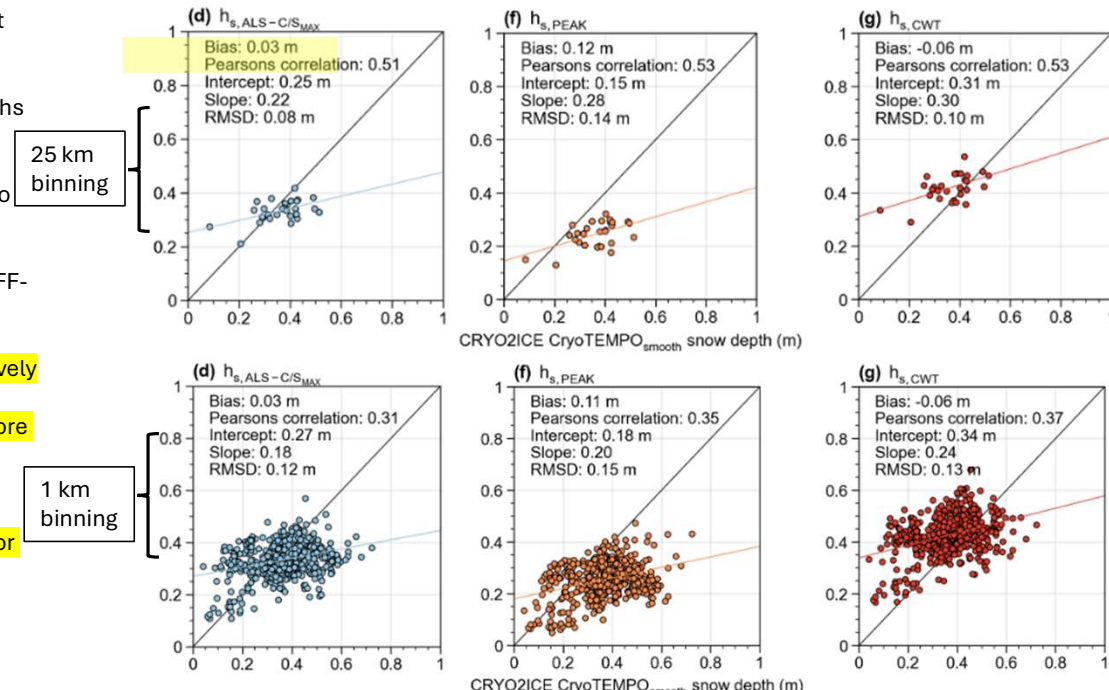
Results

- Smoothing window applied on 309, 215, and 1502 radar freeboard observations for ESA-E, FF-SAR, and CryoTEMPO, respectively, post-processing → not much data
 - ESA-E and FF-SAR have stricter requirements for waveforms to be permitted
- ESA-E and FF-SAR radar freeboards are similar, w/avg of 31 ± 19 cm and 29 ± 15 cm, respectively
 - CryoTEMPO average is 7 ± 1 cm
 - Discrepancy due to CryoTEMPO being able to retrack waveforms that are more specular, whereas ESA-E and FF-SAR require more diffuse waveforms
 - SAMOSA+ retracker doesn't classify waveforms before retracking
- Rest of study focuses on Cryo2Ice w/CryoTEMPO as ESA-E and FF-SAR have too little data
- IS2 + CryoTEMPO-derived snow depths vary considerably more (16 cm stdev) than CASSIS or AMSR2 (3 and 8 cm stdev, respectively)
 - CASSIS obs are 12 cm higher than IS2 + CryoTEMPO snow depths
 - AMSR2 snow depths agree within 1 cm of CryoTEMPO snow depths
- Comparison btw 1km binned airborne snow depths results in all seven snow depth combinations having correlations btw 0.31-0.37
 - Lowest bias (3cm) from ALS-C/S-band MAX w/RMSE 12cm

- Comparison btw 25km binned airborne snow depths results in correlations btw 0.51-0.53 for Cryo2Ice CryoTEMPO and CWT, PEAKS, and ALS-C/S-band MAX → similar bias (~3cm) as w/1km binning
- Overall, Cryo2Ice CryoTEMPO and ALS C/S-band MAX agree most closely

Discussion and outlook

- Both interfaces could, theoretically, be retrieved from airborne Ku-band data if a retracking algorithm was able to isolate some of the smaller peaks along the trailing edge
- This study, like De Rijke-Thomas et al. (2023) clearly discusses how returns differ on airborne and satellite scales due to different viewing geometries and footprint sizes
 - There is a need to link in-situ, airborne, and satellite estimates & determine how they differ
- "we have not evaluated the relationship between roughness and the different retracked interfaces"



Radar | Antarctic | Cryo2Ice | Multi-frequency

A tutorial on synthetic aperture radar

Introduction

- Flight direction = azimuth; slant range = direction perpendicular to azimuth direction
- Azimuth antenna beamwidth of conventional SLAR: $\Phi_a = \lambda/d_a$ and azimuth resolution $\delta_a = \Phi_a r_0 \rightarrow$ replaced by SAR where $\delta_a = d_a / 2 \dots$ no dependence on range

Basic SAR principles

- SAR sensors often use chirp signals (FM pulse waveforms) where amplitude is constant but instantaneous freq increases linear according to $f_i = k_r t$ where k_r is chirp rate
 - This gives bandwidth $B_r = k_r \tau$
- Chirp is followed by echo window time where radar “listens” and received signals on board
 - Fast time – time in range direction; slow-time = range-line
- Transmission + listen procedure occur every pulse repetition interval (PRI) seconds, which is the reciprocal of pulse repetition frequency (PRF) : PRI = 1/PRF
- Swath width = ground-range extent of the radar scene

$$r(t) = \sqrt{r_0^2 + (vt)^2} \approx r_0 + \frac{(vt)^2}{2r_0} \text{ for } vt/r_0 \ll 1$$

- Slow time = time associated w/platform movement
- Range variation of point target directly related to azimuth phase by $\psi(t) = -4\pi r(t)/\lambda$
- Along-track (azimuth) resolution = $\delta_a = d_a / 2$
- Across-track (slant-range) resolution $\delta_r = c_0 / 2B_r$ where c_0 is the speed of light and B_r is bandwidth
- Along-track (azimuth) resolution is provided by construction of synthetic aperture

- Synthetic aperture length $L_a = \Phi_s r_0 = \lambda r_0 / d_a$
- We want a narrow virtual beamwidth and therefore longer synthetic aperture $\Phi_{sa} = \lambda / 2L_{sa}$
- $\delta_a = r_0 \Phi_{sa} = r_0 \lambda / 2L_{sa} = d_a / 2$

- δ_a improves w/small antenna bc they “see” a point on the ground for a longer period (T_{ill}): $T_{ill} = \lambda r_0 / v d_a$
 - Smaller antenna = longer virtual antenna length
- Real and imaginary part of echo signal data are amplitude and phase, respectively
- Return echoes are sampled in fast time (range) and slow time (azimuth) → i.e., 2D
 - Slow-time is measuring data across consecutive pulses to determine target Doppler frequency
- Speckle occurs due to coherent sum of many scatterers with a random distribution within range cell
 - Intensity/phase of this speckle are Gaussian distributions → hence why it can be averaged out
- Multi-looking is a non-coherent averaging of the intensity image and reduces speckle while degrading image resolution → speckle decreases as resolution improves
- W/single-channel SAR, fine-azimuth resolution and wide swath can't be obtained simultaneously

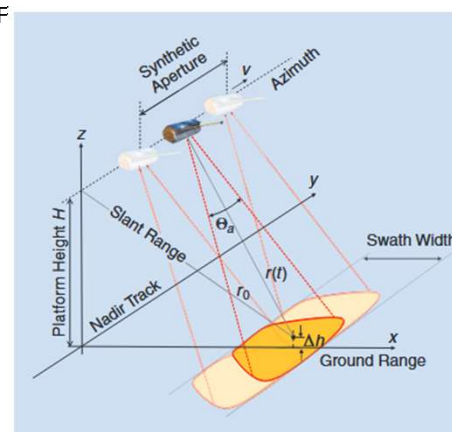


FIGURE 2. Illustration of the SAR imaging geometry. r_0 stands for the shortest approach distance, Θ_a for the azimuth beamwidth and v for the sensor velocity.

Polarimetry

- HV = transmit H, receive H and V; VH = transmit V, received V and H

- Most polarimetric SAR systems are monostatic
- Details given on polarimetric decomposition techniques → helpful for classification

Moreira et al. (2013)

Interferometry

- Interferometry requires two scenes to determine the phase difference between them → allows for range information that is accurate to a small fraction of the radar wavelength
 - Phase unwrapping is needed bc measured range difference is ambiguous within the λ
- Across-track interferometry – radar images acquired from mutually displaced flight tracks
 - $\Delta r \cong \frac{B_\perp}{r_0 \sin(\theta_i)} \Delta h \rightarrow$ can solve for Δh quite easily once we get Δr
 - Accuracy of phase measurement limited by magnitude of interferometric coherence (degree of correlation btw two scenes)
 - Multi-looking reduces coherence loss, at cost of reduced spatial resolution
 - Larger baseline = more sensitivity to Δh , but length of baseline is limited by (a) baseline decorrelation as larger baseline means echoes from individual scatterers within the scene will become more different... and (b) larger baseline = larger height ambiguity (which are usually resolved via phase unwrapping)
 - $h_{amb} = \frac{\lambda m r_0 \sin(\theta_i)}{B_\perp}$ at larger look angles, the $\sin(\theta)$ term decrease, so with larger B_\perp there is larger ambiguity in far-range
 - Bad for rough terrains w/big Δh
 - Differential SAR interferometry (DInSAR)
 - Multiple flights over same scene → range diff over temporal period used to get subsidence, for example

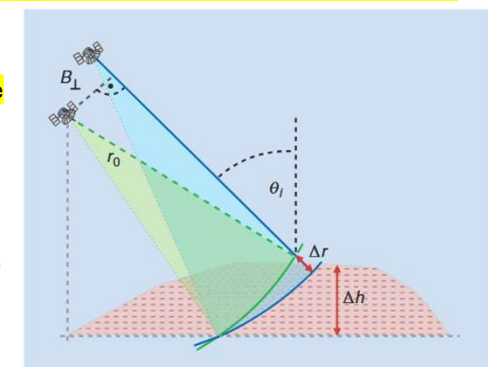


FIGURE 11. Across-track SAR interferometry employs antennas that move on parallel but mutually displaced flight paths (the flight paths are not shown since they are pointing into the page). The slant range r_0 , the incident angle θ_i , and the effective baseline B_\perp are all defined in a plane perpendicular to the flight paths. A change in the surface height by Δh causes a change in the range difference by Δr .

Polarimetric SAR interferometry

- Combination of interferograms acquired at different polarizations -- key observable is complex interferometric coherence
- Good for resolving vertical structures

Tomography

- Get synthetic aperture in elevation direction to retrieve whole distribution of vertical scatterers

Future developments

- Great description of resolution vs. swath width problem at the beginning of this section
- Digital beam forming, MIMO

Title

Author et al. (YYYY)

Introduction

Subsection | Keywords

Measurements of the Underside of Topography of Sea Ice by Moored Subsea Sonar

Melling et al. (1995)

Introduction

- The paper details acquisitions of draft and ice motion from moored ULS → Beaufort Sea

Description of instruments

- Ice motion: **Acoustic Doppler Current Profiler (ADCP)** → operating frequency of 76.8-1228.8 kHz
- Ice draft: **Ice profiling sonars (IPS)** → compute two-way travel time of acoustic pulse within a pre-defined min-max range window

- Pendulum sensors measure tilt, pressure sensor, and a clock
 - Pressure sensor is what determined the depth of the IPS below sea level → this changes w/storms, tides, so it is calculated (generally) every few minutes
- HP beamwidth <2° giving a nominal footprint diameter of 1-2
- Sampling interval is highly dependent on ice drift, as if it is sampled too sparsely, there will be undersampling, but if sampled too rapidly, data will be redundant
- IPS range precision 0.015 m

Calibration and error

- Sound speed at ice-water interface varies little throughout the year, thus a constant sound speed introduces an error of less than 0.5% in Doppler velocity calculations
- Ice drift is computed via Doppler shift in sound wave relative to mooring heading direction
- Depth of IPS: $D(t) = \frac{1}{g} \int_0^{p(t)} \frac{dp}{\rho(z,t)}$; two-way travel time: $T(t) = 2 \int_0^{R(t)} \frac{dr}{c(D-r,t)}$
- Two-way travel time varies w/density of ocean water, which has seasonal variation, thus a seasonal range correction is applied → depth not impacted as much by density changes

Sample of observations

- Eulerian ADCP ice motion estimates agree well w/Lagrangian buoy motion in the region
- Transition from ice to seawater results in strong increase in variability of Doppler velocity
 - But ultimately, the corresponding IPS data is needed to validate surface type
 - Spikes in Doppler velocity represent air bubbles, capillary waves, etc... from ocean waves
- Smooth FYI have low backscatter compared to diffuse echoes from rougher, MYI
 - Reasoning provided in Melling et al. (1998) introduction
- Primary influence on IPS depth is meteorological, as tides are small in the Arctic
 - Shown to vary up to 65 cm over first 40 days of deployment
- Average speed of sound between the IPS and the surface needs to be updated frequently to get accurate range estimates of sea ice draft → thus, discrimination of open-water vs. ice is critical**
 - W/correct speed of sound in water, range can be converted based on 2-way travel time
 - This needs to be done as routine CTD measurements is not feasible
- Apparent draft of target cannot be used for surface type discrimination because (a) agitation of leads by wind waves causes a-w interface to vary in range and (b) wave breaking causes injection of clouds of air bubbles to a depth of several meters which scatter sound strongly at freq of IPS
 - In short, **wave agitation prevents draft of open water to be used in correction of sound velocity** → lots of volume scattering can occur

- Combination of range and reverberation of echoes is what is used for ice-water discrimination
 - Reverberation = persistence of diffuse scattering
 - At same range, open water (thin FYI) has intermediate (very short) reverberation, and rough MYI has very long reverberation

Concluding remarks

- Statistics of topographic profiles/draft differ in space and time due to variations ice drift** → mapping observations to regular intervals in space is preferred method of analysis
- Since ULS is dependent on ice motion, as this is needed to calibrate range estimates and needed for Doppler velocity estimates, it is primarily useful in regions of ice motion like FS/Beaufort Sea
- Technique is not ideal for MIZ environments where pack ice can be influenced by ocean swell**
 - Messes up pressure measurements at sonar depth

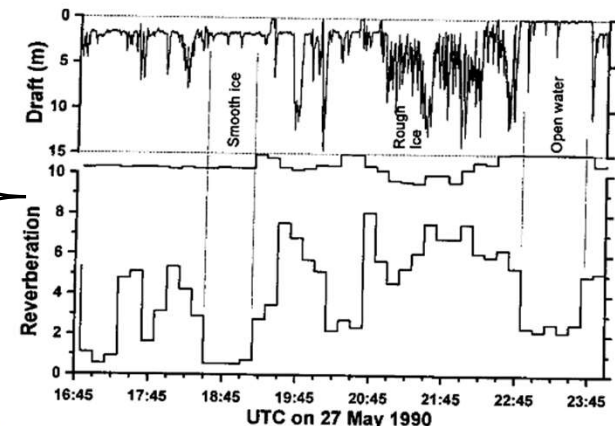


FIG. 10. An IPS record (top curve) displaying a variety of surface conditions. Note the very short reverberation of echoes from smooth ice that demonstrates the near-specular character of the reflection. Calm open water (right) is significantly rougher. See Fig. 9 for details.

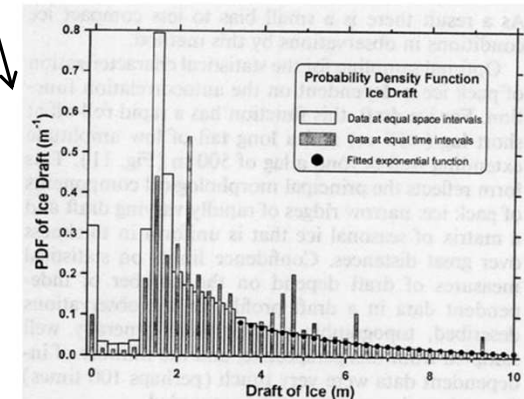


FIG. 13. Probability density of ice draft, from values interpolated to regular increments along the curvilinear survey path (open boxes). Symbols define an exponential curve fitted to the domain of deformed ice (draft 3.5–27 m). Shown also is the probability density computed from the observed data, which are regularly spaced in time (filled boxes).

Sonar | IPS | ADCP | Doppler velocity | Draft

Sound Scattering from Sea Ice: Aspects Relevant to Ice-Draft Profiling by Sonar

Introduction

- Looking at varying strength of sonar echoes and seeing what this tells us abt the surface
- IPS is vertically positioned so sonar beam hits ice at near normal incidence angle, but at the high frequencies used for IPS, the specular echo from the underside of thick FYI is weak due to “change in acoustic impedance across the porous skeletal layer forming the bottom of the ice”

Field measurements

- Water-structure profiler (WASP) sonar to observe varying conditions from freeze-up to late-winter
 - September 1995–February 1996 in Beaufort Sea
 - 10s sampling interval at 52m depth → 200 kHz IPS and 300 kHz Doppler sonar
- No data btw mid-Sep and 22 Oct → so no observations of subsurface bubble clouds
 - To get this data, separate deployment in June/July 1996 along Pacific coast of Canada

Calibration

- Lognormal form provides closest representation of observed PDF to calm sea surface
- Gain of WASP adjusted so that weakest 5% of echoes from calm sea surface would saturate receiver at deployment depth, implicit in this decision is assumption that target strength of sea ice would always be less than that of an ice-free surface
 - Because of wave action, bubbles, etc...

Observations

- Significant fluctuations in amplitude of echo from ping to ping, w/little indication of any correlation btw echo amplitude and target type (e.g., level vs. ridged ice)
- Fitting of Rayleigh function to echo amplitude observations provides much worse fit than a lognormal function over smooth and deformed ice
- Echo returns are incoherent, meaning that the amplitude reflection/backscattering coefficient is dependent on surface properties and solid angle of sonar beam
- For keels >2m, magnitude of backscatter is independent of draft and most fall within a domain of about ~10dB in width
- Echoes from level ice fluctuate more widely than echoes from deformed ice
- Reduced saturation w/increasing draft
 - Level ice in medium/thick category: fraction of saturated echoes is 32% at 0.8m draft vs. 5% of 1.8m draft → minimal saturation for ridged ice
- Increase in modal echo amplitude w/draft is a consequence of smaller sound transmission losses for targets of greater draft

Discussion

- The consistently close lognormal fit to observations indicate that multiple scattering is occurring
- Coherent reflections were rarely detected w/narrow-beam sonar → surface echoes weak overall
 - -30 dB for thick ice (~1.5m), -25 dB for medium (~0.6m), and >-22dB for thin ice (<0.3 m)
- For wind speeds <10m/s and significant wave height <0.8m, echoes from subsurface clouds of air bubbles generated by breaking waves do not result in significant misclassification as sea ice
 - This can change, though, w/frequency of sonar and larger wind speeds

Implications for ice profiling

- IPS will be receiving weak, incoherent returns due to very narrow beamwidth ($\leq 3^\circ$)
- Ice scatters sound more effectively at higher frequency, but attenuation also increases
 - Given need for sonar to be at least 40 m depth to avoid keels, 400 kHz may be upper bound to operating frequency
- Median scattering coefficient of level ice increases as draft decreases (bc more specular, I think?), but the transition from thin ice to open water is gradual
 - Surface classification based on echo strength is likely to provide ambiguous decisions
- Receiver gain was too high → echoes from thin ice/open water often saturated sensor
 - 60-dB dynamic range is recommended
- Backscatter from bubble clouds decreases sharply btw 150–500kHz, so operating frequency near high end of this range is preferable

Conclusions

- Coherent reflection is not usually received due to geometric misalignment
- For all surface targets, amplitude of incoherent returns follow lognormal distribution
 - Thin ice/open water has range of amplitudes btw 55–95% percentiles of 20 dB
 - This is ~10 dB for ridge keels
 - Median values of backscattering coefficient at 400 kHz range from -6.8 dB for calm water to -30 dB for thick level ice and ridge keels
 - Weaker returns for deformed ice, I think this is because the returns are more diffuse than calm water and thin ice, but not 100% certain

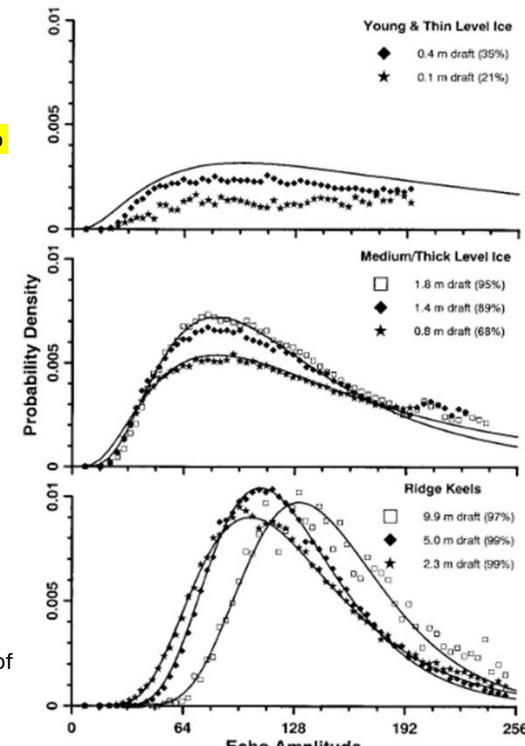


Fig. 6. Probability density of echo amplitude for three regimes segregated by range. The annotation indicates the approximate corresponding values of draft and (in brackets) the fraction of returns that did not saturate the receiver. Lognormal functions are plotted as curves.

The Ice Transport through the Fram Strait

Introduction

- ~25% of FS area can be newly formed ice → ice production in this region shouldn't be overlooked
- Anticyclonic circulation over NE Greenland Shelf, and coastal polynya south of Nordstrunden → polynya thought to be sustained via upward mixing

Observations

- Norwegian Ice Drift Experiment (ICEX) beginning in 1976
 - 52 drift tracks, 50 of which from buoys and 2 from manned stations
- Sea ice accelerates at fairly constant value of $0.5 \times 10^{-7} \text{ m s}^{-2}$ in center of FS from 83°N - 78°N
- Average winter drift speed is 2X that of the summer drift speed, and pressure gradient between FS and central Norwegian//Greenland Sea is much larger in winter
- Towards center of Fram Strait, R^2 between meridional components of drift and geostrophic wind drift speed is high (>0.70), but it varies greatly over the strait → this indicates increasing influence of non-wind effects closer to the coasts
- Increasing wind effect on ice drift due to increased divergence and reduced internal stress in MIZ
- Average southward wind direction in all months except August when it is near zero or northward
- Average annual ice drift speed due to local wind stress is 0.018 m/s , whereas average ice drift speed overall is 0.079 m/s , indicating that ocean currents drive 77% of total drift at 81°N
- Current transport increases as you go south, driving 75% of drift in N FS, 79% in central FS, and 82% in S FS → lag effect from wind stress more north is felt here
- 50% of the variation ($R^2=0.5$) of ice drift speed in central part of FS explained by air pressure distribution in Norwegian-Greenland Sea relative to FS (i.e., ΔP)
- Max sea ice drift speeds along the continental shelf break

Ice thickness

- Cross-strait SIT gradient: 1-2m in marginal areas and 5-6m approaching continental shelf
- Thinner ice in eastern FS comes from seasonal zones over Siberian shelves (Kara + Barents seas), while the thicker ice in western FS comes from Beaufort Sea/N Greenland
- Increased ridging west in FS as compared to east
- Minimal winter ice in eastern FS as W Spitsbergen current melts out/prevents growth of thin ice
- Field observations show 85% of ice flow consists of MYI/SYI
- Ice drillings taken from LANCE in July-August 1981-1984, and in July 1984 from POLARSTERN
 - 382 drillings made on level ice at reasonable distance from ridges
- Linear regressions between SIT (T), freeboard (F), and draft (D): $T = (8.35 \pm 0.11)F$ and $D = (7.35 \pm 0.11)F$ which gives draft-to-SIT conversion of $8.35/7.35 = 1.136$
 - $R=0.80$ and standard error is 0.68 m
 - Assuming $\rho_w = 1030 \text{ kg m}^{-3}$, this gives average $\rho_i = 907 \text{ kg m}^{-3}$
- When you think about it, an average density of 907 kg m^{-3} for samples that are >80% MYI, this indicates that MYI density is likely not 882 kg m^{-3} as indicated by Alexandrov et al. (2010)
- Thinner ice from 10°W to 5°W probably due to winter ice formation in Nordstrunden polynya
- Mean cross-strait weighted SIT of ~4m, and clear bimodal distribution is shown in SIT PDF

Vinje and Finnekåsa (1986)

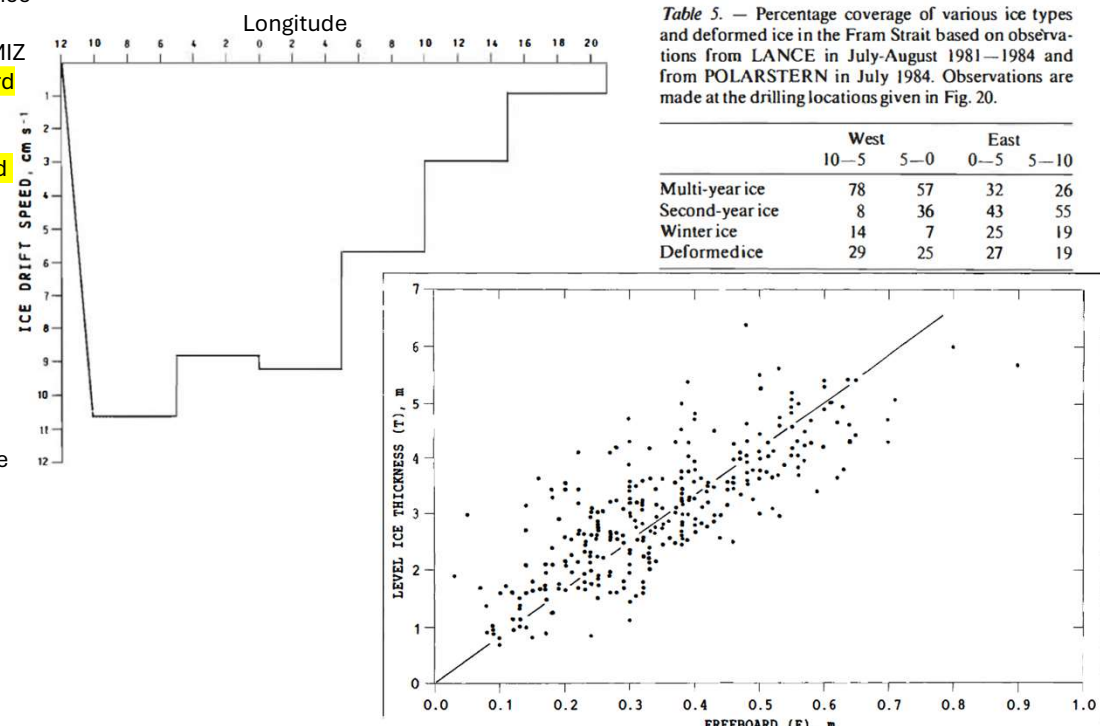
The ice volume transport

- Weighted annual average of 5000 km^3 per year, with 2/3 occurring during the winter
- Seasonal/interannual variation computed using air pressure gradient to estimate monthly drift speed profile w/monthly SIT and SIC estimates
 - Max in January ($0.213 \text{ million m}^3 \text{ s}^{-1}$), min in August ($0.079 \text{ million m}^3 \text{ s}^{-1}$)
 - Avg annual export over 9 years (1976-1984) of study at 81°N is $4,880 \text{ km}^3$ per year
 - Close agreement btw $4,880$ and $5,000 \text{ km}^3 \text{ yr}^{-1}$ indicates SIV estimates using pressure gradient approach can be useful – which Kwok (and others) later did

Conclusions/Impressions

- I couldn't include everything, but this paper details everything about sea ice in FS. Refer to it if I have any questions on topics from shape of floes to wind-induced drift speeds and SIT
- Drilling estimates, and subsequent draft-to-SIT conversion, done on summer ice w/no snow

Table 5. — Percentage coverage of various ice types and deformed ice in the Fram Strait based on observations from LANCE in July-August 1981–1984 and from POLARSTERN in July 1984. Observations are made at the drilling locations given in Fig. 20.



Sonar | Draft-to-thickness conversion | Fram Strait

SWOT and the ice-covered polar oceans: An exploratory analysis

Armitage and Kwok (2021)

Introduction

- SWOT – 21 day repeat orbit, altitude of 890 km, inclination of 77.6°
- Ka-band Radar Interferometer (KARIN) measures elevation in two off-nadir swaths 10-60km either side of the satellite ground track
- SWOT provides improved horizontal resolution, faster repeat times, and denser spatial coverage than pulse-limited or SAR altimeters
- This paper explores Ka-band backscatter over sea ice/open water over range of incidence angles spanned by SWOT swath, and quantify quality of SWOT-derived freeboards/SSH

KARIN

- SAR instrument operating at near-nadir over look angles ~0.6-4°
- Central frequency 35.75 GHz, bandwidth of 200 MHz, range resolution of 75 cm
- Two antenna are 5 m, giving KARIN along-track resolution of 2.5 m separated in across track direction by a 10 m baseline
 - Low rate (LR) mode – open ocean; HR mode (5 m X 10-70 m) required to ID leads
- Differential path delay $\Delta r = r_1 - r_2$ and phase difference of (1) $\Delta\phi = 2\pi\Delta r / \lambda$ where λ is carrier wavelength of 8.4 mm for KARIN
- If roll angle is zero, (2) $\Delta r = B\sin\theta$ where θ is the angle btw surface scatterer and nadir
- Combining (1) and (2) gives $\theta = \sin^{-1}(\frac{\Delta\phi}{B} \frac{\lambda}{2\pi})$ and then $h = H - r_1 \cos\theta$ where H is the satellite altitude and h is surface elevation relative to the reference ellipsoid
- Phase wrapping – KARIN measures phase in modulo 2π (how many 2π cycles occur) and therefore there is wraparound effect where a small height measurement could be, for example, 0.3 or $2\pi + 0.3 \rightarrow$ height ambiguity near ~10m and ~50m in near/far range
 - Thus, not a huge deal over ice-covered oceans as most elevations < 3m
- Drop-off in σ^0 w/look angle is sharp for highly specular leads, in contrast to nadir altimeters

Near-nadir Ka-band radar backscatter in the ice-covered ocean

- Dual-frequency global precipitation measurement (GPM) Ka- and Ku-band radar
- Backscatter over consolidated sea ice ($SIC > 99\%$) is lower than in MIZ areas where open water backscatter dominates → backscatter falls off more quickly w/look angle
- They also use SARAL AltiKa – 1.4km res, pulse-limited radar altimeter at 98.5° inclination and operating at nadir → goal is to examine nadir Ka-band backscatter
- At nadir- AltiKa σ^0 is quite flat over sea ice (~10 dB) in Arctic during Oct-Apr, whereas leads have much more variability (mean ~17 dB)

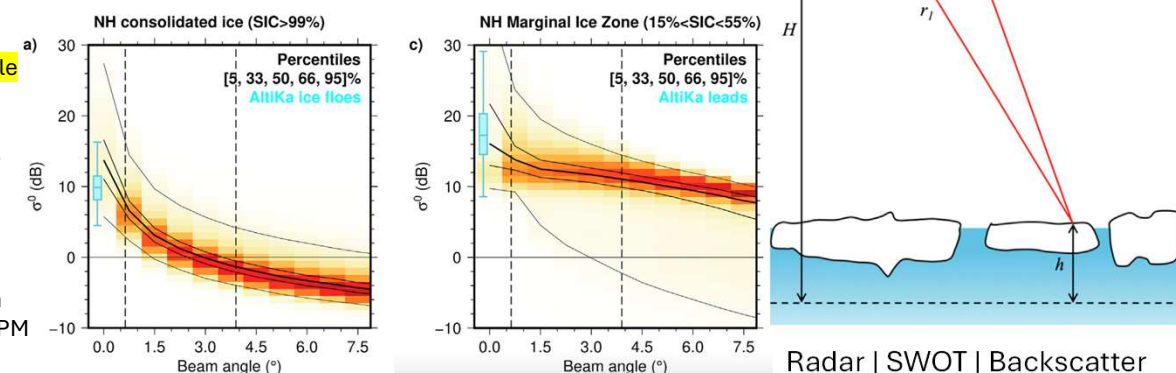
SWOT height retrievals over the ice-covered ocean

- SWOT simulator: KARIN params + DEM + surf type mask + scattering models (incidence angle dependent)
- σ_h increases w/range for all surfaces, but particularly for consolidated sea ice which has highest σ_h compared to leads/MIZ → rapid drop-off w/look-angle as shown w/GPM

- A height precision of 3 cm, which is order of precision for freeboards/ssh estimates on typical 25x25km grid (Kwok and Cunningham 2015), is ~15-40 km² in near-to-mid swath and ~90-170 km² for far swath (for consolidated sea ice surfaces) in Arctic
 - 3-10 km² over MIZ conditions and 1-2 km² for specular water
- Effect of surface roughness estimated using OIB ATM distributions
 - Additional surf roughness over MYI results in poorer height precision across entire swath → largest effect is in near-swath (σ_h increases by 14%)
 - Near-swath σ_h could be used to characterize surface roughness
- For mirror-like leads σ^0 is large at nadir then rapidly drops off – for wind-disturbed leads, σ^0 is flatter at range of incidence angles → challenges w/lead ID and ssh retrievals
 - At some incidence angles, σ^0 from leads/sea ice will be indistinguishable
 - σ^0 from leads will have behavior reflecting both (a) mirror-like surfaces and (b) wind-roughened surfaces, so this needs to be accounted for in discrimination algorithm
- SWOT retrievals of SSH should be at least as good as conventional radar altimeters w/potential to offer greater resolution + better spatial coverage
- Freeboard/SIT estimates on 25x25km grids w/precision of 3 cm → SWOT can achieve same height precision in NH w/expected 16-40 (3-7) fold improvement in near-to-mid (far) swath
- Don't consider Ka-band interferometric penetration depth into snow → depth of effective phase center relative to top of scattering volume
 - Studies have looked at this w/nadir AltiKa, but not side-looking interferometric radar

Summary and outlook

- Issue w/distinguishing between leads will be tricky w/2 (general) backscatter scenarios



SWOT Observations Over Sea Ice: A First Look

Introduction

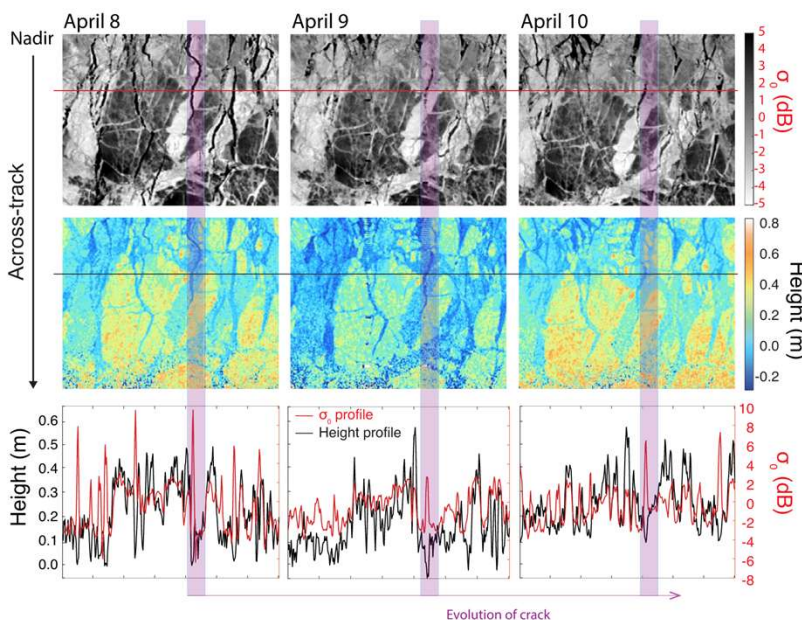
- First SWOT sea ice study; launched 16 Dec 2022; two parallel 50-km wide swaths
- 45 crossovers in 21 days at highest point of orbit

Data description

- KARIN is a SAR instrument that operates at near-nadir look angles from 0.8° - 3.5°
- Along-track res of 2.5 m, range res of 75 cm, 10 m baseline, 35.75 GHz freq, 200 MHz BW
- 500 m across-track LR data w/1 day repeat orbit during ‘fast-sampling’ phase 30 Mar-10 Jul 2023; heights referenced to IS2 ATL07 MSS

SWOT phenomenology over the polar oceans

- Backscatter contrast btw leads/floes reduced in at larger incidence angles/far range
- Ka-band signals are sensitive to snow grain size due to Mie Scattering because wavelength is ~ 0.8 cm vs. ~ 2 cm w/Ku-band (CS2)
- No consensus on primary scattering interface; height from interferometer is the phase center of the scattering volume → differs from conventional altimetry



- Notice that leads have high σ_0 , which is only the case near-nadir (crack is near-nadir)... they conclude “the scattering contrast between ice floes and leads can effectively discriminate between the two surfaces” → they don’t look at the case in the far-range where floes/leads are hard to differentiate → they acknowledge this on page 9

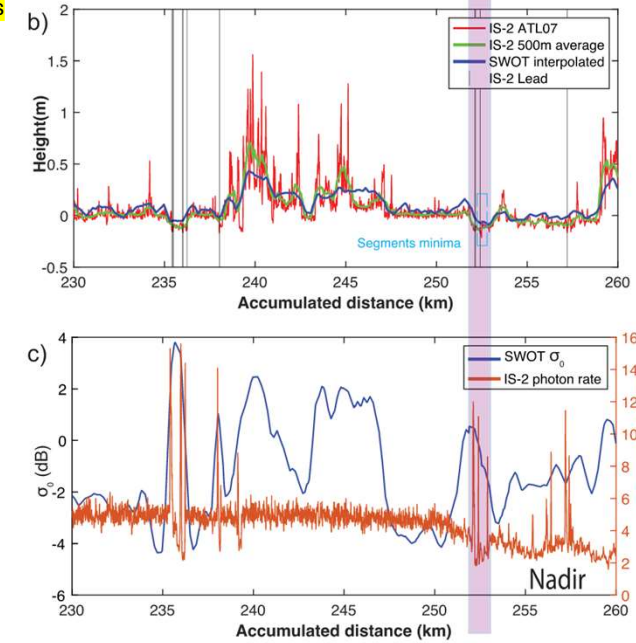
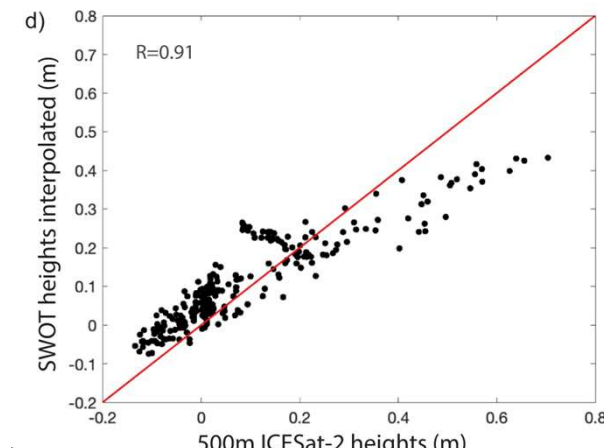
Intercomparison with near-coincident IS2 observations

Kacimi et al. (2025)

- SWOT and IS2 co-registered to account for ~ 2.14 (1.20) hr time separation in Arctic (Antarctic)
- IS2 data averaged using 500m moving window to replicate SWOT resolution
- Correlation btw IS2 and SWOT 30-km segments is 0.91 in Arctic, 0.65 in Antarctic
- Over 30-km segments, difference btw IS2 and SWOT is -0.02 ± 0.08 m (-0.01 ± 0.09 m) in Arctic (Antarctic)
- IS2 photon rate compared w/de-trended SWOT σ^0 (i.e., anomalies) → broadly, specular returns ID’d by IS2 correspond to bright returns from SWOT and low surface heights
 - They estimate freeboard using lowest heights in 30-km segment → tells us how close SSH retrievals are → they find minima are in same features (same lead) for IS2 and SWOT
 - Mean IS2 (SWOT) freeboards are ~ 0.22 (0.18) m, w/difference of 0.04 ± 0.08 m in Arctic
 - 0.30 (0.31) m w/difference of -0.01 ± 0.09 m in Antarctic
 - Difference in penetration depth can likely explain differences – especially in Arctic where IS2 fb is larger, but also inability of SWOT to sample rougher areas over short length scales

Conclusions

- SWOT surface heights show close agreement w/IS2, as shown by close agreement in freeboards
- Future work: understand Ka-band penetration at non-nadir look angles and ice/water classification across all look angles



Radar | SWOT | IS2 | Freeboard

First arctic-wide assessment of SWOT swath altimetry with ICESat-2 over sea ice

Müller et al. (2026)

Introduction

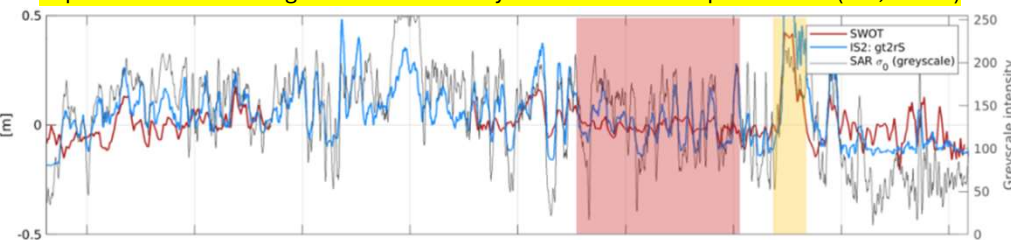
- KaRIn does not sample in nadir, but provides ssh within 60 km left and right swath
- Extends the work of Kacimi et al. (2025) by doing Arctic-wide assessment over a longer period**
 - 550 crossovers between IS2 and SWOT w/max separation time of 30 min

Data

- L2 Unsmoothed KaRIn SWOT data w/spatial resolution of ~500 m
 - This data is provided on spatial grid w/250 m resolution available through PODAAC
- All fields used to estimate surface height are explained – refer to this when trying out SWOT
- IS2 ATL07 v6 strong beams *height_segment_height*
- Only looking at surface heights here, not freeboards**
- Sentinel-1 SAR HH used for visual aid/comparison at triple intersections (S1, IS2, SWOT)

Comparison and results

- Overall, SWOT and IS2 have similar variability in surface height profiles, but SWOT struggles to capture small-scale height variations as they are smoothed compared to IS2 (red, below)



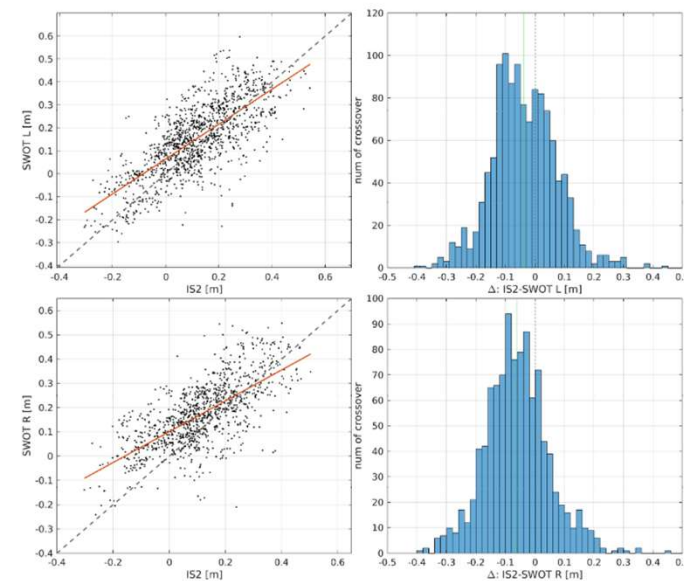
- Over (nearly) homogenous ice surfaces, only interrupted by leads/ridges, SWOT has distinct height signatures – but the full explanation behind these uncertainties remains unclear as not all instances correspond to presence of leads/ridges
 - Structure orientation seems to play a role
 - Systematic cross-track errors of 50 cm → height correction from crossover calibration likely insufficient/error prone over closed sea ice areas
 - No direct crossover adjustments can be conducted under these conditions
- Correlations btw IS2 and SWOT are 74% and 69% for left and right swath, respectively**
 - Mean differences are -4 cm (left) and -6 cm (right) → not significant given stdev of ~11 cm for both swaths
 - Trend line indicates mean values of SWOT are systematically lower than IS2
 - Less variation in height values than IS2
- Standard deviations of point-wise elevation differences are in range of 4-8 cm, w/higher values of CAA/Beaufort Sea/Greenland Sea/NE Greenland Shelf
 - Histogram of stdev of elevation differences scatter around 0.08 ± 0.04 m

- All described differences^{^^} refer to observations over all surfaces (sea ice + open water)
 - Filtering for just sea ice surfaces reduces # data significantly and results in mean stdev of 0.08 ± 0.04 m with correlations unchanged

Discussion and conclusions

- At time of writing, Version C (which they used) geophysical corrections are in separate dataset and need to be interpolated as they are on 2 km grid – this is not the case in Version D
- Crossover calibrations are missing over Arctic, so they have to use calibrations marked as "suspect" within the Arctic**
 - Only SWOT-SWOT overflights during open ocean conditions are used and are interpolated for the observations in between
 - In ice covered Arctic regions, this can lead to large uncertainties
- Edge of SWOT swaths (~5km on each side) are very noisy and shouldn't be used in analyses**
- Variability in along-track profiles from SWOT, S1 SAR (backscatter intensity) and IS2 are remarkably coherent → thus SWOT can capture details over a range of surfaces
- "SWOT LR dataset can resolve small open water and sea ice areas only to a limited extent"
- Uncertainty about Ka-band penetration into snow at off-nadir incidence angles
- Roughened surface waters and frost flowers lead to uncertain surface heights in swath data
- No SWOT observation-based sea ice surface classification exists

Scatter plot of IS2 surface height against interpolated SWOT surface elevations per crossover. Histograms of mean value differences for left (top row) and right (bottom row) SWOT swaths. In the histograms, the mean values (-4 cm for left and -6 cm for right swath) are indicated by the green line, while the zero line is indicated as a dashed line.



Swath Mapping Altimetry over Sea Ice: First Results from the Surface Water and Ocean Topography (SWOT) Mission

Fischer et al. (2025)

Introduction

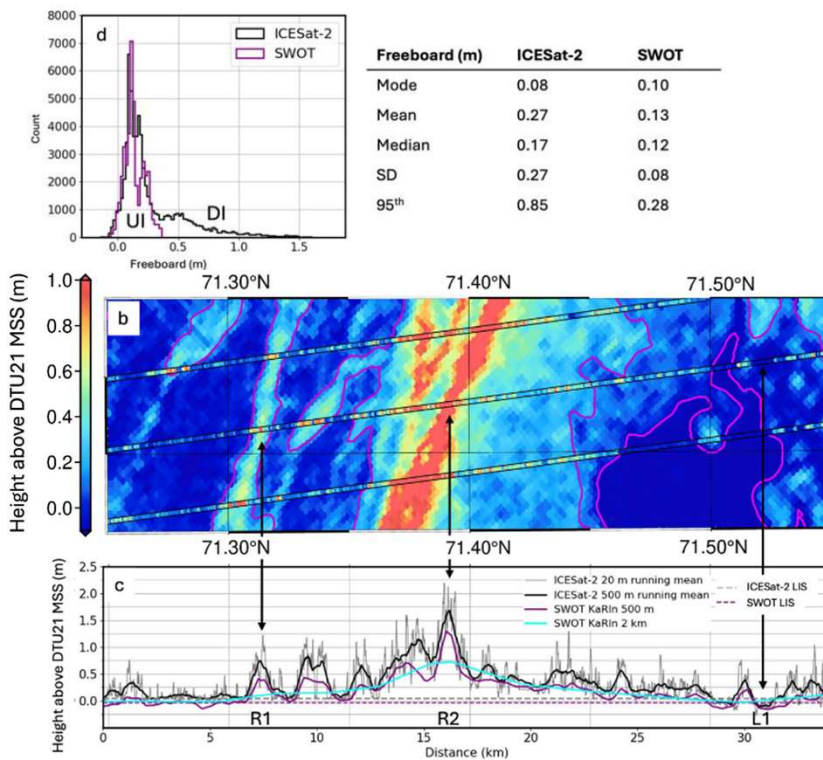
- Using SWOT and IS2 to look at sea ice morphology, drift, leads, pressure ridging in landfast ice and freeboards in Beaufort and Chukchi Seas using fast-sampling phase (1 day) data Par-Jun 2023

Data

- Unsmoothed LR L2 SWOT KaRIn data – 250 m horizontal sampling rate
- IS2 ATL03 in 20-m and 500-m running mean sea ice height profiles
- SWOT-IS2 collocation → two locations in BG and along coast where Δt 76-79 min in Apr 2023
- Crossover correction removes cross-swath height gradient of ~1m

Results

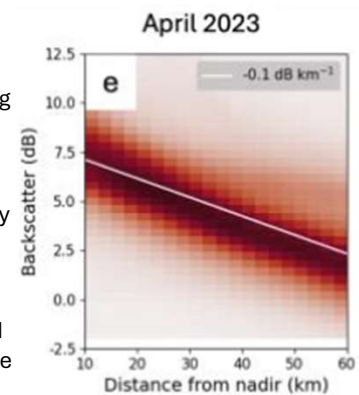
- SWOT shows remarkable agreement w/IS2 (within 2 cm) over level and undeformed ice surfaces, but underestimates the height of the large deformed floe (sail height -- 0.32 m SWOT vs. 1.06 m IS2)
 - Tail of distribution is not captured by SWOT



- In April: σ^0 is 0-10 dB, deformed floes ~6-8 dB and undeformed ice/refrozen leads ~0-5 dB
 - Newly open leads > 10 dB due to high salinity sim layer and/or frost flowers
 - Backscatter looks different in June, however (see text if interested)
- In April: -0.10 dB km^{-1} slope w/distance from nadir, with near-nadir backscatter of 7.1 dB, dropping to 2.3 dB 60 km from nadir
 - Wider spread in June, w/slope -0.12 dB km^{-1} ranging from 7.1 dB near-nadir to 1.6 dB off-nadir
- Feature tracking/pattern matching algorithm applied to SWOT backscatter to calculate sea ice displacement
 - They report values, but don't validate or provide any indication of accuracy
 - Really only possible for fast-sampling phase

Summary

- Excellent KaRIn agreement w/IS2 over undeformed ice and leads on scales 0.5-50km, but underestimates roughest ice
- In region they assessed, SWOT underestimated mean freeboard by 0.14 m and the 95th percentile by 0.57 m
- QFs worked well over leads and deformed ice, but some undeformed sea ice surfaces were classified as open ocean



- SWOT QFs able to ID leads and deformed floes, w/level sea ice surfaces flagged as “ambiguous”
- SWOT able to ID ridges in landfast ice example, but underestimates the height

Radar | SWOT | Morphology | Drift | Landfast ice | Freeboard

Geostatistics and remote sensing

Curran and Atkinson et al. (1998)

Introduction

- “Geostatistics is a set of techniques for estimating the local values of properties that vary in space from sample data”
- Variogram – “a function that relates variance to spatial separation and provides a concise description of the scale and pattern of spatial variability.”
- Semivariance – measure of dissimilarity between spatially separated observations
- Kriging – estimates are obtained by weighting each of several sample data that are proximate to the estimate → exact weights are determined from the exact form of spatial dependence as represented by the variogram
 - Weights are chosen such that the estimate is unbiased and has minimum variance
- “Kriging variance depends only on the variogram and the configuration of sample observations in relation to the estimate: the observed values have no influence.”
 - This is a way to determine the optimal sampling strategies as well
- Cokriging – “accounts simultaneously for the autocorrelation in each variable (represented by the variograms) and the crosscorrelation between the variables (represented by the crossvariograms)”
- Five main applications of geostatistics in remote sensing
 - (1) Exploring spatial variation, (2) determine optimal spatial sampling of image data and (3) ground data, (4) estimation: classification, (5) estimation of continuous variables
- “In all geostatistical techniques, the central tool is the variogram, and it is this which provides the link between classical (aspatial) statistics and geographic space.”
- “Support” refers to the scale of observation
- “A problem with kriging is that the variance of the kriged estimates generally is less than that in the original data and this is referred to as smoothing.”
 - “Not only is the variance of the estimates reduced but also the sample variogram is altered such that the pattern of spatial variation is different from that of the original data.”
- Conditional simulation is an alternative to kriging
 - “conditional simulation produces a map in which the general pattern of spatial variation in the original data is recreated, and which, consequently, is a ‘possible reality’.”
 - You can simulate many times to create many maps, unlike kriging which creates one, and the multitude of maps embodies the inherent uncertainty in the original spatial sample
- Disadvantages of conditional simulation
 - Variance added to replace the variance lost through smoothing is unrelated to original data
 - Values on a pixel-by-pixel basis are half as accurate as the kriged estimate
 - Kriged estimates create best map on pixel-by-pixel basis, whereas conditional simulation leads to best map on global basis

Summary

The fundamental tool of geostatistics is the variogram, and from it one may

- 1) estimate summary statistics such as the dispersion or sample variance;
- 2) estimate regularized variograms for new spatial resolutions;
- 3) estimate optimally at unsampled locations from sample data;
- 4) design optimal sampling strategies *before* the actual survey; and
- 5) conditionally simulate at unsampled locations from sample data.

Uncertainty propagation in models driven by remotely sensed data

Crosetto et al. (2000)

Introduction

- They propose a general procedure to support a characterization of uncertainty in RS products
 - Composed of uncertainty analysis (UA) and sensitivity analysis (SA)
 - UA = final uncertainty after propagation through processing
 - SA = how much individual sources of uncertainty contribute to total output uncertainty
- Focus of the paper is UA, SA is only briefly described

Uncertainty analysis

- UA assumes that bias is negligible – i.e., not an assessment of accuracy
- Analytical techniques of uncertainty propagation require a continuously differentiable function
 - E.g., Gaussian propagation of uncertainty in the paper
- Monte Carlo (MC) simulations are a method of numerical error propagation
- MC can be applied w/o making assumptions about model structure
- For MC, first ID sources of error, then a stochastic model capable of generating a population of error-corrupted versions of the same reality (i.e., realizations) is made
 - Each realization is a sample from the same population and differences between realizations represent uncertainty present in the input data (I_i) or parameters (p_i)
- Steps involved in MC:
 - (1) Repeat N times:
Generate randomly a set of realizations from input factors (sources of uncertainty)
Evaluate model using realizations of I_i and p_i and compute output uncertainty
 - (2) Compute stats from set of outputs, which represents a PDF. The PDF gives full characterization of the stochastic features of output uncertainty with an arbitrary level of precision, which is related to the number of samples N
- Again, UA describes uncertainty associated with input data and parameters, but accuracy is conditional on the quality of the stochastic models (i.e., processing chain) associated with I_i and p_i
 - This requires external information
- MC can evaluate models of any complexity

Sensitivity analysis

- They describe FAST – Fourier Amplitude Sensitivity Test → variance based techniques that employ MC simulations

Synergistic use of uncertainty and sensitivity analyses

- In building stages of a processing chain, it is important to use UA and SA to determine sources of uncertainty and their relative influence, so you can focus on reducing the influences of certain uncertainties that could dominate
- UA and SA can be used to examine which models perform best/optimally for a certain situation
- UA and SA can help w/optimal allocation of resources for input data acquisition

Error modeling

- They describe a general error model for quantitative raster data

- Systematic error = bias
- Spatially uncorrelated error = white noise
- Systematic error affects all estimates the same way, but this is not the case with random error as these are reduced with the large # of observations due to central limit theorem
- They have a detailed section on masking clouds in RS images, which I skipped as not relevant

Case study

- Burned area on African continent over 1982-1993 using Pathfinder AVHRR data
 - They go into great detail about random errors and systematic biases, ranging from solar zenith angle, thresholds to detect burned vegetation, etc...
 - MC simulation for UA and SA
 - SA included random and systematic biases (I think)
- ## Conclusions
- MC treats models as black boxes and therefore is a flexible tool for UA
 - Question: it seems like in their MC simulation they include systematic and random errors, how does this work? Does the output of the SA analysis tell you how much they contribute?
 - This must be the case

Uncertainty in Remote Sensing and GIS: Fundamentals

Atkinson and Foody (2002)

Error

- Errors are differences between true and predicted values, and relate to individual measurements rather than statistics
- Uncertainty is associated with statistical inference and prediction... **error ≠ uncertainty**

Accuracy

- Accuracy is defined by bias and precision

Bias

- Most often expressed as the mean error: $ME = \frac{1}{n} \sum_{i=1}^n (\hat{z}(x_i) - z(x_i))$
- The larger the systematic errors, the greater the bias

Precision

- Spread of errors around the mean error $\rightarrow s_e = \sqrt{\frac{\sum_{i=1}^n (\bar{e}_i - \hat{e}_i)^2}{n-1}}$ where s_e is standard deviation

Accuracy

- Accuracy = Unbias + Precision
- RMSE is sensitive to both systematic and random errors, and thus can predict accuracy

$$RMSE = \sqrt{\frac{\sum_{i=1}^n (\bar{z}_i - \hat{z}_i)^2}{n}}$$

- Essentially, error relates to a single value and is data-based. Accuracy relates to the average (and, thereby, statistical expectation) of an ensemble of values: it is model-based."

Model-based Prediction and Estimation

- Prediction – used in relation to variables; Estimation – used in relation to parameters
- Standard error derived from central limit theorem: $SE = \frac{s}{\sqrt{n}}$
- Precision is defined as the inverse of the prediction variance, and prediction variance is the square of the standard error
- Prediction variance is sufficient to predict full distribution of the error only if data is unbiased (predicted mean tends towards true mean with larger sample size) and the error distribution is known to be Gaussian \rightarrow this is where the SE equation comes from /why its used
 - But nothing can be said about bias (or therefore accuracy) here
- Kriging is a least-squares regression-type predictor; therefore, it predicts with minimum prediction variance
 - Kriging output is a map of predicted values and a map of prediction variance
- "A problem with the kriging variance is that it depends only on the variogram and the spatial configuration of the sample in relation to the prediction: it is not dependent on real local data values."
 - But not a big deal when local variation is similar from place to place (autocorrelation), thus you need to use a semivariogram to look at autocorrelation length scales (I think)

- Confidence intervals – "Knowledge of the standard error allows the researcher to make statements about the limits within which the true value is expected to lie. In particular, the true value is expected to lie within 1 SE with a 68% confidence, within 2 SE with a 95% confidence and within 3 SE with (approximately) a 99% confidence."
 - Issue is, **acceptable confidence intervals is an arbitrary choice**

Accuracy assessment

- Cross-validation is an accuracy assessment used w/o independent datasets, but not as preferable as some circularity in data being compared to itself
- "This use of the word validation is often inappropriate. For example, we do not show a classification to be valid. Rather, we assess its accuracy."
- Correlation measures the association between data (i.e., precision)
- Spatially autocorrelated errors implies local bias

Further Issues I: Spatial Resolution

- "The support is the size, geometry and orientation of the space on which each observation or prediction is made." \rightarrow i.e., sampling/sensor resolution

Further Issues II: Classification

- Soft classification can be helpful, as mixed pixel classes can indicate spatial variety

Further Issues III: Conditional Simulation

- Conditional simulation \rightarrow predict unknowns values while maintaining, in the predicted variable, the original variogram
 - A solution to kriging, as w/kriging the predicted variable is likely to be smoothed in relation to the original sample data \rightarrow some of the variance is lost
- "Conditional simulation represents the decision to put greater emphasis (less uncertainty) on the reproduction of spatial character and less emphasis (more uncertainty) on prediction."

Further Issues IV: Non-stationarity

- Stationarity: a single model is fitted to all data and is applied equally over the geographic space
 - E.g., Known leaf area index (LAI) vs. NDVI used to fit regression model, which is then used to predict LAI for pixels where only NDVI is known, but regression model and coefficients are unchanging
- Non-stationary approach – allow parameters of model to vary with space

The Certainty of Uncertainty: GIS and the Limits of Geographic Knowledge

Couclelis (2003)

Modes of Geospatial Knowledge Production

- **Data-driven approach** → data characteristics determine which processing method can be applied and what final product quality can be obtained
 - E.g., processing of remotely sensed data
- **Method-driven approach** → starts with some standardized model of data processing, which imposes specific minimum requirements on input data and determines the quality of the product to the extent to which the data conform to the method's requirements
 - E.g., Application of standardized land classification method
- **Product-driven approach** → desirable final product is identified first and this determines the selection of appropriate methods which in turn impose their own requirements on the input data
 - E.g., Process modeling using pre-existing models
- Commonsense reasoning == all forms of reasoning except deduction
- Abduction – produces a best explanation (product) out of a set of observations (data) such that the explanation satisfies a number of methodological/empirical constraints (methods)
 - E.g., an explanation may be the interpretation of a pattern seen in the data
 - Finding a best explanation is intractable in most cases
- Deduction – the foundation for all of our statistical methods – methods-driven case
- Nonmonotonic reasoning – the adoption of assumptions ('axioms') that may have to be abandoned in light of new information → e.g., product-driven approach

Discussion and Conclusions

- Not all uncertainties are due to human limitations → there are some things that simply cannot be known
- Knowing what can't be known, therefore allows us to focus on the things that can be eventually known
- "The nightmare today is not in the uncertainty itself but in its inadequate, unscientific expression: in the hand-waving, the wishy-washy statements, the ignorance concealed under pretty pictures, the pretense that something can be known that in fact cannot. There is too much of that going on."

Great quote^

Subsection | Keywords

Remote-sensing image analysis and geostatistics

van der Meer (2012)

Introduction

- Review of how geostatistics is used in remote sensing by examining literature from 2000-2010

Pixels, images and regionalized variables

- **Stationary** – the variable/process is stochastic, and its statistical properties remain constant over time, ensuring the data doesn't have trends/predictable long-term patterns (Google AI def)
- "Strict stationarity applies to a stochastic process whose joint probability distribution (and parameters such as mean and variance) does not change in (time or) space; in other words, the mean and variance exist and are independent of spatial location."
- At time of writing, **no well-agreed upon method of testing for stationarity**

The (semivariogram and remote sensing

- Omnidirectional and directional variograms
- Equations for semivariance provided and explained
 - **Semivariance** is half the mean squared difference between each pair of values for a given lag (distance), $h \rightarrow$ do this for many h and get semivariogram
- **Nugget variance** – non-zero y-intercept of curve \rightarrow random (sensor) noise, non-spatial
 - Nugget needs to be estimated based on variogram model which introduces bias
- **Range distance** – distance in lag intervals at which curve trends to level off
 - Gives indication of length of correlation btw observations/pixels
- **Sill variance** – maximum value of the variance that is reached at distance of the range
- "the variogram can be used to derive an optimal scale or spatial resolution to perform these observations."
- "**Regularization** is the process whereby samples get more regular (less variable) when support (pixel) size increases" \rightarrow basis for upscaling & downscaling remote sensing observations
 - I.e., smoothing?
- Square root of the range measures the mean length scale of the data

Univariate kriging and remote sensing

- **Kriging** – estimates unbiased as weights must sum to 1 and estimation variance is minimized
- Very helpful for downscaling and upscaling

Indicator kriging

- Indicator variables are used to estimate a distribution; a cutoff value is defined and all sampling points that have a higher (lower) value than the cutoff are assigned 0 (1)
 - Apply kriging, get range of values 0-1 that indicate probability that a certain location exceeds the cut-off value \rightarrow probability mapping at finer resolution than the support

Cokriging and remote sensing

- "Kriging uses the spatial correlation of one variable, while **cokriging exploits the cross-correlation between variables to produce local estimates**"
 - "Typically, cokriging uses a well-known densely sampled variable to map a less well-known sparsely sampled variable where the two show a strong cross-correlation."

Stochastic simulation and remote sensing

- Stochastic simulation generates alternative, equally probable models (realizations) of the spatial distribution of an attribute over a field
- Simulation differs from kriging in that it considers global statistics more important than local accuracy
 - Conditional simulation honors original variance of input data
- The models honor "sample statistics and variogram but each individual realization **will not necessarily provide the best linear unbiased estimate at an unknown location.**"
 - Requires assumption of Gaussian distribution (I think)
- "The realizations that the simulation produce are a set of n representations of the same variable, which can be viewed as a conditional probability distribution (whose variance is the kriging variance for any unsampled location)"

Discussion

- "**Support** is the physical size of a single measurement, **regularization** is the process of averaging these over larger areas and the variogram is the tool to show the change of spatial variability with object size"
- Important issue is assumption of stationarity and whether this holds in remote sensing images / observations \rightarrow this should be checked when doing an analysis
- Sensor design industry / space agencies needs to consider things like optimal scale and change of support rather than just engineering concepts
- Geostatistics has focus on spatial dimension, but further attention needs to be paid to time dimension

Example of issue w/stationarity in optical imagery: you assume the spectral signature of a land-cover class (e.g., forest) is stable over time. Then, you train a land-cover classifier using Landsat images from 2010-2024

You assume (a) forest reflectance in 2010 is roughly the same as 2024, (b) cropland reflectance patterns haven't changed (e.g., what if earlier green up due to more warming earlier in season bc climate change) and (c) seasonal behavior is the same each year

From ChatGPT^

Downscaling in remote sensing

Atkinson (2013)

Introduction

- Downscaling = decrease in the pixel size of remotely sensed images
- The support (space over which each observation is defined) is the measurement parameter of particular interest in relation to downscaling (the other measurement being spatial extent)

Downscaling continua

- Regression approaches – downscale by regressing a direct measurement of the fine resolution target and some coarse resolution covariate... e.g., NDVI (fine) and land surface temp (coarse)
 - Effect of support and presence of spatial variation at fine scale not really accounted for
- Area-to-point (ATP) prediction – downscaling of continua through interpolation
 - ATP Kriging – requires estimation of semi variogram defined on a point support
 - Many variants have followed, e.g., a multivariate ATPK

Super-resolution mapping → usually done for land cover

- “The use of interpolation based on a variety of methods to increase the apparent spatial resolution of a single input image (or set of input images) whilst also transforming it into a classification” → e.g., images of several wavelength bands that are used to “zoom in” via interp
 - Transformed continuous variables as inputs to categorical variables as outputs
- Two step procedure: (1) initial image converted to classified image at original resolution, then (2) this image is converted into a classification at a finer resolution
- Techniques separated into two classes based on source of prior knowledge:
 - (a) Goal is to maximize spatial correlation btw neighboring sub-pixels – requires objects in scene to be larger relative to pixel size
 - (b) Prior knowledge comes from model (e.g., semi variogram) or training data (RS image)
 - Often applied when objects are small relative to pixel size
- Interpolation techniques for this mapping – sub-pixel swapping, Hopfield NN, geostatistics, Markov random field

Discussion

- Approaches using training images are preferred instead of simpler functions
 - There are more differences between pixels, and thus, information than using just a semi-variogram or two-point histogram
- Using training data in the form of a semi-variogram leads to smoothing as there is just less info than if the training data is an image → detail at sub-pixel level is highly generalized
- Quality training data is essential
- Early methods of downscaling paid little attention to prediction uncertainty in the downscaled output
- Now that we have decades of data, for example Landsat images, these can be used as training data → effectively borrowing of info btw images to separate real change from noise

Impressions

- Largely focused on imagery, but useful to understand the general concepts of downscaling

Good practices for estimating area and assessing accuracy of land change

Introduction

- “In this article, we synthesize the current status of key steps and methods that are needed to complete an accuracy assessment of a land change map and to estimate area of land change”
- Accuracy assessment separated into response design, sampling design, and analysis

Sampling design

- “The **sampling design** is the protocol for selecting the subset of spatial units (e.g., pixels or polygons) that will form the basis of the accuracy assessment”
 - “The most critical recommendation is that the sampling design should be a probability sampling design. An essential element of probability sampling is that randomization is incorporated in the sample selection protocol.”
 - “Probability sampling is defined in terms of inclusion probabilities, where an inclusion probability relates the likelihood of a given unit being included in the sample”
- Whether to use strata, cluster, or to implement systematic/random selection protocol are three key decisions that influence choice of sampling design
- “**Stratification** is a partitioning of the ROI in which each assessment unit is assigned to a single stratum.”
- “In **cluster sampling**, a sample of clusters is selected and the spatial units within each cluster are therefore selected as a group rather than selected as individual entities.”
- “The two most common selection protocols implemented in accuracy assessment are simple **random and systematic sampling** (we define “systematic” as selecting a starting point at random with equal probability and then sampling with a fixed distance between sample locations).”
- Stratified random sampling is the recommendation

Response design

- “**Response design** encompasses all steps of the protocol that lead to a decision regarding agreement of the reference and map classifications”
 - Four features: spatial unit, source(s) of info used to determine reference classification, labeling protocol for reference classification, and definition of agreement
- Reference (i.e., validation) data should be at an equal or finer level of detail than the data
- Reference data has to be higher quality or more accurately classified than data it is being compared to
- Reference data also runs into stationarity problem – is it right to compare 2010 validation data with 2020 data?
- Minimal mapping unit should be provided
- When labeling, having low-moderate-high flags for classes may be helpful with understanding the uncertainty in a classification – also a mixed class may be informative
- **Errors/uncertainties in the reference dataset should be included**

Analysis

- Confusion (error) matrix
- Measures of accuracy are selected based on design of study – design-based inference
- Producer vs. users' accuracy

Example of good practices: estimating area and assessing accuracy of forest change

- 2000-2010 Landsat deforestation example

Summary

- **The entire paper is summarized in bullet points in this section** – refer to this if I need to, does a good job of briefly describing all that was discussed in the paper

Deep Learning for Remote Sensing Image Understanding

Zhang et al. (2015)

- This is an **editorial** that is the introduction to a special issue of a journal.
- “Deep learning is about learning hierarchical feature representations. Deep architectures with multiple levels attempt to learn hierarchical structures and seem promising in learning simple concepts first and then successfully building up more complex concepts by composing the simpler ones together.”

Spatial Autocorrelation and Uncertainty Associated with Remotely-Sensed Data

Griffith and Chun (2016)

Introduction

- Remote sensing data often has high spatial autocorrelation which has the impact of variance inflation which, in turn, impacts uncertainty quantification and assessment of the data
- “The purpose of this paper is to outline methodology for quantifying uncertainty in remotely-sensed data that relates to spatial autocorrelation latent in these data”

The Florida Everglades Data

- 1 Jan 2002 Landsat 7 image
- They look at NDVI and Normalized Burn Index (NBI) which have spatial autocorrelation >0.85

Spatial Regression Model Based Sampling Variability of the Spatial Autocorrelation Parameter

- Very mathematical and jargon filled – skimmed
- Describes model-based inference of spatial autocorrelation ρ
- Spatial autocorrelation parameter is ρ and ranges from -1 to 1

Sampling Experiment Designed Based Sampling Variability of the Spatial Autocorrelation Parameter

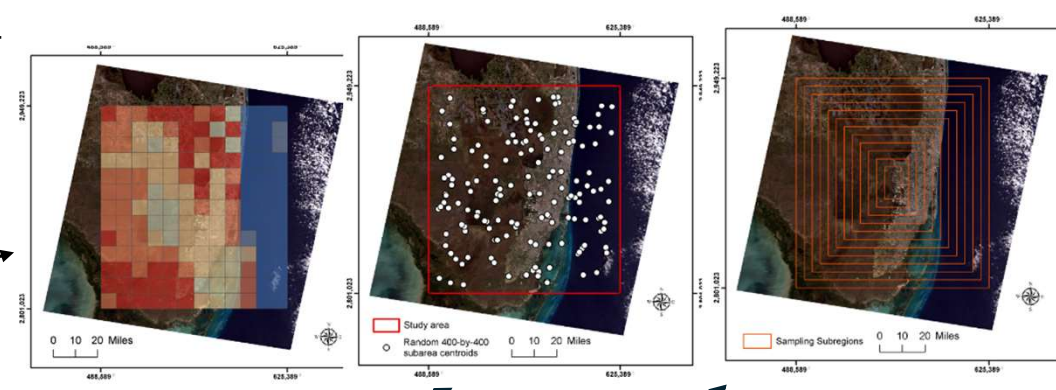
- Three sampling strategies designed to quantify variability in ρ across a geographic landscape
 - Essentially splitting the image into subregions in different ways
- Sampling strategy 1 (coterminous): strong-positive ρ for NDVI, moderate-strong ρ for NBI
 - Ocean shows negative ρ
 - Just positive ρ values give estimates 0.88 and 0.83 for NDVI and NBI
- Sampling strategy 2 (random subregions): ρ averages of 0.69 (NDVI) and 0.64 (NBI)
 - Like coterminous results
 - Ocean shows negative ρ
 - Just positive ρ values give estimates 0.85 and 0.81 for NDVI and NBI
 - Uncertainty quantification less reliable than coterminous sampling (based on confidence intervals) → range of ρ for conf intervals much smaller than sampling strategy 1
 - “random sub-regions furnish useful measures of uncertainty, but random pixels do not”
- Sampling strategy 3 (increasing domain subregions): ρ of 0.929 and 0.842 for NDVI/NBI
 - Smaller standard errors than other two sampling strategies
 - Larger ρ w/increasing domain size → as anticipated

Discussion

- Effective sample size is about 5% of total sample size → lots of redundant information in spectral measures/indices
- Variance inflation factor: NDVI is factor of ~5, NBI is a factor of ~4
 - This means confidence intervals w/variance estimates are ~2x as wide as they should be
 - There is considerably more uncertainty attributable to sampling error than appears to exist if latent spatial autocorrelation is not considered
- Thus, sample size and variability are distorted by spatial autocorrelation

Conclusions and Implications

- “Uncertainty associated with remotely-sensed data should be cast in terms of its latent spatial autocorrelation,”
- “Ignorance of spatial autocorrelation can result in unreliable results.”



Because Neff is less than N, variance is biased low
Confidence interval, CI, defined as:

$$CI = \bar{x} \pm z \frac{s}{\sqrt{n}}$$

Where \bar{x} is sample mean, z is confidence level value, s is sample standard deviation, and n is sample size. Thus, if Neff << N but you used N, your confidence interval will be smaller/narrower than it should be (larger denominator) which can lead to more results being statistically significant than they should be.

VIF tells us how much the variance of an estimate is inflated because of correlation between predictors – so if VIF is high, then the S term in the confidence interval rises as $s = \sqrt{var}$

Geostatistics | Spatial autocorrelation | Variance |
Confidence interval | Effective sample size

How well do we really know the world? Uncertainty in GIScience

Goodchild (2020)

Introduction

- Geospatial data are a representation of geography, not geography itself
- “Nearby things are more similar than distant things” also applies to uncertainties → most errors are in reality strongly and positively **autocorrelated**
- There is a lack of attention paid to uncertainty in GIScience

New directions and challenges

- Movement to “let the data speak for itself” and base theory on this, rather than the other way around, **has two major issues:**
 - Not all patterns are equally likely and established principles like spatial dependence, heterogeneity, and resolution limit what can be found in practice on Earth’s surface
 - **Uncertainty** – how do we account for uncertainty when making predictions, for example, using AI?
 - “Should analysis begin with a collection of alternative data sets, each of which represents a possible true state of geographic reality that is consistent with the known uncertainties?”
- In the age of Big Data, how do we integrate data from various sources, of various provenance and quality, into a single best estimate and how do we determine that estimate’s uncertainty?
 - Emphasis on the reliability/quality of data sources here
- New types of data introduce new types of uncertainty that are difficult to model using traditional techniques
- “Replicability crisis” – needs to be a greater attention to replicability
- Spatial heterogeneity → uncertainty is present in the data then how much variation in one area compared to another is attributable to uncertainty and how much to spatial heterogeneity?

Spatial sampling, data models, spatial scale and ontologies: Interpreting spatial statistics and machine learning applied to satellite optical remote sensing

Atkinson et al. (2022)

Introduction

- "This paper summarizes the development and application of spatial statistical models in satellite optical remote sensing" → review paper
- Not a review of methods

Remote sensing as a source of data

- "The support is a geostatistical concept representing the space on which a measurement is made, or observation is defined, and it has three parameters; size, geometry and orientation"
 - "It represents one element of the spatial (space-time) sampling strategy, with the other elements being the pattern of observations and the extent."
- "This means potentially that the Euclidean space itself is discretized into a regular grid of possible values. Operations that are made directly on that grid generally deny the underlying continuous space of the real world," → interesting point

Information in remotely sensed data

- Range provides information on the scales of spatial variability (and amount of redundant information in an image) → upper limit on the extent of any correlation
- Size of support doesn't matter; what matters is the size of the support in relation to the spatial variation in the data

Characterizing imagery using spatial statistics

- Geostatistics
 - "given that it is so obvious that stationary covariance-based Gaussian processes are unrealistic and inappropriate representations, why are they still so ubiquitous in remote sensing?"
- Mixed models and the Bayesian inference paradigm
 - "A spatial regression model can be conceptualized as being an additive model that in simple case combines two effects; a linear fixed effect and a spatial random effect, plus an error term"
- Objects
 - Fuzzy objects and fuzzy definitions are important → most spatial objects have a fuzzy component → e.g., where does a mountain truly begin?

The rise and rise of machine learning

- Machine learning
 - Support vector machines, random forest
 - Machine learning models focus on the data and don't focus on the reality
- Deep learning (CNN used as example)
 - Earlier classifiers predict first-order representations, CNNs predict these + higher-order ones
 - "CNN exploits second-order and higher-order relations (e.g., texture) in the input image patch to target the classification of higher-order representations" such as land use
 - CNNs generally take an image patch as an input which is coarse spatial support → harder to label multiple objects within an image, CNNs better at identifying something in an image
- Explainable AI
 - E.g., having model output IF-THEN rules w/result of classification to see how it got there

Semantic and ontological considerations

- Choice of goal, method, and spatial resolution
- A hierarchical ontology for remote sensing
 - Example: land use is a higher order feature than land cover → characteristics of land cover define land use
 - Determine the hierarchical ontology, then determine the goals, and then select the appropriate methods

Summary

- Summary reiterates main points of the paper in bullet pts and should be my first go-to

Geostatistics | ML | AI | CNN | Spatial regression | Optical remote sensing

Artificial Intelligence for Remote Sensing Data Analysis: A review of challenges and opportunities

Zhang and Zhang (2022)

Introduction

- Comprehensive review of AI from 2016-2022

Machine Learning

- Pre-DL era: SVM, RF, and manifold learning
- DL
 - Convolutional-based methods – CNNs for computer vision-related tasks
 - Generative-based methods – autoencoders, generative adversarial networks
 - Sequence-based methods – recurrent neural nets, natural language processing mainly, not much remote sensing
- Data sets and training samples
 - General lack of quality training data as deep NNs have millions of parameters to be optimized
 - Three DL strategies for small sample sizes: training sample generation, few-shot learning, and transfer of knowledge from other datasets
 - Training sample generation → create your own labeled samples
 - Few-shot learning → learn latent representation from unlabeled images and transfer the model to new tasks/targets using a few labeled samples

Computational Intelligence

- “Computational intelligence helps AI algorithms and models find their theoretical optimal solution (or suboptimal in practice), which is crucial for RS data analysis.”
- Evolutionary algorithms
 - Simulate natural selection to optimize solutions for complex problems/data
- Neural architecture search
 - ML technique that automatically designs optimal DL network architectures
- Quantum computing

AI Explicability

- Explainable models
- Physics-combined models
 - “Data-driven AI algorithms may violate key physical constraints and cannot generalize outside of their training set. Therefore, practical researchers still prefer models with a clear physical meaning rather than simply data fitting.”

Data Mining

- Scene classification and object detection
- Data reconstruction and information restoration
- Environmental parameter extraction
- Regression analysis
- State estimation and event localization

Natural language processors (NLP)

- Language models that interpret an image and explain it
- Description generation for RS images
- RS image question answering – directly retrieving answers from RS images
- RS image generation with sequential data – text-to-image generation
- RS image with audio sequence – audio-to-image generation

AI Security

- “For example, the deployed AI system might be attacked by specific deception algorithms [266], known as adversarial attacks, which can generate subtle perturbations imperceptible to a human observer but may greatly mislead state-of-the-art AI systems to make wrong predictions.”
- Adversarial attacks
 - Make it unlikely that DL models will be used in safety-critical RS fields
- Adversarial defenses
 - (a) Improved training schemes → add adversarial examples to training data and train deep NNs with mixed clean/adversarial samples → *adversarial training*
 - (b) Improved network architectures

Conclusions and remarks

- Future interesting topics:
 - AI approaches for real-world RS tasks
 - Explainable AI algorithms for RS data
 - Security-related AI approaches for RS data
- This paper is essentially a paper that lists off what other papers have done, while neatly categorizing them, and then references those papers

A survey of uncertainty in deep neural networks

Gawlikowski et al. (2023)

Introduction

- Deep learning algorithms are largely unable to provide uncertainty estimates for a deep NN's decision and they frequently have overly confident predictions
- "The most common way to estimate the uncertainty of a prediction (the predictive uncertainty) is based on separately modelling the uncertainty caused by the model (epistemic or model uncertainty) and the uncertainty caused by the data (aleatoric or data uncertainty)."
 - Predictive uncertainty is reducible by improving the model, data uncertainty is not

Uncertainty in deep neural networks

- Four steps leading from raw info to uncertainty estimates in DNNs
 - Data acquisition
 - DNN building process
 - Applied inference model → the model applied for inference, e.g., ensemble of NNs, Bayesian NNs, etc...
 - Prediction's uncertainty model
- Five most important factors causing uncertainty in deep NNs:
 - the variability in real world situations,
 - the errors inherent to the measurement systems,
 - the errors in the architecture specification of the DNN,
 - the errors in the training procedure of the DNN,
 - the errors caused by unknown data.

Uncertainty estimation

- Four key methods:
 - Single deterministic methods – "prediction based on one single forward pass within a deterministic network"
 - Bayesian methods – all kinds of stochastic DNNs
 - Ensemble methods – "combine the predictions of several different deterministic networks at inference."
 - Test-time augmentation methods – "give the prediction based on one single deterministic network but augment the input data at test-time in order to generate several predictions that are used to evaluate the certainty of the prediction"
- But the reliability of the uncertainty estimates also needs to be accounted for

Uncertainty measures and quality

- Evaluating quality of uncertainty estimates can be hard:
 - Quality of uncertainty estimate depends on underlying method for estimating uncertainty
 - Lack of ground truth uncertainty estimates and defining ground truth uncertainty is hard
 - Lack of unified quantitative evaluation metrics – especially across different tasks like classification, segmentation, and regression

Calibration

- "A predictor is called well-calibrated if the derived predictive confidence represents a good approximation of the actual probability of correctness"
- Three main groups of calibration methods based on the step when they are used:
 - Regularization methods applied during the training phase
 - DNNs inherently calibrated
 - Post-processing methods applied after the training process of the DNN
 - "require a held-out calibration data set to adjust the prediction scores for recalibration."
 - Neural network uncertainty estimation methods
 - "reduce the amount of model uncertainty on a neural network's confidence prediction, also lead to a better calibrated predictor. This is because the remaining predicted data uncertainty better represents the actual uncertainty on the prediction."

Data sets and baselines

- "In this section, we collect commonly used tasks and data sets for evaluating uncertainty estimation among existing works."

Applications of uncertainty estimates

- Brief overview of applications of uncertainty estimates in active learning, reinforcement learning, and domain fields like medical image analysis and earth observation

Conclusions and outlook

- Reasons why DNNs are not consistently used in real-world applications:
 - Missing validation of existing methods over real-world problems
 - Models are generally for specific use cases and are not readily applicable to complex real-world environments
 - Lack of standardized evaluation protocol
 - Inability to evaluate uncertainty associated to a single decision
 - Uncertainty estimated is based on whole test set, but what if we need an uncertainty estimate for one specific decision? Will be biased towards performance rest of test dataset
 - Lack of ground truth uncertainties → no validation of uncertainties
 - Explainability issue

Title

Author et al. (YYYY)

Introduction

Subsection | Keywords